UiO : University of Oslo

Jon Austad

Theoretical Investigations of Molecular Electronic Structure in a Magnetic Field

Thesis submitted for the degree of Philosophiae Doctor

Department of Chemistry
Faculty of Mathematics and Natural Sciences

Hylleraas Centre for Quantum Molecular Sciences

2020

Series of dissertations submitted to the
Faculty of Mathematics and Natural Sciences, University of Oslo
No. 2295

ISSN 1501-7710

Cover: Hanne Baadsgaard Utigard.
Print production: Reprosentralen, University of Oslo.

Acknowledgment

I joined the Oslo group of theoretical chemistry in my last semester as a bachelor student. Then, I got my master's degree with Trygve Helgaker and Erik Tellgren as my supervisors, and now, finally, my Ph.D. As such, I've been a part of this excellent community for nine years. I've seen the Centre of Theoretical and Computational Chemistry end, and I've seen the Hylleraas Centre of Quantum Molecular Sciences rise. Naming all the generous, kind and interesting people I've interacted with over the years is impossible, but I'll mention a few.

My supervisors, Trygve and Erik, have guided me through this project and have granted me more encouragement and patience than I could possibly deserve. Alex Borgoo also acted as unofficial supervisor for a time, and helped me get back on track when things looked bleak. To Glenn B.S. Miller, who started studying chemistry at the same semester as I, and who defended his Ph.D years before me: Thank you for a lasting friendship – and for your linguistic feedback! To Patrick, Volodja, Kai, Chamdan, John, Jostein, Sigbjørn, Julie, Llouis, and all the other temporary inmates of our little office: I will never forget the general atmosphere you created, how helpful you all were, and how enjoyable it has been to be your colleague. So long, and thanks for all the fish!

Also a great thank you to Henrik Austad and Vidar Løkken for your indispensable advice on programming, operating systems, backup routines and all the CPU time you have generously granted me on your personal servers. I assure you, there are few privately owned servers out there that have done more number crunching on quantum mechanical systems in magnetic fields.

However, there is one person in particular who deserves more credit and praise than anyone else: My wife, Marianne. Being a struggling scientist is hard on the environment in general and on the family in particular. When I was disorganized, she helped me retrieve the loose ends. When I despaired, she encouraged. When I sacrificed all my duties at home and with the family to concentrate on my work, she covered for me. Without her, this would project would be nothing but a dead dream. That is a debt I can never repay. From the bottom of my heart: *Thank you!*

List of Articles

I. *Kohn–Sham energy decomposition for molecules in a magnetic field*, published in Molecular Physics [1].

II. *Bonding in strong magnetic fields: role of spin and angular momentum*, submitted for publication.

III. *Effects of strong magnetic fields on water from rigorous quantum calculations*, to be submitted for publication.

Contents

Part I

Introduction and theory

Chapter 1

Introduction

When the Schrödinger equation was solved for the hydrogen molecule and the helium atom in the 1920s, it was made clear that any molecular system could be accurately described with quantum mechanics [2, 3, 4]. The term *quantum chemistry* appeared around the same time. Given such a prominent maturity, one might be tempted to assume quantum chemistry to be a finished field by now. Nothing could be further from the truth.

Quantum chemistry relies on manybody quantum mechanics, which has proven to be a resilient adversary for a century. Some of the obstacles appear intractable even today. While the rules of the game dictate that all physical properties can be exactly computed, and although all forces involved are well understood, the same rules excludes an accurate depiction of all but the simplest model systems. Furthermore, even those solutions are rarely analytical. It became abundantly clear from the very beginning that manybody quantum mechanics belong to the murky realm of heavy number crunching.

Modeling of larger systems in particular require certain approximations, both in how the wave function is described, and in how the Schrödinger equation is solved. It is not enough to compromise between accuracy and tractability: Choices must be made, both about what parts of the physics should be maintained, and about what should be glossed over. These choices must reflect the investigations at hand. Entire hierarchies of approximations (and corresponding corrections) have arisen over the years. The scaling of cost of even the crudest usable approximations is rarely linear in nature; if the system size is doubled, the computational expense is polynomially increased at best. Safely navigating these waters, knowing when to use what, and how – that is the trade of a quantum chemist. Nothing is simpler than producing meaningless data which superficially look nice.

One area of computational quantum chemistry that has been beyond the reach of conventional computational methods for a long time is the regime of strong magnetic fields. Mathematically, magnetic fields introduce serious complications, the gauge problem being the main antagonist. For weak fields, certain approximations can be made, but they are safe to use only when experimental results are available for comparison. However, magnetic fields experimentally attainable here on Earth are paltry compared to certain stellar phenomena [5]. Even with terrestrially available fields, experiments can be hard to conduct and interpret. Magnetic fields in general, and strong fields in particular, are causing both theoretical and experimental concerns. Fritz London proposed an elegant solution to some of these problems in 1938 [6] which allows the magnetic vector potential[1] to be included in the orbitals. This solves the gauge origin problem [7], but the all conventional numerical methods must be reformulated and reimplemented in the new formalism. As always, when a solution to one particular problem is introduced, a large number of different issues tend to tag along.

The LONDON program was written with this in mind [8, 9]. As a scientist, it has been my most important tool. As a software developer, my main headache.

1.1 Scope

This thesis is my contribution to the continued advancement of high accuracy quantum chemistry methods for magnetic fields, and to fill in some of the white spots on the map of strong field chemistry. I have developed, implemented and explored computational methods for strong magnetic fields. The behavior of these methods, and their strengths and weaknesses, have been central points of investigation. I have used these methods to probe molecular systems hitherto unavailable to scientific scrutiny.

From a development perspective, I have mostly concerned myself with *Møller-Plesset perturbation theory* (MPPT). My research, however, has also relied heavily on methods implemented in the LONDON suite by others. These include more accurate methods, such as *coupled cluster* theory (CC) and *configuration interaction* theory (CI), and less accurate methods like *Hartree-Fock* theory (HF). Furthermore, I have dealt with *density functional theory* (DFT) which is a different beast altogether, particularly in the presence of magnetic fields. All these methods will be given due treatment in Chapter 3.

The research includes three papers which address three different aspects of magnetic quantum chemistry. The first paper explores the underlying mechanisms of

[1] Magnetic vector potentials will be introduced in Section 2.2.

DFT. Specifically, we investigated a field-dependent DFT formalism by using wave-function methods (HF, MPPT and CC) to produce a density, and then compare these with more or less conventional DFT functionals. The gist of this project was to further the understanding of the theoretical framework of magnetic DFT.

The second paper revolved around helium atoms and clusters in strong magnetic fields. High accuracy calculations were performed in order to fully understand the interactions between helium atoms, and also explore the electronic structure of the molecule for different bond lengths, orientations to the field, and field intensities. The interest of helium on highly magnetic objects, such as white dwarfs stars, is not new [10, 11].

In the final paper, a practical issue was scrutinized: Are the physical properties of water affected by magnetic fields attainable on Earth? The issue has seen significant attention over the years, but a scientific consensus has not yet emerged [12, 13]. Our short answer to this riddle is no, the physical properties of water are not affected by magnetic fields of available intensity, but saying so with confidence is surprisingly hard.

The work underlying this thesis is therefore threefold, and on three different abstraction levels. The overarching theme is the development and usage of magnetic wave-function methods with the London orbital approach. These methods have been used to increase our comprehension of other levels of theory, explore exotic molecular properties, and provide practical answers to relevant issues here on Earth.

1.2 Magnetic fields and where to find them

This thesis is a theoretical study dealing extensively with magnetic fields and their effect on chemistry.

In the vernacular sense, one might be tempted to consider a refrigerator magnet or a compass needle as "weak" magnets, while a magnetic door lock or an NMR spectrometer are "strong" – and the effects such powerful magnets can produce are certainly impressive. There have even been fatal accidents with MRI scanners and loose steel canisters [14]. Yet, the field strengths of such machines are typically just a few tesla (T). The famous levitating frog experiment was conducted at 16 T [15] and continuous magnetic fields for experimental research above 40 T have been available for decades [16]. However, all of these contraptions produce weak fields in the chemical sense: None of them perceptibly affect molecular interactions. The tesla is usually considered a rather large unit, but the atomic units are preferred for quantum chemistry. In this thesis, the SI based Hartree system is used throughout. One atomic unit (a.u.) for magnetic fields (B_0) corresponds to approximately 235 kT

and is several orders of magnitude stronger than anything available to experimental research. Somewhat curiously, magnetic fields of moderate to high intensity have until recently been largely unavailable to the theoretical chemists as well: The necessary adjustments of the physical descriptions – or rather, the inapplicability of the conventional field free approximations – causes vast computational problems for interesting chemical systems.

It should be emphasized that the universe contains magnetic fields many orders of magnitude larger than anything examined in this thesis. The LONDON program allows for a delightful generality, even still there are mysteries out there currently beyond its grasp. For example, when the Coulomb interactions are a mere perturbation to the magnetic forces, the pressure so high that electrons and protons merge into neutrons, and the object rotates so fast that the linear velocity near the surface approaches a quarter of the speed of light [17], then a completely different theoretical approach is required.

Table 1.1 contains some examples of magnetic fields of various orders of magnitude in an attempt to put the matter into perspective. Even experimentally attainable fields can cause counterintuitive things to happen [34, 35], but for the really exotic properties, much stronger fields are required. As an example of an exotic property, Figure 1.1 shows how a magnetic field introduces currents in a H_2 molecule to the point that the triplet state allows for a stable, molecular bond: The induced currents of the singlet and triplet have different direction, causing an increase and decrease in energy, respectively. This in turn causes the triplet state to be strongly bonding in a magnetic field [36], but only if the molecular axis is perpendicular to the field. This effect is called perpendicular paramagnetic bonding [37, 38].

A sufficiently strong field will cause a paramagnetic molecule to become diamagnetic [39, 40, 41]. Strong magnetic fields can also significantly alter the geometries of well known molecules, such as benzene [42].

For the early history of the strong-field chemistry, consult [43, 44, 45, 46, 47].

Table 1.1: *Magnetic fields by order of magnitude*

Regime [T]	**Description**
10^{-18}	Lower bound for SQUID magnetometers (about 5 aT) [18]
10^{-9}	The heliosphere (1–35 nT) [19]
10^{-6}	The magnetic field of planet Earth (up to 67 μT) [20]
10^{-3}	Typical refrigerator magnet (about 5 mT)
10^{0}	Rare earth magnets, magnetic door locks and MRI scanners [14]
10^{1}	Typical NMR spectrometers ($>$ 10 T), Levitating frog experiment (16 T) [15], Strongest continuous field on earth (45 T) [16]
10^{2}	Strongest non-destructive pulsed field on earth, exceeding 100 T [21, 22]
10^{3}	Strongest destructive pulsed fields [23, 24] up to 2.8 kT, by means of explosives [25, 26]
10^{4}	White dwarf *Grw+70° 8247*; surface field strength of about 32 kT [27]
10^{5}	1 a.u. = 235 kT = B_0 Coulomb and magnetic interactions of equal magnitude Lower bound for neutron star magnetic field [28] Atoms deformed into prolate spheroids [29]
10^{8} to 10^{10}	Magnetars [30] Non-linear fields (Schwinger limit); $S_{mi} = \frac{c^2 m_e^2}{q_e \hbar} \approx 4.41$ GT [31, 32, 33]

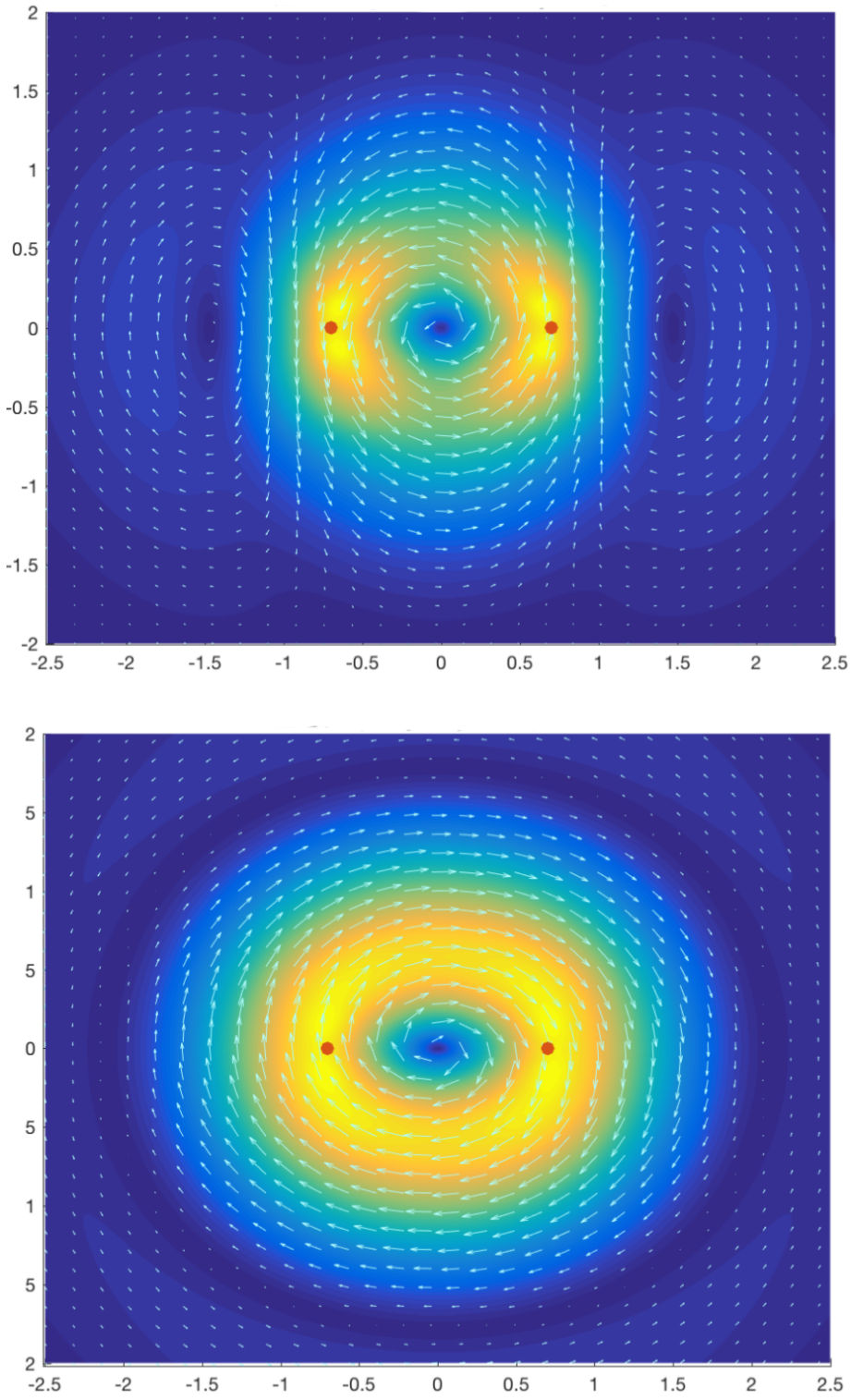

Figure 1.1: *The molecular current density of a H_2 molecule, with the current density of isolated atoms subtracted; singlet molecule above, triplet below. The unit of the X- and Y-axis are a_0 (bohr). The magnetic field introduces currents which causes the triplet state to be stable and bonding. Image courtesy of Erik Tellgren.*

Chapter 2

Many-body quantum mechanics

In this chapter, the formalisms of manybody quantum mechanics will be introduced, along with some useful approximations and tools.

2.1 The Schrödinger equation

There are many different approaches for doing quantum mechanics, some are more convenient for some problems and less so for others [48]. The notation used in this thesis will rely heavily on second quantization, bra-kets and commutators. These are common tools for quantum chemists.

The conventional view is that the wave function, Ψ, contains all physical information about a quantum system. Any observable can be represented by an operator, $\hat{\Omega}$, whose eigenvalues are the possible outcomes of a measurement.

The operator $\hat{\Omega}$ maps a wave function to another (possibly identical) wave function. The expectation value is given by the integral

$$\langle \hat{\Omega} \rangle = \int \Psi^* \hat{\Omega} \Psi \, \mathrm{d}\tau. \tag{2.1}$$

This follows from the Born rule, which states that the probability of measuring a value ω_i, corresponding to an eigenstate Φ_i, is $|\langle \Phi_i \,|\, \Psi \rangle|^2$.

The most important operator of manybody quantum mechanics by far is the Hamiltonian, $\hat{H}$. It describes the energy spectrum and all dynamics. Time evolution of quantum states as a function of time t can be written like this,

$$\hat{H} \,|\Psi(t)\rangle = i\hbar \frac{\partial}{\partial t} \,|\Psi(t)\rangle \,, \tag{2.2}$$

which is the time dependent Schrödinger equation. This is a first order differential equation in time. The solution to the *time-independent* Schrödinger equation provides the stationary states,

$$\hat{H}\left|\Psi\right\rangle = E\left|\Psi\right\rangle, \tag{2.3}$$

where E is the total energy of the system. This is the setting in which the work of this thesis has been conducted. The Hamiltonian operator depends on the relevant physics of the system to be described. In quantum chemistry, the exact Hamiltonian contains a term for the kinetic energy of all particles involved, and energy terms for the twobody interactions between them. Threebody interactions and beyond have no physical relevancy in chemistry and are not included in the Hamiltonian.

2.1.1 The Born-Oppenheimer approximation

Typically, the *Born-Oppenheimer* (BO) approximation is employed to reduce the number of interactions, details are described below. The BO approximation lies at the heart of most conventional quantum chemistry.

The complete Hamiltonian can be split up in many ways. One is to extract the kinetic energy of the nuclei and treat the rest as an "electronic Hamiltonian",

$$\hat{H} = \hat{T}_{\text{nuc}} + \hat{H}_{\text{el}}, \tag{2.4}$$

where

$$\hat{T}_{\text{nuc}} = -\sum_{\mu=1}^{N_{\text{nuc}}} \frac{1}{2M_\mu}\nabla_\mu^2. \tag{2.5}$$

is the kinetic energy of the nuclei. The electronic Hamiltonian then becomes

$$\hat{H}_{\text{el}} = \hat{T}_{\text{el}} + \hat{W} + \hat{V}_{\text{ext}} + \hat{V}_{\text{nuc}}. \tag{2.6}$$

The kinetic energy operator for the electrons is similar to the kinetic energy operator for the nuclei:

$$\hat{T}_{\text{el}} = -\frac{1}{2}\sum_{p}^{N_{\text{el}}} \nabla_p^2. \tag{2.7}$$

The remaining terms of $\hat{H}_{\text{el}}$ are the potential operators. These are

$$\hat{V}_{\text{nuc}} = \sum_{\mu<\nu} \frac{Z_\mu Z_\nu}{|\mathbf{r}_\mu - \mathbf{r}_\nu|}, \quad \hat{V}_{\text{ext}} = \sum_{p,\mu} \frac{Z_\mu}{|\mathbf{r}_\mu - \mathbf{r}_p|} \quad \text{and} \quad \hat{W} = \sum_{p<q} \frac{1}{|\mathbf{r}_p - \mathbf{r}_q|}, \tag{2.8}$$

where the Greek indices indicate nuclei and Latin indices indicate electrons, so that $1 \leq p, q \leq N_{\text{el}}$ and $1 \leq \mu, \nu \leq N_{\text{nuc}}$.

The lightest atom in existence is hydrogen, whose nucleus consists of a single proton. Even in this case, the nucleus is more than a thousand times heavier than an electron. It is therefore reasonable to assume that electrons experience the attractions from the nuclei as an external potential and not as a twobody interaction. Consequently, it is assumed that the electrons immediately adapt to any configuration of the nuclei. This is the "classical" (and somewhat heuristic) justification for the BO approximation[1]. In practice, it is well suited for ground state calculations, but is often too crude for highly excited states: The BO approximation works best when the states are comfortably far apart.

The definition of many computational methods rely on the assumption that the movement of the nuclei is separated from the electron. While it is clear that the BO approximation works well for a large number of chemical systems, there are fundamental problems that should be kept in mind. The above argument is formulated in the paradigm of chemical structure as an "intrinsic property" of a molecule, but this is inconsistent with requirements of quantum theory [50].

When the BO approximation is invoked, the nuclear-nuclear repulsion is independent of electron coordinates and remains constant for a given geometry. Therefore, the nuclear-electron interactions are onebody operators, just like the electronic kinetic energy. Only the electron-electron interactions depend simultaneously on more than one particle. Splitting the electronic Hamiltonian into one- and twobody operators provides a compact representation. The one-electron Hamiltonian $\hat{h}$ is defined as

$$\hat{h}_i = -\nabla_i^2 + \sum_{\mu=1}^{N_{\text{nuc}}} \frac{Z_\mu}{|\mathbf{r}_\mu - \mathbf{r}_i|}, \tag{2.9}$$

thus rewriting the electronic Hamiltonian to

$$\hat{H}_{\text{el}} = \sum_{i=1}^{N_{\text{e}}} \hat{h}_i + \hat{W}. \tag{2.10}$$

[1] Albeit, Born and Oppenheimer themselves did not use this argument [49].

It is common to write the components of $\hat{W}$ in similar manner; $\hat{g}_{ij} = \frac{1}{r_{ij}}$. For the remainder of this thesis, I will assume that $\hat{H}$ and $\hat{T}$ means $\hat{H}_{\text{el}}$ and $\hat{T}_{\text{el}}$ unless otherwise specified.

The BO approximation requires that the center of mass can be separated from the internal degrees of freedom. In a magnetic field, this is a hard problem [51, 52, 53]. For this reason, calculating the expectation values of properties that rely directly on the movement of the nuclei, such as vibrational spectra, is tricky when magnetic fields are present. However, the properties investigated in this thesis do not depend on the motion of the nuclei.

2.1.2 The Hellman-Feynman theorem

Any N-electron, antisymmetrized wave function Φ yields an energy which cannot lie below the true ground state energy as provided by the ground state wave function Ψ_0:

$$E\left[\Phi\right] = \frac{\left\langle \Phi \left| \hat{H} \right| \Phi \right\rangle}{\left\langle \Phi \,|\, \Phi \right\rangle} \geq E_0 = E\left[\Psi_0\right]. \tag{2.11}$$

This in turn allows Φ to be systematically varied until some energy minimum is found. This is the Rayleigh-Ritz variational principle.

The Hellman-Feynman theorem simplifies differentiation of the energy. Assuming a parametric dependency in the Hamiltonian on some continuous variable λ so that

$$\hat{H}_\lambda \left|\psi_\lambda\right\rangle = E_\lambda \left|\psi_\lambda\right\rangle, \tag{2.12}$$

and inserting this expression into Equation (2.11), and then differentiating with respect to λ,

$$\frac{\partial E_\lambda}{\partial \lambda} = \frac{\partial}{\partial \lambda} \left\langle \psi_\lambda \left| \hat{H}_\lambda \right| \psi_\lambda \right\rangle = E_\lambda \underbrace{\left[\left\langle \frac{\partial \psi_\lambda}{\partial \lambda} \middle| \psi_\lambda \right\rangle + \left\langle \psi_\lambda \middle| \frac{\partial \psi_\lambda}{\partial \lambda} \right\rangle \right]}_{\frac{\partial}{\partial \lambda}\left\langle \psi_\lambda \,|\, \psi_\lambda \right\rangle} + \left\langle \psi_\lambda \middle| \frac{\partial \hat{H}_\lambda}{\partial \lambda} \middle| \psi_\lambda \right\rangle. \tag{2.13}$$

Because $\left\langle \psi_\lambda \,|\, \psi_\lambda \right\rangle = 1$, it follows that $\frac{\partial}{\partial \lambda} \left\langle \psi_\lambda \,|\, \psi_\lambda \right\rangle = 0$, and only

$$\frac{\partial E_\lambda}{\partial \lambda} = \left\langle \psi_\lambda \middle| \frac{\partial \hat{H}_\lambda}{\partial \lambda} \middle| \psi_\lambda \right\rangle \tag{2.14}$$

is left. This assumes ψ_λ to be an eigenstate of the Hamiltonian. The Hellman-Feynman theorem can be shown to work on a more general level if needed [54]. This is a nifty result, but it only applies to variational methods. HF and CI theory are variational methods, but MPPT and CC theory are not. All these methods will receive due introduction in Chapter 3.

A further caveat is that the Hellman-Feynman theorem requires the wave function to not depend parametrically on λ. Often, this is true even if λ represents a magnetic field. However, when London orbitals are used, the wave function depends explicitly on the field. Magnetic properties like magnetizabilities and shielding constants can be described by a Taylor expansion of the energy (more in Section 2.1.3), and can therefore not be derived with the aid of the Hellman-Feynman theorem. Differentiation with respect to variables that do not affect the model space of the parametrized wave function are still acceptable, so an electric field, for example, is not a problem.

2.1.3 Magnetic properties

The response of a system to changes in a magnetic field can be investigated in several ways. It is usually recommended to employ analytical differentiation when possible, since usage of numerical differentiation is expensive and messy. Unfortunately, implementing the analytical derivatives tend to be labor intensive and hard. As discussed in Section 2.1.2, the Hellman-Feynman theorem does not hold for magnetic dependencies and London orbitals. This means the derivatives of not only the Hamiltonian, but also of the wave function, is required. Polynomial fitting is a less desirable solution in terms of accuracy and reliability, but sometimes pragmatism must prevail over purity.

The total energy of a molecular system as a function of the magnetic field can be written as a Taylor expansion

$$E(\mathbf{B}) = E_0 + \frac{1}{2}\sum_{\alpha} J_\alpha B_\alpha - \frac{1}{2!}\sum_{\alpha\beta} \chi_{\alpha\beta} B_\alpha B_\beta + \frac{1}{3!}\sum_{\alpha\beta\gamma} X_{\alpha\beta\gamma} B_\alpha B_\beta B_\gamma + ... \qquad (2.15)$$

where E_0 is the field-free energy. The first derivative is the angular momentum, and the magnetizability is the second-order term. The higher orders are all called hyper-magnetizabilities, and denominated by $X_{\alpha\beta\gamma\delta...}$ where the number of indices determine the exact order of the property. In a closed shell system, $E(\mathbf{B}) = E(-\mathbf{B})$ and all odd terms disappear due to symmetry. The first relevant hyper-magnetizability for

a closed shell system is therefore

$$X_{\alpha\beta\gamma\delta} = -\frac{\partial^4 E(\mathbf{B})}{\partial B_\alpha \partial B_\beta \partial B_\gamma \partial B_\delta}\bigg|_{\mathbf{B}=0}. \tag{2.16}$$

It is intractable to compute such a fourth-order tensor with polynomial fitting. For highly symmetric molecules, such as small, homoatomic clusters, most of the tensor will contain redundant information and high-order magnetic properties have consequently been calculated [55] for this kind of systems.

In paper 1, a sixth order polynomial fitting over not just the total energy as a function field, but different Kohn-Sham components (see Section 3.5), was employed.

2.1.4 Second quantization and commutators

The second quantization formalism was made for quantum field theory, and is particularly useful for keeping track of an arbitrary, and possibly changing, number of particles. In quantum chemistry, the number of particles is usually constant, unless ionization and similar effects are studied. However, second quantization simplifies the book keeping and offers compact a representation of the mathematics involved.

Instead of describing the coordinates of particles explicitly, they are represented by creation and annihilation operators. A creation operator will add a particle with a particular set of quantum numbers to the wave-function, and an annihilation operator will remove one.

It is assumed that some set of orthonormal single particle spin orbitals exists and that they can be assigned single particle energies[2]. Adding all particles in ascending order to the true vacuum state gives the simplest approximation to a many-particle ground state. This defines the Fermi vacuum,

$$\hat{a}_1^\dagger \hat{a}_2^\dagger ... \hat{a}_N^\dagger \left|\text{vac}\right\rangle = \left|\psi_0\right\rangle \tag{2.17}$$

which is a many-particle wave function that frequently serves as a starting point for more elaborate descriptions. Indices of single-particle states (orbitals) below the Fermi level are denoted with the letters $i, j, k...$, letters $a, b, c...$ are used above the Fermi level, and $p, q, r...$ denote arbitrary single-particle states. An unoccupied orbital is usually called virtual. The Fermi level necessarily lies between the highest occupied orbital and the lowest virtual orbital.

All the possible single particle orbitals – whatever they may be – are sorted by energy, and the particles of the system are created from lowest energy and upwards.

[2]This is a modest assumption. Some examples are orbitals provided by the 1-electron part of $\hat{H}$, the Fock operator, the Kohn-Sham operator or by some other quasi-particle theory.

This is not necessarily the ground state, but since all the low energy orbitals are at play, it is usually a fair starting point. It is much more useful than the true vacuum since all the particles are "in game", and different configurations can be described by applying creation and annihilation operators in equal amount. Due to the Pauli exclusion principle, no fermions can share the same set of quantum numbers. Therefore, attempting to create an existing particle, or annihilating a non-existing one, renders the wave function void:

$$\hat{a}_i^\dagger \left|\psi_0\right\rangle = \hat{a}_a \left|\psi_0\right\rangle = 0. \tag{2.18}$$

Annihilating an existing particle creates a "hole". If a particle is then created in a different orbital, a new state with the same number of particles is created. This is called a particle-hole excitation, and is typically depicted like this:

$$\hat{a}_a^\dagger \hat{a}_i \left|\psi_0\right\rangle = \left|\psi_i^a\right\rangle, \quad \hat{a}_a^\dagger \hat{a}_b^\dagger \hat{a}_i \hat{a}_j \left|\psi_0\right\rangle = \left|\psi_{ij}^{ab}\right\rangle \tag{2.19}$$

and so on, where the states $\left|\psi_{ijk\ldots}^{abc\ldots}\right\rangle$ are n-particle-n-hole excitations for some $1 \leq n \leq N_{\text{el}}$. As long as the number of particle creations is identical to the number of annihilations, the total number of particles is preserved. Any wave function can be described as a linear combination of different particle-hole excitations from some N-electron state. For creation and annihilation operators, the commutator rules are

$$\left[\hat{a}_p^\dagger, \hat{a}_q^\dagger\right]_+ = 0, \quad \left[\hat{a}_p, \hat{a}_q\right]_+ = 0 \quad \text{and} \quad \left[\hat{a}_p^\dagger, \hat{a}_q\right]_+ = \delta_{pq}, \quad \text{where} \quad \delta_{pq} = \begin{cases} 1 & p = q \\ 0 & p \neq q \end{cases} \tag{2.20}$$

is the Kronecker delta. In the second quantization representation, the anticommutation relations in Equation (2.20) are central axioms. For more details, consult [56, 57].

2.2 Vector potentials and gauge transformations

Maxwell's equations for electromagnetism,

$$\nabla \cdot \mathbf{E} = \frac{\rho}{\epsilon_0}, \quad \nabla \mathbf{B} = 0, \quad \nabla \times \mathbf{E} = \frac{\partial \mathbf{B}}{\partial t} \quad \text{and} \quad \nabla \times \mathbf{B} = \mu_0 \left(\mathbf{J} + \epsilon_0 \frac{\partial \mathbf{E}}{\partial t}\right), \tag{2.21}$$

define relations between the magnetic field $\mathbf{B}$ and the electric field $\mathbf{E}$. The other *dramatis personae* in the equations above are the current density $\mathbf{J}$, the charge

density ρ, the vacuum permittivity $\epsilon_0 = \frac{1}{4\pi}$ a.u. and the vacuum permeability $\mu_0 = \frac{4\pi}{c^2}$. In classical physics, this is often the most convenient way to formulate and use electromagnetic relations. It is, however, also possible to define these relations in terms of the magnetic vector potential $\mathbf{A}$ and the electrostatic potential Φ. Whereas $\mathbf{E}$ and $\mathbf{B}$ are actual, physical fields, the potentials are mathematical constructions. They can be arbitrarily chosen, as long as the following demands are satisfied:

$$\mathbf{E} = -\nabla\Phi + \frac{\partial \mathbf{A}}{\partial t} \quad \text{and} \quad \mathbf{B} = \nabla \times \mathbf{A}. \tag{2.22}$$

When the fields are static, the requirement for the electric field is simplified to

$$\mathbf{E} = -\nabla\Phi. \tag{2.23}$$

The existence of electromagnetic potentials is ensured by the Helmholtz theorem, also called the fundamental theorem of vector calculus. It states that a well behaved[3] vector field $\mathbf{F}$ may be decomposed into a solenoidal and an irrotational field – that is, one field whose divergence is zero, and one whose curl is zero, respectively. The vector field is written as

$$\mathbf{F} = -\nabla\Phi + \nabla \times \mathbf{A}, \tag{2.24}$$

which determines Φ and $\mathbf{A}$ up to a gauge term given by the gradient of a function [58].

The *canonical momentum* operator for an electron is

$$\hat{\mathbf{p}} = -\mathrm{i}\nabla. \tag{2.25}$$

However, the presence of a magnetic field requires the inclusion of the magnetic vector potential. Since $-q = 1$ in atomic units, the operator becomes

$$\hat{\boldsymbol{\pi}} = -\mathrm{i}\nabla + \mathbf{A}. \tag{2.26}$$

The operator $\hat{\boldsymbol{\pi}}$ represents the *physical momentum* (also called the *kinetic momentum* in the literature). $\hat{T}$ and $\hat{H}$ are then adjusted accordingly. This is called the *minimal substitution* [59].

Next, we consider quantum mechanics with external fields. Assume a gauge transformation function f so that

$$\phi(\mathbf{r}) \mapsto e^{-\mathrm{i}f(\mathbf{r})}\phi(\mathbf{r}) = \phi'(\mathbf{r}) \tag{2.27}$$

[3] "Well behaved" is a loose term, but formally speaking, the requirement is twofold. First, the vector field must be fast decaying, and second, it must be smooth. The latter entails that both $\nabla\mathbf{F}$ and $\nabla \times \mathbf{F}$ are finite everywhere.

where

$$\mathbf{A}(\mathbf{r}) \mapsto \mathbf{A}(\mathbf{r}) + \nabla f(\mathbf{r}). \tag{2.28}$$

As usual, $\phi(\mathbf{r})$ is the wave function. The gauge transformations cancels out exactly for the canonical momentum (Equation (2.26)), because

$$\begin{aligned}\hat{\boldsymbol{\pi}}'\phi' &= (-\mathrm{i}\nabla + \mathbf{A} + \nabla f)\, e^{-\mathrm{i}f(\mathbf{r})}\phi = e^{-\mathrm{i}f(\mathbf{r})}\left(-\mathrm{i}\nabla - \nabla f + \mathbf{A} + \nabla f\right) \\ &= e^{-\mathrm{i}f(\mathbf{r})}\left(-\mathrm{i}\nabla + \mathbf{A}\right)\phi = e^{-\mathrm{i}f(\mathbf{r})}\hat{\boldsymbol{\pi}}\phi. \end{aligned} \tag{2.29}$$

When written as an expectation value, this becomes

$$\left\langle \phi' \,\middle|\, \hat{\boldsymbol{\pi}}' \,\middle|\, \phi' \right\rangle = \int \phi^* e^{if(\mathbf{r})} e^{-\mathrm{i}f(\mathbf{r})} \hat{\boldsymbol{\pi}}\phi \, d\mathbf{r} = \int \phi^* \hat{\boldsymbol{\pi}}\phi \, d\mathbf{r} = \left\langle \phi \,\middle|\, \hat{\boldsymbol{\pi}} \,\middle|\, \phi \right\rangle. \tag{2.30}$$

Clearly, the expectation value is not affected by the gauge transformation. Since the momentum is gauge invariant, so is the kinetic energy, and therefore the Hamiltonian itself because electrostatic interactions are field independent.

The London orbital formalism is actually invariant for all gauge transformations on the form $\mathbf{A} \to \mathbf{A} + \mathbf{c}$, where $\mathbf{c}$ is some Cartesian vector [60]. However, for the purposes of this thesis, gauge *origin* invariance is enough. My work is restricted to uniform magnetic fields and the vector potentials are on the form $\mathbf{A} = \frac{1}{2}\mathbf{B} \times (\mathbf{r} - \mathbf{G})$. The reference point $\mathbf{G}$ is the gauge origin. In this case, f is

$$f(\mathbf{r}) = \mathbf{r} \cdot \left(\frac{1}{2}\mathbf{B} \times \mathbf{c}\right) \quad \text{which gives} \quad \nabla f(\mathbf{r}) = \frac{1}{2}\mathbf{B} \times \mathbf{c}. \tag{2.31}$$

There are only two actual degrees of freedom, since the component parallel to the field does not contribute to $\mathbf{A}$. The wave function must be complex when a magnetic field is present, but it can still be described by real basis functions. However, in an incomplete basis, the wave function lacks the required flexibility to conform to the oscillations[4]. Figure 2.1 illustrates how the wave function for a H_2 molecule behaves in a field for two different gauge origins. The density $|\psi(\mathbf{r})|^2$ is unaffected by the gauge origin, but the wave function itself changes. The oscillations introduced are hard to model with Gaussians alone. The London factor introduces these oscillations, thus providing the wave function with the necessary flexibility to cope with gauge origin transformations.

This solves the gauge origin problem and retains the basis set formulation of the manybody methods. Several new issues are unfortunately introduced. Complex

[4]For atoms, this is not a problem, since the gauge origin can be safely placed in the center.

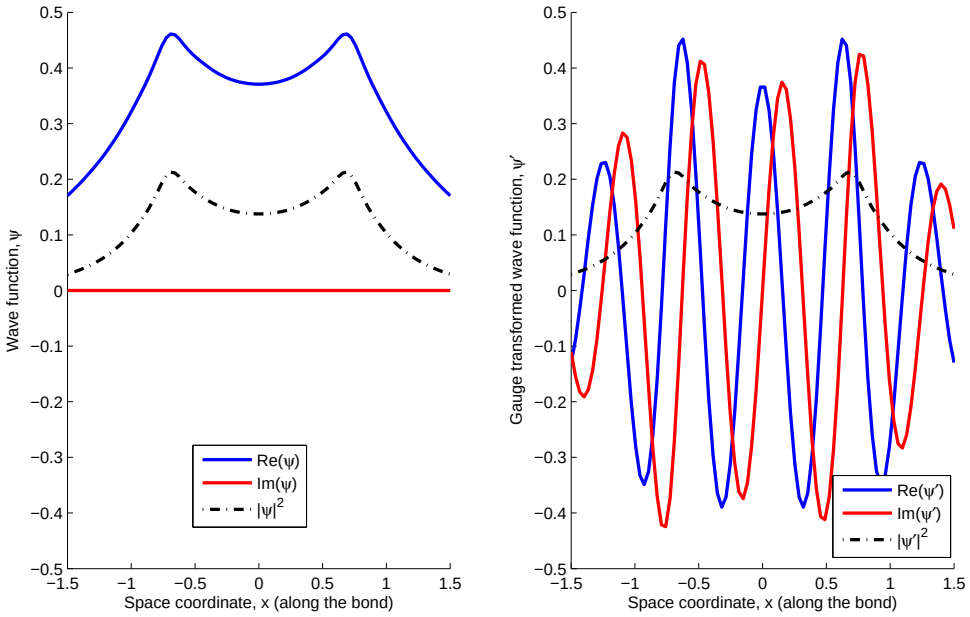

Figure 2.1: *The real and imaginary parts of the wave function for a hydrogen molecule in a magnetic field of* $0.1B_0$*. The only difference between the left an the right plot is the placement of the gauge origin. In the left figure, the gauge origin is placed at the electronic center of mass, in the right, it is placed far away. Image courtesy of Erik Tellgren.*

numbers require more flops and memory, and should therefore be avoided if possible. Also, certain useful short-cuts and symmetries which can be exploited for real numbers are no longer valid. London orbitals also cause the basis functions themselves to be complex, something most conventional integral routines cannot handle [61, 62, 63]. For example, given a real density matrix $\mathbf{D}$ and an overlap matrix $\mathbf{S}$, the number of electrons is $N = \sum_{pq} S_{pq} D_{pq}$. This is no longer true for a complex density matrix. Since the matrices are Hermitian, the correct (but often redundant) definition is rather

$$N = \sum_{pq} S_{pq} D^*_{pq} = \sum_{pq} S_{pq} D_{qp}. \tag{2.32}$$

The density operator- and matrix will be properly introduced in Chapter 3. Another illustrative example is the twoelectron integrals:

$$\langle rs \,|\, pq \rangle = \langle pq \,|\, rs \rangle = \langle qp \,|\, sr \rangle^* \neq \langle qp \,|\, sr \rangle \,, \tag{2.33}$$

which reveals how some of the commonly exploited symmetries are still valid, while others are not [64]. Here, the conventional notation

$$\langle pq \,|\, rs \rangle \equiv \iint \phi^*_p (\mathbf{r}_1) \, \phi^*_q (\mathbf{r}_2) \, \frac{1}{|\mathbf{r}_1 - \mathbf{r}_2|} \phi_r (\mathbf{r}_1) \, \phi_s (\mathbf{r}_2) \;\, \mathrm{d}\mathbf{r}_1 \mathrm{d}\mathbf{r}_2, \tag{2.34}$$

has been employed.

As an aside, London orbitals have also been used in the relativistic regime [65], showing that this formalism is viable for heavier elements as well. For a mathematical description of gauge invariance in a more general setting, please consult [31].

2.3 Molecules and magnetism

All physical matter is affected by magnetic fields, but "magnetism" is not one singular, unique property. Rather, it is a class of physical phenomena, and the material in question may simultaneously be under the influence of several. The source of magnetism in all forms are the spin magnetic momenta of the elementary particles and electric current. In the context of this thesis, the only elementary particles of relevancy are the electrons.

Consider a field-dependent one-electron Hamiltonian

$$\hat{h} = \frac{1}{2} \hat{\boldsymbol{\pi}}^2 + V = \frac{1}{2} \left(\hat{\mathbf{p}} + \mathbf{A} \right) \left(\hat{\mathbf{p}} + \mathbf{A} \right) + V. \tag{2.35}$$

In a uniform magnetic in the z direction, the expression can be rewritten as

$$\hat{h} = \hat{h}_0 + Bs_z + \frac{1}{2}B\hat{L}_z + \frac{1}{8}B^2\left(x^2 + y^2\right) \tag{2.36}$$

where

$$\hat{h}_0 = \frac{1}{2}\hat{\mathbf{p}}^2 + V \tag{2.37}$$

is the field-free single particle Hamiltonian and L_z and s_z are the angular and spin magnetic momenta. The term Bs_z is the spin Zeeman contribution. The spin Zeeman term gives rise to the conventionally known spin states: singlets, doublets, triplets, and so on. The last terms deserve a bit more scrutiny as they describe orbital interactions. Defining

$$\hat{h}_{\text{para}} = \frac{1}{2}B\hat{L}_z \quad \text{and} \quad \hat{h}_{\text{dia}} = \frac{1}{8}B^2\left(x^2 + y^2\right) \tag{2.38}$$

we see that h_{para} is linear in the field and h_{dia} is quadratic. It is the electronic rotational motion in the field which gives rise to $\hat{h}_{\text{para}}$. This rotation generates an orbital magnetic momentum, which interacts with the field in a dipolar fashion; it will either increase or decrease the energy, all depending on the orientation of the spin to the field. This term is paramagnetic. The final term is diamagnetic and is caused by the precessional motion of the electron in the field. This, in turn, induces a destructive magnetic momentum, thus increasing the energy of the system.

Closed shell molecules are normally diamagnetic, since all electrons are bound up as pairs with opposing spin. In fact, as seen in Equation (2.38) all molecules *must* have a diamagnetic term, but they may also have a paramagnetic term in addition, which causes attraction to the external field. A radical is obviously paramagnetic, but also a molecule such as O_2: The ground state has two electrons in degenerate orbitals, and in accordance with Hund's rules, they consequently align spinwise. The two aligned spins give rise to a paramagnetic term which is much stronger than the diamagnetic term from the remaining seven doubly occupied orbitals. However, since the diamagnetic term scales with the square of the field, while the paramagnetic term is linear, all molecules become diamagnetic in a sufficiently strong field. Typically, closed shell molecules are exclusively associated with diamagnetism, but closed shell paramagnetic molecules are also possible. This is an exotic effect. In the case of boron monohydride (BH), the molecule is diamagnetic if the molecular axis is parallel to the field, and paramagnetic in a perpendicular orientation. The diamagnetic terms causes the electron distribution around an atom to become less diffuse and symmetric [66]. This "diamagnetic shrinking" is not yet experimentally observable *in vitro*, as the fields attainable on Earth are comparatively weak.

Chapter 3

Computational methods

Quantum chemistry encompasses an astounding amount of different many-body theories, each with numerous variations and flavors. Even a cursory introduction to all of them is beyond the scope of this thesis, but the methods presented in the following sections have been used extensively and merit a description.

3.1 Hartree-Fock theory

HF theory is the foundation upon which most *ab initio* methods are constructed. The main assumption in HF theory is that the exact manybody wave function can be adequately approximated with a single Slater determinant. The resulting determinant can then be used as a Fermi vacuum for more exact descriptions. Minimizing the energy as the expectation value from a full Hamiltonian applied on a single Slater determinant gives effective single particle equations. This can be interpreted to describe particles interacting with a "mean-field" from the others, rather than the full Coulomb interaction [67].

The time-independent non-relativistic Schrödinger equation, Equation (2.3), was introduced in Section 2.1. The solutions to this equation provides what we define to be the exact energy of a system. Solving the manybody Schrödinger equation exactly in the conventional sense is typically intractable for chemically relevant systems, which is why entire hierarchies of approximations have arisen. The so called correlation energy E_{corr} is, by definition, the difference between the exact energy of a system and the HF energy:

$$E_{\text{corr}} \equiv E - E_{\text{HF}}. \tag{3.1}$$

One note of importance: In the quantum chemistry vernacular, the "exact energy" is usually defined as the Full Configuration Interaction (FCI) energy (E_{FCI}) in the basis set limit[1]. This is not the only way to solve the Schrödinger equation exactly, but it is the most common approach. Of course, all exact descriptions must necessarily provide the same energy, and can therefore be seen as rewritings of each other.

3.1.1 Slater determinants

The fermionic many-particle wave function is constructed from orthogonal single-particle spin orbitals $\chi_p(\mathbf{x})$. The coordinates $\mathbf{x}$ contain both the spatial coordinates $\mathbf{r}$ and the spin σ of the particle. The orbital index is labeled p. A single-particle orbital χ_p depending on $\mathbf{x}$ is a spinor. The Hartree product was introduced by Douglas Hartree in 1928 [68], and is a product of spinors,

$$\Phi_{\mathrm{H}} = \chi_\alpha(\mathbf{x}_1)\,\chi_\beta(\mathbf{x}_2)\cdots\chi_\sigma(\mathbf{x}_N)\,. \tag{3.2}$$

It is an ansatz for the wave function, but a rather poor one: The wave function needs to be antisymmetric under the interchange of two particles, so as to satisfy the Pauli exclusion principle, and a product is obviously not. The antisymmetrizing issue was solved with the introduction of the Slater determinant, Φ_{SD}. It is defined like this:

$$\Phi_{\mathrm{SD}} \equiv \frac{1}{\sqrt{N!}} \begin{vmatrix} \chi_1(\mathbf{x}_1) & \chi_2(\mathbf{x}_1) & \cdots & \chi_N(\mathbf{x}_1) \\ \chi_1(\mathbf{x}_2) & \chi_2(\mathbf{x}_2) & & \chi_N(\mathbf{x}_2) \\ \vdots & & \ddots & \vdots \\ \chi_1(\mathbf{x}_N) & \chi_2(\mathbf{x}_N) & \cdots & \chi_N(\mathbf{x}_N) \end{vmatrix}. \tag{3.3}$$

The interchange of two particles is the same as interchanging two columns, thereby changing the sign of the determinant. It is inconvenient to write out the determinant in full, but it can be rewritten in terms of the antisymmetrizing operator $\hat{A}$ and the Hartree product. The antisymmetrizing operator is a summation of permutation operators, $\hat{P}$. The permutation operator simply interchanges the ordering of a given number of columns, for example like this:

$$\hat{P}_{12}\Phi(\chi_1\chi_2\chi_3\cdots\chi_N) = -\Phi(\chi_2\chi_1\chi_3\cdots\chi_N)\,. \tag{3.4}$$

It must commute with the Hamiltonian since the Hamiltonian is invariant to the permutation of particles. The antisymmetrizing operator $\hat{A}$ is therefore defined as

$$\hat{A} \equiv \frac{1}{\sqrt{N!}} \sum_p \varepsilon_p \hat{P}_p \tag{3.5}$$

[1]Basis sets will receive due attention in Section 3.1.2, FCI will be introduced in Section 3.2.

where ε_p is 1 for even numbers of pairwise interchanges and -1 for odd. This term is known as the Levi-Civita tensor. In general, $\varepsilon_{m_1 m_2 \ldots m_N} = (-1)^p \varepsilon_{12\ldots N}$, where p is the number of pairwise permutations required to sort the indices in ascending order. If any indices are equal, the term is zero[2]. The antisymmetrized wave function is necessarily antisymmetric, therefore it follows that

$$\hat{A}^2 = \hat{A}. \tag{3.6}$$

This operator allows the Slater determinant to be rewritten in terms of the Hartree product (Equation (3.2)), so that

$$\Phi_{\mathrm{SD}} = \hat{A}\phi_1(1)\phi_2(2)...\phi_N(N) = \hat{A}\Phi_{\mathrm{H}}, \tag{3.7}$$

and the energy of a Slater determinant is then written as

$$\begin{aligned} E_{\mathrm{SD}} &= \left\langle \Phi_{\mathrm{SD}} \middle| \hat{H} \middle| \Phi_{\mathrm{SD}} \right\rangle = \left\langle \hat{A}\Phi_{\mathrm{H}} \middle| \hat{H} \middle| \hat{A}\Phi_{\mathrm{H}} \right\rangle = \sum_p \varepsilon_p \left\langle \Phi_{\mathrm{H}} \middle| \hat{H} \middle| \hat{P}\Phi_{\mathrm{H}} \right\rangle \\ &= \sum_p \varepsilon_p \left\langle \Phi_{\mathrm{H}} \middle| \sum_{i=1}^{N_{\mathrm{e}}} \hat{h}_i + \sum_{i<j}^{N_{\mathrm{e}}} \hat{g}_{ij} + \hat{V}_{\mathrm{nn}} \middle| \hat{P}_p\Phi_{\mathrm{H}} \right\rangle, \end{aligned} \tag{3.8}$$

where $\hat{g}_{ij} = \frac{1}{r_{ij}}$ and the nuclear-nuclear term can immediately be set aside as a constant, since they are independent of the coordinates of the electrons. For the one-body part of the Hamiltonian[3], only the first term of $\hat{A}$ comes into play: The orbitals making up the Slater determinant are orthonormal, meaning terms like

$$\left\langle \phi_1(1)\phi_2(2) \middle| \hat{h}_1 \middle| \phi_2(1)\phi_1(2) \right\rangle = \left\langle \phi_1(1) \middle| \hat{h}_1 \middle| \phi_2(1) \right\rangle \underbrace{\langle \phi_2(2) \,|\, \phi_1(2) \rangle}_{0} \tag{3.9}$$

disappear. Therefore, only a simple sum of expectation values are left:

$$\sum_{i=1}^{N_{\mathrm{e}}} \left\langle \Phi_{\mathrm{H}} \middle| \hat{h}_i \middle| \Phi_{\mathrm{H}} \right\rangle = \sum_{i=1}^{N_{\mathrm{e}}} \left\langle \phi_i(i) \middle| \hat{h}_i \middle| \phi_i(i) \right\rangle = \sum_{i=1}^{N_{\mathrm{e}}} h_i. \tag{3.10}$$

For the twobody operator, things are slightly more complex. All permutations involving tree or more electrons will give zero contributions by similar argument, but

[2] As it should be lest the Pauli exclusion principle is violated.

[3] $\hat{h}$ was introduced in Equation (2.9).

twobody permutations allows for non-zero terms. Two distinctly different terms are possible:

$$J_{ij} = \langle \Phi_{\mathrm{H}} \,|\, \hat{g}_{ij} \,|\, \Phi_{\mathrm{H}} \rangle \quad \text{and} \quad K_{ij} = \left\langle \Phi_{\mathrm{H}} \,\middle|\, \hat{g}_{ij} \,\middle|\, \hat{P}_{ij}\Phi_{\mathrm{H}} \right\rangle . \tag{3.11}$$

The Coulomb term J_{ij} is a quantum mechanical counterpart to electrostatic repulsion, but the exchange K_{ij} has no classical analogue. The energy of a Slater determinant is then

$$E_{\mathrm{SD}} = \sum_{i=1}^{N_{\mathrm{e}}} h_i + \frac{1}{2} \sum_{ij}^{N_{\mathrm{e}}} (J_{ij} - K_{ij}) + V_{\mathrm{nn}}. \tag{3.12}$$

The gist of HF theory is to find the one Slater determinant that offers the lowest possible energy. The method is consequently variational, and

$$E_{\mathrm{HF}} = \min_{\Phi_{\mathrm{SD}}} E_{\mathrm{SD}}. \tag{3.13}$$

Differentiation of the energy expression with respect to the orbitals, subject to orthonormality constraints, yields the condition for a stationary point. The stationary point found may or may not be a minimum – it could also be a saddle point. Saddle points can be avoided, but there is no guarantee that the minimum found is the global minimum [69]. The mountain valley problem is beyond the scope of this thesis, but on a practical note, a reasonable initial guess for the orbitals tends to work well most of the time. HF theory is a robust and reliable method, and is extensively used as a starting point for more elaborate schemes.

Everything described so far has been completely general, but in practice, assumptions about spin constraints of the system are usually made. For a thorough description, consult [70]. If all spatial orbitals are required to be doubly occupied, the method is called *Restricted Hartree-Fock* (RHF). With singly occupied spin orbitals, the method is rather called *Unrestricted Hartree-Fock* (UHF). A hybrid between the two schemes, which employs doubly occupied orbitals whenever possible and singly occupied orbitals for unpaired electrons, is known as *Restricted Open-Shell Hartree-Fock* (ROHF).

3.1.2 Basis sets

The idea of the HF method is to approximate the wave function with one single Slater determinant, and so the method is necessarily variational as elaborated in

Section 3.1.1. In principle, any scheme which optimizes the wave function by minimizing the energy to reach a minimum is valid. However, mathematical validity does not imply practicality. The conventional solution is to expand the Slater determinant in a basis and vary the coefficients until a self consistent solution is found, as described below.

The Slater determinant consists of orbitals. These orbitals χ_i will now be described as a linear combination of basis functions

$$|\chi_i\rangle = \sum_{\alpha} C_{\alpha i} |\alpha\rangle \tag{3.14}$$

where the matrix $\mathbf{C}$ contains the coefficients multiplying each basis function. This description of an orbital introduces an additional approximation; unless the orbital can be perfectly described by a finite number of basis functions, an exact description is off the table.

Due to the basis set expansion, only $\mathbf{C}$ is changed during optimization. Consequently, the entire problem can be rephrased as a system of equations to be solved. These are the famous Roothaan-Hall equations:

$$\mathbf{FC} = \mathbf{SC}\epsilon. \tag{3.15}$$

The overlap matrix is represented by $\mathbf{S}$, whose elements are

$$S_{ij} = \int \chi_i^* (\mathbf{r}) \chi_j (\mathbf{r}) \; d\mathbf{r}. \tag{3.16}$$

The undetermined Lagrange multipliers are encapsulated by ϵ. The algorithm requires a set of initial coefficients from which a Fock matrix $\mathbf{F}$ is computed. Using the same notation for twoelectron integrals as in Equation (2.34), the elements of $\mathbf{F}$ become

$$f_{\mu\nu} = h_{\mu\nu} + \sum_{\rho\sigma} \sum_{i=1}^{F} C_{\rho i}^* C_{i\sigma} \left[\underbrace{\langle \mu\rho \,|\, \nu\sigma \rangle}_{E_{\text{direct}}} - \underbrace{\langle \mu\rho \,|\, \sigma\nu \rangle}_{E_{\text{exchange}}} \right]. \tag{3.17}$$

After construction, this matrix is (block) diagonalized. This provides a new ansatz for $\mathbf{C}$, and the cycle can be repeated until convergence. At convergence, ϵ are the HF orbital energies. The HF state is invariant to unitary transformations, but the canonical solution entails complete diagonalization [71].

Basis sets come in many shapes and forms. They are some kind of mathematical functions; Gaussians, exponentials, sine functions, polynomials or the like. While a

complete basis in all cases should produce the same wave function, this choice is *not* arbitrary and depends on the investigations to be undertaken. The Kato theorem states that the electron density at a nucleus acquires the form of a cusp [72, 73]. Accordingly, the basis functions should ideally produce a good cusp as well. Exponentials may seem a like natural choice for basis functions, but they require costly numerical integrals. Gaussians allow for analytical integrals, which is a huge cost saver. More Gaussians are needed to produce a good cusp than exponentials, and their long range decay may be a bit rapid, but the total evaluations are still significantly cheaper. The LONDON code is written for Gaussian type orbitals (GTOs) with a complex plane wave – the London factor.

Even when the choice of Gaussians has been made, the size and properties of the basis sets vary. Gaussian type basis sets have been tailored for more or less any property chemists have been wanting to study with varying degrees of success. Some basis sets are optimized for getting the correlation energy right, some are optimized for specific molecular properties, etc.

A strong magnetic field is a notoriously tricky customer. The gauge problem is one issue, but there is also the anisotropic deformation: The field change the shape of the orbitals in a non-trivial way, both as a function of intensity and orientation. Conventional basis sets assume a spherical symmetry of the s-orbitals, thus the same exponents are used in all Cartesian directions. This cannot handle anisotropic deformation unless d-orbitals or higher are present:

$$e^{-a\left(x^2+y^2+z^2\right)-bz^2} = e^{-ar^2}e^{-bz^2} = e^{-a\mathbf{r}^2}\left(\underbrace{1}_{\text{s}} - \underbrace{bz^2}_{\text{d}} + ...\right). \tag{3.18}$$

One way to do it is to simply go to the basis set limit. Obviously, this is not feasible, and specific anisotropic basis sets have been constructed [74, 75, 75, 76]. Anisotropic deformation is a significant cause of error in the strong-field regime, so having basis sets that can account for it is a useful improvement. This approach is unfortunately not without hurdles. The basis sets must then be optimized for the magnetic field at hand, and this is a significant challenge which adds to the overall complexity and cost. Furthermore, such optimizations may be non-trivial, and the uncertainties are difficult to measure. For atomic calculations, regular Gaussians can work quite well, however [77].

Anisotropic deformation is beyond the scope of this thesis. Therefore, rather than working with exotic basis sets that accounts for it, I have focused on the gauge problem alone: The gauge dependency also detracts from basis set convergence [60]. I have relied on conventional basis sets and let the London factor deal with the gauge problem. Thus, one of the obstacles to fast basis set convergence has been removed

and all conventional basis sets, whose behavior is well established, can be used out of the box. This is important, since experimental basis sets are often optimized only for atoms.

The deformation issue is still highly relevant for extreme fields. For moderate fields, up to a few atomic units, the deformation can be adequately handled by conventional sets of decent size. It is certainly possible to use anisotropic basis sets with a London factor as well, of course. This would be an interesting endeavor to undertake in the future.

The *correlation consistent* basis sets of Dunning and coworkers are optimized to get the correlation energy of the valence electrons correctly [78, 79, 80, 56]. This is a useful property in general, but it is especially important for dispersion effects. Unfortunately, that purpose requires *augmentations* (diffuse functions) since long-range effects are poorly described otherwise. Most of my work has relied on this family of basis sets, with the uncontracted augmented triple ζ acting as the work horse. Normally, uncontracted basis sets are avoided, as they provide extra cost and scant little benefit, but they have a certain flexibility that is otherwise unavailable: The problems introduced by anisotropic deformations from intense magnetic fields are offset a little.

Basis set notations can unfortunately be rather impenetrable when different modifications and distinctions are added to well established formalisms. Thus `cc-pVTZ` becomes `aug-cc-pCVTZ` when augmentations and core functions are added. Specifying the uncontracted set is marked by adding the prefix `u`, typically preceded by an `L` to denominate the London factor. This convention has been used throughout this thesis.

3.1.3 Basis set superposition errors

When two atoms are in close proximity, their respective basis functions will overlap. This provides a local and artificial effective increase in the size of the basis for each atom. The quality of description of the wave function therefore depends on the position of the atoms, and any variational method will predict a slightly lower energy than should be the case. In other words, the accuracy of the calculations depends on the distance between the atoms. This is known as *basis set superposition error* (BSSE). The conventional remedy is the *counterpoise correction*.

Typically, the effects of BSSE are small, and can often be ignored if the property to be investigated involve energy differences orders of magnitude larger than the BSSE. However, for subtle effects like dispersion, the quantitative influence can be proportionally quite large. In some cases, even qualitatively wrong. For example, HF

theory predicts an energy minimum for the He_2 dimer at about 8.5 bohrs distance in zero field when using the `Lu-aug-cc-pVTZ` basis set, as seen in Figure 3.1a. This gives the impression of there being a dispersion effect at work (which is true), and that HF theory correctly predicts it (which is false): Since dispersion is an effect of purely dynamical correlation, this minimum is completely spurious. For stronger fields, however, there is a paramagnetic bonding. This effect is purely caused by the kinetic energy of the system, which HF theory models very well. A bit more subtle is the fact that the energy of the paramagnetic bonding is grossly overestimated.

The counterpoise correction offers an amelioration most of the time. The atoms in a quantum chemistry calculation is actually two different things. The first is the atomic charge. The second is the basis functions, typically optimized for the atom involved. For practical calculations, these two entities share coordinates, and the descriptive labels are (somewhat imprecisely) used interchangeably. A ghost atom is the basis functions corresponding to an atom, but with no nuclear charge. Replacing all atoms but one with ghosts will create a local overlap between the basis functions, just as if the atom was surrounded by actual atoms. The wave function is then described with a similar artificial increased quality. Subtracting the energy of a free atom should then provide insight into the nature and magnitude of the BSSE.

However, there is no such thing as a free lunch, particularly when magnetic fields are involved. The counterpoise correction ameliorates the issue, but it is not an exact description. It also adds an additional computational burden. Furthermore, a molecular system is not necessarily well described by the possible fragments. Matching states is tricky and error prone, but this puzzle must also be solved in order to get the correct counterpoise correction. For excited states, this can become unmanageable. Under the influence of a magnetic field, state crossings may occur [81].

The overlap does not depend solely on the distance between the two centers, but also on their orientation to the field. Figures 3.2a and 3.2b show the BSSE for He_2 in the lowest singlet and triplet states when $|\mathbf{B}| = B_0$.[4] BSSE converges quickly to zero when the inter atomic distance increases, but the close range behavior is certainly not easily predictable. For the singlet, there is a saddle point when the molecular axis is oriented at an angle $\frac{\pi}{4}$ rad to the field. The reason for this is the anisotropic deformation of the orbitals. For example, a spherical orbital may be transformed into an oblate or prolate spheroid. In the first case, the overlap will increase perpendicularly to the field, in the latter, parallel to it. No orbitals may be deformed in a non-anisotropic manner, which is also true for the non-spherical orbitals. This could explain a slightly lower effect of BSSE at such an angle. For the

[4]These calculations are not performed at the HF level. However, the point about BSSE stands for any approach that relies on basis sets.

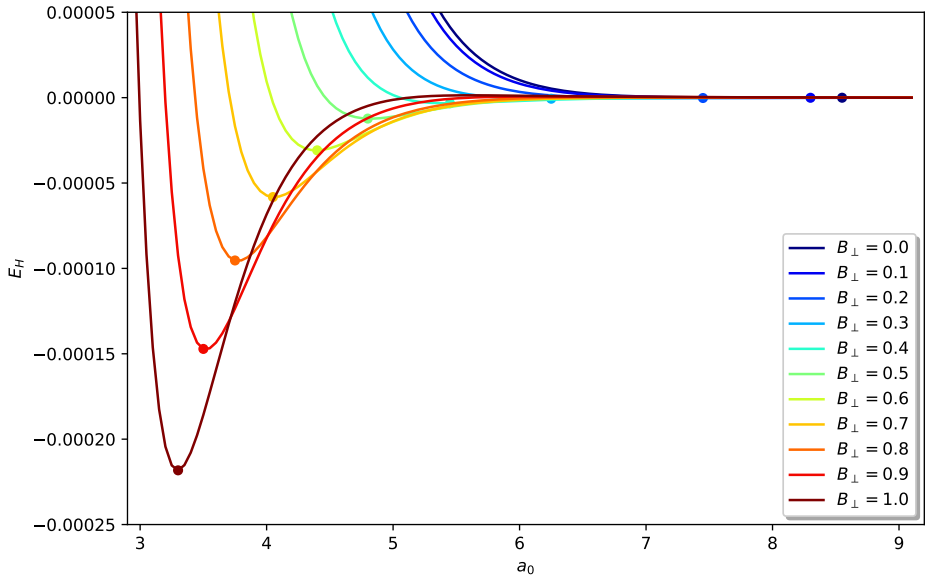

(a) *Without the counterpoise correction*

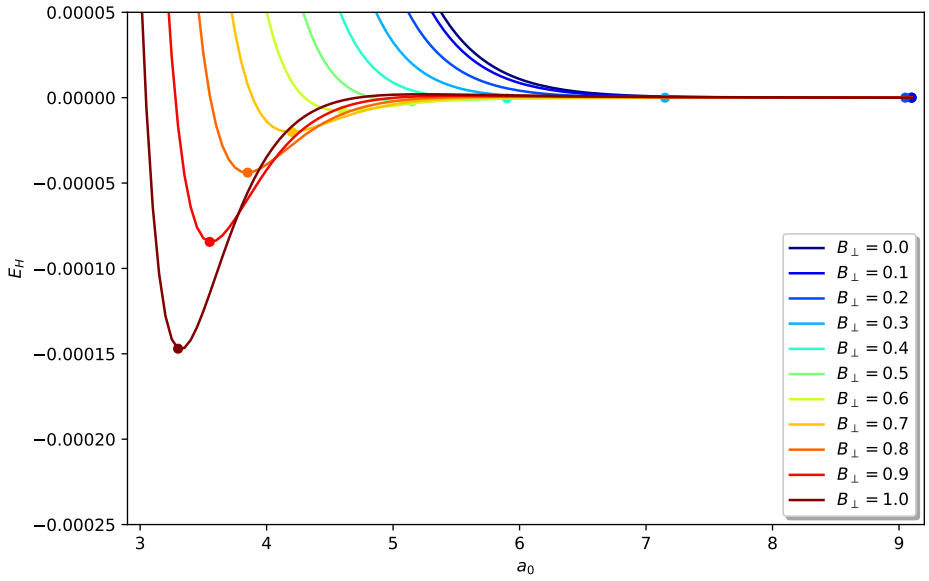

(b) *With the counterpoise correction*

Figure 3.1: *This is the HF energy for a He_2 singlet dimer in various perpendicular fields, with and without the counterpoise correction. The energy at $R = \infty$ has been subtracted. The basis set is* `Lu-aug-cc-pVTZ`.

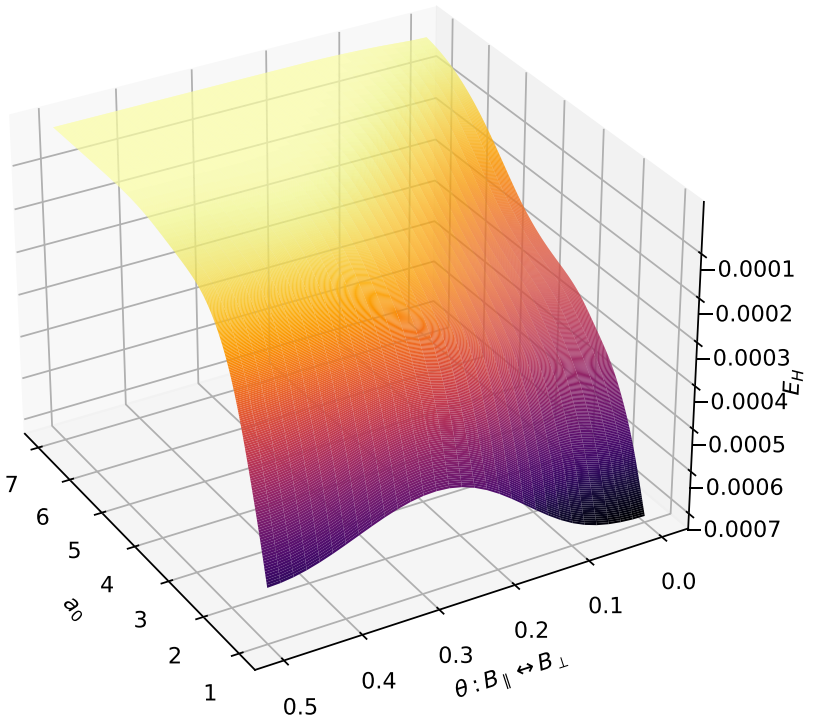

(a) *Singlet*

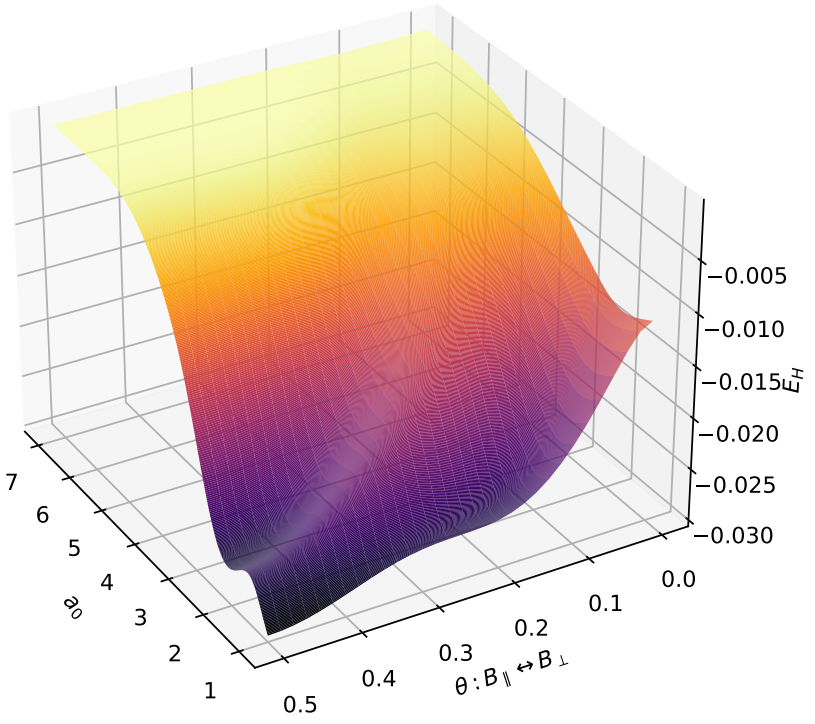

(b) *Triplet*

Figure 3.2: *This is the BSSE contribution to a helium dimer in a field of 1 a.u. magnitude, as a function of distance between the atoms and orientation to the field for the lowest singlet and triplet. The calculations are performed at the FCI/*`Lu-aug-cc-pVTZ` *theory level.*

triplet, the picture is more complex, and the magnitude of the BSSE is larger. This is a challenge, as the investigated properties can be rather subtle.

3.2 Configuration interaction theory

The full description of many-particle system requires more than one Slater determinant. CI theory is in many ways the most obvious way to improve HF theory. If a single Slater determinant is insufficient, then the wave function can be represented as a linear combination of many Slater determinants instead. The typical approach is to first define the Fermi vacuum (see Section 2.1.4), and then add all necessary new determinants, each for a particular particle-hole configuration. As mentioned in Section 3.1, when all possible configurations are included, the method is called FCI and provides the "exact solution".

While it is possible to describe all possible holes for a particular system, the number of excitations is infinite. In a finite basis, however, this is not a problem. The FCI wave function is the numerically exact wave function in a given basis.

Two terms that invariably pop up are *dynamic* and *static* correlation. From a practical perspective, they are two completely different beasts and require different solutions. A bond breaking typically entails the latter, while van der Waals interactions is a phenomenon exclusively described by the former. From a mathematical perspective, the distinction between dynamic and static correlation is a little more fuzzy. If more than one determinant is important for describing the system, so that the HF level of theory is a poor model, then the system is said to have static correlation. Informally said, if all the determinants are sorted by weight, then the first few determinants with a high weight are the cause of static correlation, and the "tail" of the expansion corresponds to dynamic correlation. There is no formal distinction and edge cases can certainly occur.

Obviously, bond breaking tend to involve degenerate determinants of great importance. If, on the other hand, the system is utterly dominated by one determinant, and all the correlation effects are caused by a (often large) number of less important determinants, the system has dynamic correlation. In this case, HF theory may be an excellent starting point, and all the dynamic effects can, perhaps, be treated perturbatively or by similar standard approaches. When determining the properties of noble gas clusters, dynamical correlation is absolutely essential. MPPT (Section 3.4.1) is an excellent tool for describing dynamic correlation, but poor for static correlation.

Since the CI expansion is a linear combination of known Slater determinants, the whole CI method takes the form of an eigenvalue problem where the unknown factors

are the amplitudes for each configuration,

$$|\Psi_{\mathrm{CI}}\rangle \equiv \left(1+\hat{C}\right)|\Phi_0\rangle \quad \text{where} \quad \hat{C} = \underbrace{\sum_{ia} c_i^a \hat{a}_a^\dagger \hat{a}_i}_{1P1H} + \frac{1}{4}\underbrace{\sum_{ijab} c_{ij}^{ab} \hat{a}_a^\dagger \hat{a}_b^\dagger \hat{a}_j \hat{a}_i}_{2P2H} + \ldots \tag{3.19}$$

The coefficients for each determinant can be found by applying the Hamiltonian to all relevant combinations of determinants systematically. Then, all these expectation values can be presented as a matrix. Diagonalization of this matrix equates to solving the Schrödinger equation. That is a monumental task, but because of the anticommutator relations (Equation (2.20)), many matrix elements are zero: The expectation value of an N-body operator applied on two determinants whose excitation level differ by more than N is necessarily zero [67]. The Hamiltonian matrix is block-banded, and the width of the band is determined by the physics. In quantum chemistry, where only one- and twobody operators are relevant, the entire matrix will look like this:

$$\begin{array}{c|ccccccc}
 & |\Phi_0\rangle & \left|\Phi_{1P}^{1H}\right\rangle & \left|\Phi_{2P}^{2H}\right\rangle & \left|\Phi_{3P}^{3H}\right\rangle & \left|\Phi_{4P}^{4H}\right\rangle & \ldots & \left|\Phi_{NP}^{NH}\right\rangle \\
\hline
\langle\Phi_0| & X & X & X & & & & \\
\left\langle\Phi_{1P}^{1H}\right| & X & X & X & X & & & \\
\left\langle\Phi_{2P}^{2H}\right| & X & X & X & X & X & & \\
\left\langle\Phi_{3P}^{3H}\right| & & X & X & X & X & & \\
\left\langle\Phi_{4P}^{4H}\right| & & & X & X & X & & \\
\vdots & & & & & & \ddots & \\
\left\langle\Phi_{NP}^{NH}\right| & & & & & & & X
\end{array} . \tag{3.20}$$

Each X represents all non-zero combinations between the determinants of different excitation level. There is only one $|\Phi_0\rangle$, but many $\left|\Phi_{2P}^{2H}\right\rangle$ etc. Such matrices are huge, and despite the sparsity, brute force diagonalization is intractable. There are iterative procedures available, and in the LONDON program, the FCI solver uses Davidson's method. See [82] for details.

Despite this, the CPU-demand of a FCI solution still scales factorially with the number of electrons in a system, making it impractical for all but minuscule molecules. When applicable, it offers easy computation of both the ground state and excited states, and an accurate description of molecular properties. The method is by necessity both size extensive, size consistent and variational. A method which behaves correctly for non-interacting systems described by a single wave function is *size consistent*. A method which scales correctly with the number of electrons in a system is *size extensive* [83]. The variational principle was given due attention in Section 2.1.2.

It is possible to truncate the problem, and thus get a polynomial scaling with number of electrons. Single excitations are called *singles* (S), double excitations *doubles* (D) and so on. If only single and double excitations are included, the method is called CISD and the formal scaling is N^6 with the number of electrons. Adding triples increase this to N^8, then N^{10} with quadruples. However, the truncated CI theory is not size consistent, and therefore largely avoided: Lack of size consistency can cause considerable errors [84, 85]. In this project, FCI has been widely used, particularly in paper II.

3.3 Coupled cluster theory

CC theory has many similarities to CI theory, but the ansatz for the wave function is different. Rather than using a simple linear combination of excitation and annihilation operators, it relies on an exponential thereof. The wave function is defined as

$$|\Psi_{\mathrm{CC}}\rangle \equiv e^{\hat{T}} |\Phi_0\rangle \tag{3.21}$$

where the cluster operator $\hat{T}$ is a sum of operators of different order

$$\hat{T} = \hat{T}_1 + \hat{T}_2 + ... + \hat{T}_N \tag{3.22}$$

whose components are

$$\hat{T}_1 = \sum_{ia} t_i^a \hat{a}_a^\dagger \hat{a}_i, \quad \frac{1}{2}\hat{T}_2 = \sum_{ijab} t_{ij}^{ab} \hat{a}_a^\dagger \hat{a}_b^\dagger \hat{a}_j \hat{a}_i, \tag{3.23}$$

and so on. The $|\Phi_0\rangle$ is usually the Hartree-Fock wave function. The exponential formulation of the wave function allows for a Taylor expansion;

$$e^{\hat{T}} = \sum_{k=0}^{\infty} \frac{1}{k!} \hat{T}^k. \tag{3.24}$$

Inserting into Equation (3.23), we get

$$e^{\hat{T}} = \hat{1} + \underbrace{\hat{T}_1}_{\text{singles}} + \underbrace{\hat{T}_2 + \frac{1}{2}\hat{T}_1^2}_{\text{doubles}} + \underbrace{\hat{T}_3 + \hat{T}_2\hat{T}_1 + \frac{1}{6}\hat{T}_1^3}_{\text{triples}} + ... \tag{3.25}$$

This wave function has great similarities to the CI wave function, but is multiplicatively separable even when truncated. Therefore, it is always size extensive.

Solving the problem involves finding the cluster amplitudes t, much as CI is about finding the coefficients c. In the the limit of all possible particle-hole excitations, FCI and CC are equivalent.

The obvious solution is to exploit the variation principle. However, if this is attempted, the method will always be exponentially scaling with system size, regardless of truncation in $\hat{T}$. The standard approach is instead similarity transformations of the Hamiltonian. The Schrödinger equation for the CC wave function becomes

$$\hat{H}e^{\hat{T}}\Phi_0 = Ee^{\hat{T}}\Phi_0, \tag{3.26}$$

and multiplying the Hamiltonian from left with the de-excitation operator $e^{-\hat{T}}$ gives

$$E_{\mathrm{CC}} = \left\langle \Phi_0 \middle| e^{-\hat{T}}\hat{H}e^{\hat{T}} \middle| \Phi_0 \right\rangle. \tag{3.27}$$

This projection gives a similarity transformed Hamiltonian which is no longer Hermitian. Therefore, projection-CC methods are not variational. Since a de-excitation of the Fermi vacuum by necessity is zero, only the first term of the Taylor expansion in Equation (3.27) is non-zero. The cluster amplitudes are found when the criteria

$$\left\langle \Phi_i^a \middle| e^{-\hat{T}}\hat{H}e^{\hat{T}} \middle| \Phi_0 \right\rangle = \left\langle \Phi_{ij}^{ab} \middle| e^{-\hat{T}}\hat{H}e^{\hat{T}} \middle| \Phi_0 \right\rangle = \left\langle \Phi_{ijk}^{abc} \middle| e^{-\hat{T}}\hat{H}e^{\hat{T}} \middle| \Phi_0 \right\rangle = ... = 0 \tag{3.28}$$

are met for all relevant excitations. The naming conventions and scaling of the different excitation levels is identical to the CI terminology. For CCSD, only the two first terms in Equation (3.28) are involved.

The highest order calculated is the most expensive. Sometimes, an approximation is used instead. When this is done perturbatively, the convention is to denominate said term inside parenthesis. CCSD with perturbative triples is therefore called CCSD(T). This is informally called the gold standard of quantum chemistry. For more information about coupled cluster theory, consult [83, 86, 87].

3.4 Many-body perturbation theory

In the widest possible interpretation, *perturbation theory* is more of a general strategy for attacking complicated problems than a specific algorithm. At its core, the idea is to take a hard problem and split it into two parts. One part should be significantly easier to handle, while still resembling the original problem as much as possible. The

other part – in effect the difference between the exact and the simplified problem – is treated as a *perturbation*. This perturbation is restated as an infinite power series. In the case of quantum chemistry, this would then be something like

$$E_{\text{exact}} = \underbrace{E^{(0)}}_{\text{unperturbed}} + \underbrace{\lambda E^{(1)} + \frac{1}{2}\lambda^2 E^{(2)} + ...}_{\text{perturbations}} \tag{3.29}$$

This summation is infinite and must be truncated at some point. Higher order perturbations are generally more complex to evaluate, but also less relevant to the total sum. Perturbation theory offers an arbitrarily improvable solution to complex problems. There are several possible schemes for actually splitting the problem. The most common approach in quantum chemistry is *Møller-Plesset perturbation theory* (MBPT), which is a specific application of *Rayleigh-Schrödinger perturbation theory* (RSPT). However, there are other relevant schemes as well, such as *Brillouin-Wigner perturbation theory* (BWPT) [88]. Mathematically, these schemes have many similarities, but only RSPT will be described in-depth here. The special case of MBPT to second order will receive extra attention.

The Hamiltonian is split into two parts,

$$\hat{H} = \hat{H}_0 + \hat{H}_I \tag{3.30}$$

where $\hat{H}_0$ and $\hat{H}_I$ are the unperturbed and perturbed parts, respectively. If we only care about the time-independent ground state energy and assume that the wave function can be expanded in terms of Slater determinants, we get

$$|\Psi\rangle = |\Phi_0\rangle + \sum_{n=1}^{\infty} C_n |\Phi_n\rangle \tag{3.31}$$

where intermediate normalization has been applied. Intermediate normalization means that $\langle \Psi \,|\, \Phi_0 \rangle = 1$, rather than the usual normalization where $\langle \Psi \,|\, \Psi \rangle = 1$. The unperturbed part of the wave function and Hamiltonian gives

$$\hat{H}_0 |\Phi_0\rangle = E_0 |\Phi_0\rangle \,. \tag{3.32}$$

Because of the intermediate normalization, we get

$$\langle \Phi_k \,|\, \Psi \rangle = \sum_{n=1}^{\infty} \langle \Phi_k \,|\, \Phi_n \rangle \, C_n = \sum_{n=0}^{\infty} \delta_{kn} C_n = C_k. \tag{3.33}$$

This allows us to sort out the different energy components from the Schrödinger equation:

$$\hat{H}\left|\Psi\right\rangle = \left(\hat{H}_0 + \hat{H}_I\right)\left|\Psi\right\rangle = E\left|\Psi\right\rangle \tag{3.34}$$

$$E = \left\langle \Phi_0 \middle| \hat{H} \middle| \Psi \right\rangle \tag{3.35}$$

$$E_0 = \left\langle \Phi_0 \middle| \hat{H}_0 \middle| \Psi \right\rangle \tag{3.36}$$

$$E - E_0 = \left\langle \Phi_0 \middle| \hat{H}_I \middle| \Psi \right\rangle = E_I. \tag{3.37}$$

Next, we consider an expansion of the perturbation energy:

$$E_I = \sum_{n=1}^{\infty} E^{(n)}. \tag{3.38}$$

Introducing the resolution of identities, we obtain

$$\hat{P} \equiv \left|\Phi_0\right\rangle\left\langle\Phi_0\right| \quad \text{and} \quad \hat{Q} \equiv \sum_{n=1}^{\infty} \left|\Phi_n\right\rangle\left\langle\Phi_n\right|, \tag{3.39}$$

where

$$\left|\Psi\right\rangle = \left(\hat{P} + \hat{Q}\right)\left|\Psi\right\rangle. \tag{3.40}$$

Introducing a free parameter γ in equation (3.34), we get

$$\left(\hat{H}_0 + \hat{H}_I - \gamma\right)\left|\Psi\right\rangle = (E - \gamma)\left|\Psi\right\rangle. \tag{3.41}$$

After rearranging the terms, the expression becomes

$$\left(\gamma - \hat{H}_0\right)\left|\Psi\right\rangle = \left(\gamma - E + \hat{H}_I\right)\left|\Psi\right\rangle. \tag{3.42}$$

Next, projection by $\hat{Q}$ yields

$$\hat{Q}\left|\Psi\right\rangle = \frac{\hat{Q}}{\gamma - \hat{H}_0}\left(\gamma - E + \hat{H}_I\right)\left|\Psi\right\rangle \tag{3.43}$$

so that[5]

$$|\Psi\rangle = |\Phi_0\rangle + \frac{\hat{Q}}{\gamma - \hat{H}_0}\left(\gamma - E + \hat{H}_I\right)|\Psi\rangle\,. \tag{3.44}$$

Iterating the above equation, the perturbative expansion for the wave function becomes

$$|\Psi\rangle = \sum_{n=0}^{\infty}\left(\frac{\hat{Q}}{\gamma - \hat{H}_0}\left(\gamma - E + \hat{H}_I\right)\right)^n |\Phi_0\rangle\,. \tag{3.45}$$

So far, this is an exact result. This summation can now be used to define the expansion of E_I. Replacing γ with the exact total energy E, we get

$$E_I = \sum_{n=0}^{\infty}\left\langle \Phi_0 \left| \hat{H}_I \left(\frac{\hat{Q}}{E - \hat{H}_0}\hat{H}_I\right)^n \right| \Phi_0 \right\rangle = \left\langle \Phi_0 \left| \hat{H}_I + \hat{H}_I\frac{\hat{Q}}{E - \hat{H}_0}\hat{H}_I + ... \right| \Phi_0 \right\rangle. \tag{3.46}$$

The summation above can be truncated at any level. If a reasonable estimate for E is available, then the system can be solved self-consistently. This is the essence of BWPT. Unfortunately, this solution is not size extensive. In RSPT, γ is set to be E_0 instead (Equation (3.36)). Equation (3.46) now becomes

$$E_I = \sum_{n=0}^{\infty}\left\langle \Phi_0 \left| \hat{H}_I \left(\frac{\hat{Q}}{E_0 - \hat{H}_0}\left(\hat{H}_I - E_I\right)\right)^n \right| \Phi_0 \right\rangle. \tag{3.47}$$

Exploiting once more the fact that $\hat{Q}$ and $\hat{H}_0$ commute, the energy contribution in orders of perturbations becomes

$$E^{(0)} = E_0 \tag{3.48}$$

$$E^{(1)} = \left\langle \Phi_0 \left| \hat{H}_I \right| \Phi_0 \right\rangle \tag{3.49}$$

$$E^{(2)} = \left\langle \Phi_0 \left| \hat{H}_I \frac{\hat{Q}}{E_0 - \hat{H}_0}\hat{H}_I \right| \Phi_0 \right\rangle \tag{3.50}$$

Beyond this point, the expressions become rapidly less tractable, but the mechanism for deriving them is the same. For this project, only second order corrections has been relevant.

[5]The juggling of operators performed in Equation (3.43) is permitted, since $\hat{Q}$ and $\hat{H}_0$ commute.

3.4.1 Second order Møller-Plesset Theory

So far, the choice of $\hat{H}_0$ has been omitted. By defining $\hat{H}_0$ to be the Fock operator $\hat{F}$ so that $\hat{H} = \hat{F} + \hat{H}_I$, we get *Møller Plesset Perturbation Theory* (MPPT), which is a variant of RSPT. The order at which the perturbation series is truncated is usually denoted with a number, so second order MPPT is usually just called MP2 [86].

In a basis of UHF orbitals, the Fock operator can now be rewritten as

$$F_{pq}^{\sigma} = h_{pq}^{\sigma} + \frac{1}{2}\sum_{j,\tau} \langle p_\sigma j_\tau \,||\, q_\sigma j_\tau \rangle \,, \tag{3.51}$$

where

$$\langle p_\sigma j_\tau \,||\, q_\sigma j_\tau \rangle = \langle p_\sigma j_\tau \,|\, q_\sigma j_\tau \rangle - \langle p_\sigma j_\tau \,|\, j_\tau q_\sigma \rangle \tag{3.52}$$

is a common shorthand for antisymmetrized twoelectron integrals.

The Hamiltonian and the Fock operator can be reformulated in terms of creation and annihilation operators;

$$\hat{H} = \sum_{pq\sigma} h_{pq}^{\sigma} \hat{a}_{p\sigma}^{\dagger} \hat{a}_{q\tau} + \frac{1}{2} \sum_{pq\sigma, rs\tau} g_{pqrs}^{\sigma\tau} \hat{a}_{p\sigma}^{\dagger} \hat{a}_{r\tau}^{\dagger} \hat{a}_{s\tau} \hat{a}_{q\sigma} \tag{3.53}$$

and

$$\hat{F} = \sum_{pq\sigma} F_{pq}^{\sigma} \hat{a}_{p\sigma}^{\dagger} \hat{a}_{q\tau} = \sum_{pq\sigma} \left[h_{pq}^{\sigma} + \frac{1}{2} \sum_{j} g_{pqjj}^{\sigma\uparrow} n_{j\uparrow} + g_{pqjj}^{\sigma\downarrow} n_{j\downarrow} + g_{pqjj}^{\sigma\sigma} n_{j\sigma} \right] \hat{a}_{p\sigma}^{\dagger} \hat{a}_{q\tau} \tag{3.54}$$

where $n_{p\sigma}$ is the occupation number of orbital p with spin σ. $\hat{H}_I$ is the difference between these two operators. If a HF wave function is already available, then

$$E^{(0)} = \left\langle \Phi_{\mathrm{HF}} \middle| \hat{F} \middle| \Phi_{\mathrm{HF}} \right\rangle = \sum_{p\sigma} n_{p\sigma} \epsilon_p \tag{3.55}$$

and

$$E_{\mathrm{HF}} = E^{(0)} + E^{(1)}. \tag{3.56}$$

Hence, the zeroth order term is just a summation of orbital energies and the first order correction provides the HF energy. The second order perturbation is therefore the first interesting term. This is the MP2 contribution:

$$E_{\mathrm{MP2}} = E_{\mathrm{HF}} + E^{(2)}. \tag{3.57}$$

In the following deductions, the capital indices $A, B, C...$ denote spin-orbital numbers. The expression for the general MP2 contribution is then

$$E^{(2)} = -\frac{1}{4}\sum_{IJAB}\frac{|\langle IJ\,||\,AB\rangle|^2}{\epsilon_{IJ}^{AB}}, \tag{3.58}$$

where $\epsilon_{IJ}^{AB} = \epsilon_A + \epsilon_B - \epsilon_I - \epsilon_J$. Writing out all the components of this expression is cumbersome, but a few symmetries can be exploited to reduce the unwieldiness somewhat:

$$\sum_{IJAB}|\langle IJ\,|\,AB\rangle|^2 = \sum_{IJAB}|\langle IJ\,|\,BA\rangle|^2 \tag{3.59}$$

and

$$\sum_{IJAB}\langle IJ\,|\,AB\rangle^*\langle IJ\,|\,BA\rangle = \sum_{IJAB}\langle IJ\,|\,AB\rangle\langle IJ\,|\,BA\rangle^*. \tag{3.60}$$

So far, all possible combinations of spin and orbital occupation number has been included, even nonphysical terms like $\left\langle i^\uparrow j^\uparrow \,\middle|\, a^\uparrow b^\downarrow\right\rangle$. Mathematically, this is perfectly legitimate. Assuming UHF restrictions and accounting for spin, it can be deduced that

$$\begin{aligned} E_{UHF}^{(2)} &= \sum_{i_\sigma<j_\tau, a_\sigma<b_\tau}\frac{|\langle ij\,|\,ab\rangle^{\sigma\tau} - \delta_{\sigma\tau}\langle ij\,|\,ba\rangle^{\sigma\sigma}|^2}{\epsilon_{ij}^{ab}} \\ &= \sum_{ijab}\frac{\left|\langle ij\,|\,ab\rangle^{\uparrow\downarrow} - 0\right|^2}{\epsilon_{ij}^{ab}} + \sum_\sigma\sum_{i<j,a<b}\frac{|\langle ij\,|\,ab\rangle^{\sigma\sigma} - \langle ij\,|\,ba\rangle^{\sigma\sigma}|^2}{\epsilon_{ij}^{ab}}. \end{aligned} \tag{3.61}$$

In the RHF case, this becomes

$$E_{RHF}^{(2)} = \sum_{ijab}\frac{\langle ij\,|\,ab\rangle^*\left[2\langle ij\,|\,ab\rangle - \langle ij\,|\,ba\rangle\right]}{\epsilon_{ij}^{ab}}. \tag{3.62}$$

3.4.2 The MP2 density matrix

For any manyparticle wave function, there exists a one-electron reduced density matrix D:

$$D(\mathbf{x}_1, \mathbf{x}_1') = N\int \Psi^\dagger(\mathbf{x}_1\mathbf{x}_2...\mathbf{x}_n)\,\Psi(\mathbf{x}_1'\mathbf{x}_2...\mathbf{x}_n)\;d\mathbf{x}_2 d\mathbf{x}_3...d\mathbf{x}_n. \tag{3.63}$$

Once this density matrix is computed, any expectation value described by a singleparticle operator $\hat{\Omega}$ can easily be evaluated. This is done by tracing it with the density matrix:

$$\langle \Omega \rangle = \mathrm{tr}\left(D\Omega\right). \tag{3.64}$$

Also, if the density matrix is diagonalized, then natural orbitals and occupation numbers are readily available.

The approach for computing the relaxed density matrices in LONDON are largely inspired by Frisch, Head-Gordon and Pople's approach [89], and restricted to the RHF reference.

It is most practical to look at the different blocks of the density matrix individually. The occupied-occupied and virtual-virtual blocks are straight-forward, and may be computed in parallel with the energy contribution at a slight computational cost. The occupied-occupied and virtual-virtual blocks are

$$P_{ij} = -2\sum_{abk} \frac{\langle ik \,|\, ab\rangle \left[2\,\langle jk \,|\, ab\rangle - \langle jk \,|\, ba\rangle\right]^*}{\epsilon_{ik}^{ab}\epsilon_{jk}^{ab}} \tag{3.65}$$

and

$$P_{ab} = \quad 2\sum_{ijc} \frac{\langle ij \,|\, ac\rangle \left[2\,\langle ij \,|\, bc\rangle - \langle ij \,|\, cb\rangle\right]^*}{\epsilon_{ij}^{ac}\epsilon_{ij}^{bc}}, \tag{3.66}$$

respectively. For the off-diagonal blocks, we first need the MP2 Lagrangian [90],

$$\begin{aligned} L_{ia} = 4\sum_{jb}\left[\sum_{k} \frac{\langle kj \,|\, ib\rangle \left[2\,\langle jk \,|\, ba\rangle - \langle jk \,|\, ab\rangle\right]^*}{\epsilon_{jk}^{ab}} - \sum_{c} \frac{\langle ja \,|\, bc\rangle \left[2\,\langle ij \,|\, cb\rangle - \langle ij \,|\, bc\rangle\right]^*}{\epsilon_{ij}^{bc}}\right] \\ -2\sum_{ik} P_{jk}\left(2\,\langle kc \,|\, ji\rangle - \langle kc \,|\, ij\rangle\right) - 2\sum_{ac} P_{bc}\left(2\,\langle ca \,|\, bk\rangle - \langle ca \,|\, kb\rangle\right) \end{aligned} \tag{3.67}$$

which allows the occupied-virtual block to be obtained by iterative solution of the coupled perturbed HF equations

$$L'_{ia} = 2\sum_{bj}\left[2\,\langle ib \,|\, aj\rangle - \langle ib \,|\, ja\rangle\right] L_{jb} - \left[2\,\langle ij \,|\, ab\rangle - \langle ij \,|\, ba\rangle\right] L^*_{jb} + 2\epsilon_i^a L_{ia}. \tag{3.68}$$

The density matrix is necessarily Hermitian, so the virtual-occupied block is obtained for free.

3.5 Density Functional Theory

Density Functional Theory (DFT) is the quintessential work horse of everyday quantum chemistry [91]. At a theoretical level, it relies on a radically different approach than wave-function theories. At an implementation and computational level, however, it is startlingly similar to HF theory: It is an pseudo-eigenvalue problem which is solved self-consistently. The scaling is similar, and so are the techniques for parallelization. From a user perspective, DFT has a somewhat capricious reputation; it may offer results which compete with high-accuracy wave-function methods at a tiny fraction of the cost, but it is considerably more difficult to predict when and where it will fail. Error cancellation is often large [92, 93], and proper usage of DFT requires solid understanding of both the problem at hand and the available approximate functionals – of which a plethora exists.

3.5.1 The variational principle

The N-electron Hamiltonian of Equation (2.6) can be restated in terms of an external potential v as

$$\hat{H}\left[v\right] = \hat{T} + \hat{W} + \hat{V}_{\text{ext}}\left[v\right], \tag{3.69}$$

where

$$\hat{V}_{\text{ext}}\left[v\right] = \sum_{i} v\left(\mathbf{r}_i\right) = \sum_{i}\sum_{J} \frac{Z_J}{|\mathbf{r}_J - \mathbf{r}_i|}. \tag{3.70}$$

The wave function Ψ is, as usual, a normalizable N-electron wave-function. In other words, $\Psi \in W_N$ where

$$W_N = \left\{ \Psi \;\middle|\; \langle \Psi \,|\, \Psi \rangle = 1,\ \hat{N}\Psi = N,\ \hat{P}_{ij}\Psi = -\Psi \ \ \forall\, i < j \leq N \right\}. \tag{3.71}$$

The whole idea of having an external potential at all assumes the validity of the Born-Oppenheimer approximation.

3.5.2 The constrained search approach

The Hohenberg-Kohn (HK) formalism has had a tremendous importance for the development of DFT, but has largely been superseded by the more general constrained search formalism. More information about the HK formalism can be found in reference [94].

In the coming deductions, all wave functions of interest belong to the set W_N of Equation (3.71). From any such valid wave function, a density can be constructed as an integral over the spin coordinates σ_i of all particles, and the spatial coordinates $\mathbf{r}_j$ of all particles but one:

$$\rho(\mathbf{r}_1) = \int |\Psi(\mathbf{r}_1, \sigma_1, \mathbf{r}_2, \sigma_2, ...\mathbf{r}_N, \sigma_N)|^2 \ \mathrm{d}\sigma_1 \mathrm{d}\mathbf{r}_2 \mathrm{d}\sigma_2 ... \mathrm{d}\mathbf{r}_N \mathrm{d}\sigma_N. \tag{3.72}$$

The integral of the density over all space is necessarily the number of particles:

$$\int \rho(\mathbf{r}) \ \mathrm{d}\mathbf{r} = N. \tag{3.73}$$

The density ρ is a function of only three spatial coordinates, whereas the wave function depends on $3N$. This point is *the* reason why DFT is so important; the "curse of dimentionality" can be dispelled without sacrificing generality – at least in theory.

With the above considerations and the Hamiltonian of Equation (3.69), the Rayleigh-Ritz variational principle now becomes

$$E[v] = \inf_{\Psi \in W_n} \left\langle \Psi \left| \hat{H}[v] \right| \Psi \right\rangle. \tag{3.74}$$

Putting it all together, we get

$$E[v] = \inf_{\Psi \in W_n} \left\langle \Psi \left| \hat{T} + \hat{W} + \hat{V}_{\mathrm{ext}}[v] \right| \Psi \right\rangle = \inf_{\rho \in I_N} \inf_{\Psi \mapsto \rho} \left\langle \Psi \left| \hat{T} + \hat{W} + \hat{V}_{\mathrm{ext}}[v] \right| \Psi \right\rangle \tag{3.75}$$

where $I_N = \{\rho_\Psi \,|\, \Psi \in W_N\}$ is the set of N-representable densities. An equivalent definition can be shown to be

$$I_N = \left\{ \rho \,\middle|\, \rho \geq 0, \ N = \int \rho(\mathbf{r}) \ \mathrm{d}\mathbf{r}, \ T_W(\rho) < \infty \right\}, \tag{3.76}$$

where

$$T_W[\rho] = \frac{1}{8} \int \frac{|\nabla \rho(\mathbf{r})|^2}{\rho(\mathbf{r})} \ \mathrm{d}\mathbf{r} \tag{3.77}$$

is the von Weizsäcker kinetic energy. That is, the densities of interest are non-negative, they integrate to N and their von Weizsäcker kinetic energy is finite.

For all densities $\rho \in I_N$, the Levy-Lieb (LL) constrained search functional is

$$F_{\mathrm{LL}}[\rho] = \min_{\Psi \mapsto \rho} \left\langle \Psi \left| \hat{T} + \hat{W} \right| \Psi \right\rangle, \tag{3.78}$$

where standard rewriting of the integrals

$$(v \,|\, \rho) \equiv \int v(\mathbf{r})\, \rho(\mathbf{r})\ \mathrm{d}\mathbf{r}. \tag{3.79}$$

has been used. The minimizing restriction labeled $\Psi \mapsto \rho$ simply means we only investigate wave functions that recreate the density of choice, and that minimizer *always* exists. Now, the variational principle becomes

$$E[v] = \inf_{\rho \in I_N} \left(F_{\mathrm{LL}}[\rho] + (v \,|\, \rho) \right). \tag{3.80}$$

This rewriting of the variational principle is the *constrained search* formalism. The external potential depends on the density alone, while the kinetic energy and the contribution from the electron-electron interactions are disentangled from the expression.

The LL constrained search functional of Equation (3.78) is said to be *universal*. This means it is independent of the external potential v. The LL functional was studied by Percus [95], Levy [96], and from a mathematical perspective by Lieb [97].

3.5.3 The Lieb variational principle

In order to conjure up the expression for the Lieb variational principle, we first need to justify that $E[v]$ is concave. Assuming a real number $\lambda \in [0, 1]$, then

$$E[\lambda v_1 + (1-\lambda) v_2] \geq \lambda E[\lambda v_1] + (1-\lambda) E[v_2]. \tag{3.81}$$

This can be demonstrated from Equation (3.80);

$$\begin{aligned} E[\lambda v_1 + (1-\lambda) v_2] &= \inf_{\Psi} \left\langle \Psi \left| \hat{H}[\lambda v_1 + (1-\lambda) v_2] \right| \Psi \right\rangle \\ &= \inf_{\Psi} \left\langle \Psi \left| \lambda \hat{H}[v_1] + (1-\lambda) \hat{H}[v_2] \right| \Psi \right\rangle \\ &\geq \lambda \inf_{\Psi} \left\langle \Psi \left| \hat{H}[v_1] \right| \Psi \right\rangle + (1-\lambda) \inf_{\Psi} \left\langle \Psi \left| \hat{H}[v_2] \right| \Psi \right\rangle, \end{aligned} \tag{3.82}$$

from which Equation (3.81) trivially follows. This results relies on the linearity of the Hamiltonian in v.

Since $E[v]$ can also be shown to be continuous, there exists a convex dual functional $F[\rho]$ so that the two variational principles can be restated in terms of each other:

$$E[v] = \inf_{\rho} \left(F[\rho] + (v \,|\, \rho) \right), \tag{3.83}$$

$$F[\rho] = \sup_{v} \left(E[v] - (v \,|\, \rho) \right). \tag{3.84}$$

Equation (3.83) is the *Lieb variational principle* [98][6]. Hohenberg and Kohn derived the eponymous *Hohenberg-Kohn functional* of Equation (3.84), and their original paper from 1964 provides the proof of universality [94].

These two variational principles are related by Legendre-Fenchel transforms and therefore said to be conjugate functionals. The nitty-gritty details of convex analysis can be pursued in reference [99].

3.5.4 The adiabatic connection

The *adiabatic connection* (AC) allows the physical system with correct electron interactions to be smoothly connected to the non-interacting Kohn-Sham system [100, 101]. This may seem like a detour, but since there are great practical similarities between the two cases, the consequences are important.

First, we introduce an interaction strength parameter $\lambda \in [0, 1]$ to the constrained search functional of Equation (3.78):

$$F[\rho] = \min_{\Psi \mapsto \rho} \left\langle \Psi_\lambda \middle| \hat{T} + \lambda \hat{W} \middle| \Psi_\lambda \right\rangle = \left\langle \Psi_\lambda^\rho \middle| \hat{T} + \lambda \hat{W} \middle| \Psi_\lambda^\rho \right\rangle \tag{3.85}$$

The last equality is necessarily true, since the minimizer is proven to exist [96, 98]. The parameter λ allows the effect of the electron-electron interactions to be smoothly varied from a non-interacting system to the fully interacting physical system of the previous sections. We shall also need the λ-derivatives of Equation (3.85), which is

$$\frac{\partial F[\rho]}{\partial \lambda} = \left\langle \Psi_\lambda^\rho \middle| \hat{W} \middle| \Psi_\lambda^\rho \right\rangle \tag{3.86}$$

due to the Hellman-Feynman theorem.

[6] Equation (3.83) greatly resembles Equation (3.80), but that variational principle is constructed on the Levy-Lieb functional, F_{LL}. The two are sometimes identical.

For the next step, a bit of mathematical prestidigitation is required. By juggling with the definition of the now λ-dependent universal functional, we get

$$\begin{aligned} F[\rho] &= F_0[\rho] + F_1[\rho] - F_0[\rho] = F_0[\rho] + \int_0^1 \frac{\partial F[\rho]}{\partial \lambda}\, \mathrm{d}\lambda \\ &= \left\langle \Psi_0^\rho \middle| \hat{T} \middle| \Psi_0^\rho \right\rangle + \int_0^1 \left\langle \Psi_\lambda^\rho \middle| \hat{W} \middle| \Psi_\lambda^\rho \right\rangle \mathrm{d}\lambda \\ &= \left\langle \Psi_0^\rho \middle| \hat{T} \middle| \Psi_0^\rho \right\rangle + \left\langle \Psi_0^\rho \middle| \hat{W} \middle| \Psi_0^\rho \right\rangle + \int_0^1 \left(\left\langle \Psi_\lambda^\rho \middle| \hat{W} \middle| \Psi_\lambda^\rho \right\rangle - \left\langle \Psi_0^\rho \middle| \hat{W} \middle| \Psi_0^\rho \right\rangle \mathrm{d}\lambda \right), \end{aligned} \tag{3.87}$$

which allows the expression to be separated into different components. Now, it is time to label all these separate terms and describe their physical meaning. We have the *non-interacting kinetic energy*;

$$T_\mathrm{s}[\rho] = \left\langle \Psi_0^\rho \middle| \hat{T} \middle| \Psi_0^\rho \right\rangle, \tag{3.88}$$

the *Hartree term*;

$$J[\rho] = \int \rho(\mathbf{r}_1)\, \rho(\mathbf{r}_2)\, \frac{1}{r_{12}}\, \mathrm{d}\mathbf{r}_1 \mathrm{d}\mathbf{r}_2, \tag{3.89}$$

the *exchange energy*;

$$E_\mathrm{x}[\rho] = \left\langle \Psi_0^\rho \middle| \hat{W} \middle| \Psi_0^\rho \right\rangle - J[\rho], \tag{3.90}$$

and the *correlation energy*;

$$E_\mathrm{c}[\rho] = \int_0^1 \left(\left\langle \Psi_\lambda^\rho \middle| \hat{W} \middle| \Psi_\lambda^\rho \right\rangle - \left\langle \Psi_0^\rho \middle| \hat{W} \middle| \Psi_0^\rho \right\rangle \mathrm{d}\lambda \right). \tag{3.91}$$

These last two terms are frequently added together and called the *exchange-correlation energy*;

$$E_\mathrm{xc}[\rho] = E_\mathrm{x}[\rho] + E_\mathrm{c}[\rho]. \tag{3.92}$$

Finally, all of this can be put back together so that

$$F[\rho] = T_\mathrm{s}[\rho] + J[\rho] + E_\mathrm{xc}[\rho]. \tag{3.93}$$

The above are the so called *Kohn-Sham* (KS) components, and the flexibility they offer make them crucial for approximations to the universal functional. The energy can be written in these terms:

$$E[v] = \inf_{\rho} \left(F[\rho] + (v \,|\, \rho) \right) = \inf_{\rho} \left(T_{\mathrm{s}}[\rho] + (v \,|\, \rho) + J[\rho] + E_{\mathrm{xc}}[\rho] \right). \tag{3.94}$$

The KS components serve different purposes as well: In the first paper, we used such component wise splitting to study the influence of magnetic fields on the potentials. Having all these components allows more of the picture to be investigated than the energy alone. More details about KS DFT will be discussed in Section 3.5.5.

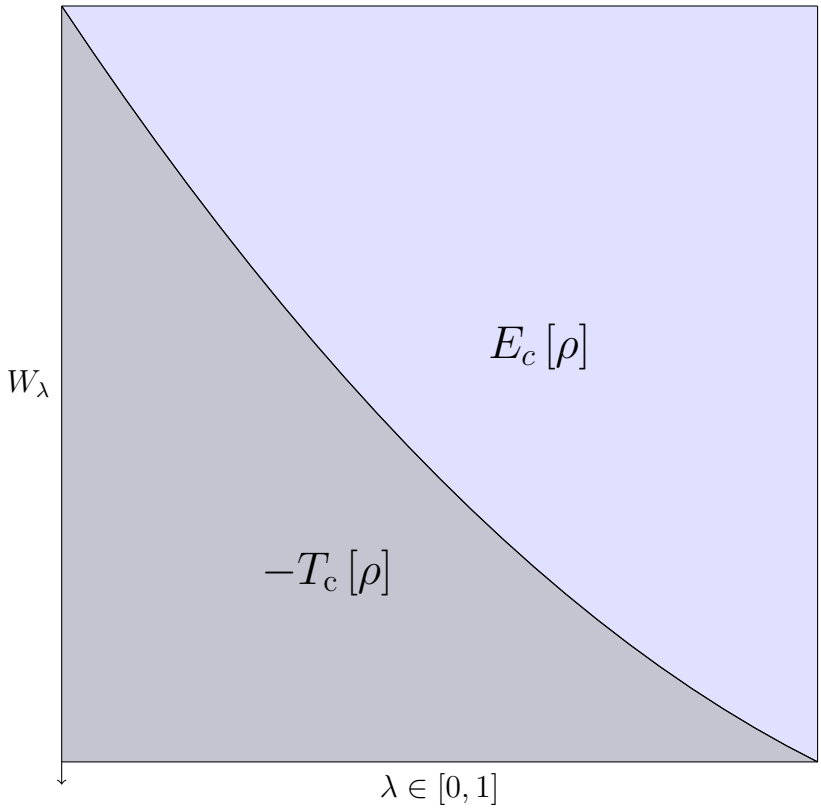

Figure 3.3: *Example of an AC curve.*

The density provides the total energy, but the kinetic energy alone is somewhat less tangible. However, it may be defined by means an adiabatic connection curve, as seen in Figure 3.3. An AC curve is simply a plot of W as a function of λ. In the resulting graph, $T_{\mathrm{c}}[\rho]$ is the negative of the area underneath the graph and delimited

by the rectangle of the extremes. This component is also the difference between the actual and the non-interacting kinetic energy:

$$T_\mathrm{c}\left[\rho\right] = T\left[\rho\right] - T_\mathrm{s}\left[\rho\right]. \tag{3.95}$$

The corresponding area above the curve in Figure 3.3 is the correlation energy.

Another useful property of the AC curve is the curvature itself, which reveals the amount of static correlation in a system: A nearly straight line indicates little to no static correlation, whereas a highly convex curve reveals a strong multi reference character of the system to be studied.

3.5.5 Kohn-Sham DFT

The Kohn-Sham ansatz states that the wave function may here be described with a single Slater determinant. Consequently,

$$F_0\left[\rho\right] = \inf_{\Phi\mapsto\rho} \left\langle \Phi \middle| \hat{T} \middle| \Phi \right\rangle = \left\langle \Phi_\mathrm{KS} \middle| \hat{T} \middle| \Phi_\mathrm{KS} \right\rangle = T_\mathrm{s}\left[\rho\right]. \tag{3.96}$$

This is useful, since it is hard to calculate T_s directly from the density. In other words, only T_c needs to be estimated from the density. Since T_s is a good approximation to T, T_c is rather modest in magnitude.

The entire and fully interacting energy expression may now be rewritten as

$$E_1\left[v\right] = \inf_{\Phi} \left[\left\langle \Phi \middle| \hat{T} \middle| \Phi \right\rangle + J\left[\rho_\Phi\right] + E_\mathrm{xc}\left[\rho_\Phi\right] + \left(v \,|\, \rho_\Phi\right) \right] \tag{3.97}$$

which can be differentiated by the route of Lagrangian multipliers and a basis set expansion. At this point, this greatly resembles the final form of the HF problem in Equation (3.17) and is similarly solved self consistently.

In Equation (3.97), we are back to optimizing over an ansatz for the wave function. In a manner of speaking, the Kohn-Sham energy is a result of a reversed application of the constrained search formalism of the previous sections.

3.5.6 The exact functional from wave-function methods

Knowing that a universal functional exists is one thing, but finding it is quite another. The idea behind the Lieb scheme is to produce an approximation to the density of a wave-function like quality, as per Equation (3.78). Unfortunately, enforcing $\Psi \mapsto \rho$ is infeasible. However, by using the Lieb variational principle and an approximation to the external potential in a basis, the problem can be handled – albeit still at a high

computational cost. This must be emphasized: In order to get the exact solution to the many-particle Schrödinger equation, a costly FCI calculation is required. In order to get the exact DFT functional as described in the previous sections, *several* FCI calculations are necessary.

The potential needs to be parametrized for an optimization procedure to work. The parametrization used is

$$v\left(\mathbf{r}\right) = v_{\text{ext}}\left(\mathbf{r}\right) + \left(1-\lambda\right) v_{\text{ref}}\left(\mathbf{r}\right) + \sum_{\alpha} C_{\alpha}\Omega_{\alpha}\left(\mathbf{r}\right) \tag{3.98}$$

where the last term is an expansion in Gaussians and the reference potential $v_{\text{ref}}\left(\mathbf{r}\right)$ is the Fermi-Amaldi potential

$$v_{\text{ref}}\left(\mathbf{r}\right) = \left(1 - \frac{1}{N}\right) \int \frac{\rho\left(\mathbf{r}'\right)}{\left|\mathbf{r}' - \mathbf{r}\right|}\, \mathrm{d}\mathbf{r}, \tag{3.99}$$

which provides the correct asymptotic behavior. The energy from a wave-function method is used en lieu the exact energy $E\left[v\right]$, while the parametrization of the potential v reduces the problem to an optimization over the coefficients C_{α}. This approach was formulated by Wu and Yang in 2003 [102].

The wave-function based functional F^{Ψ} can be evaluated as

$$F_{\lambda}^{\Psi}\left[\rho_{\text{ref}}\right] \approx \sup_{\mathbf{C}} \left(E_{\lambda}^{\Psi}\left[v\left(\mathbf{C}\right)\right] - \left(v\left(\mathbf{C}\right) \mid \rho\right)\right) \tag{3.100}$$

where E^{Ψ} is the energy from some wave-function method. This scheme requires the wave-function method to produce a relaxed density matrix, so that the Lieb functionals and gradients may be evaluated. The Lieb gradient is given by

$$G_{\alpha}^{\text{L}} = \frac{\partial E\left[v\right]}{\partial C_{\alpha}}, \tag{3.101}$$

and if the basis set expansion from Equation (3.98) is inserted for the potential and the energy expression from Equation (3.83) for the energy, then

$$\begin{aligned}
\frac{\delta E\left[v\right]}{\delta C_{\alpha}} &= \frac{\delta E_{\lambda}^{\Psi}\left[v\left(\mathbf{C}\right)\right]}{\delta C_{\alpha}} - \frac{\partial}{\partial C_{\alpha}}\left(v\left(\mathbf{C}\right) \mid \rho^{\text{ref}}\right) \\
&= \frac{\delta E_{\lambda}^{\Psi}\left[v\right]}{\delta v}\frac{\partial v\left(\mathbf{C}\right)}{\partial C_{\alpha}} - \left(\Omega_{\alpha} \mid \rho^{\text{ref}}\right) \\
&= \left(\Omega_{\alpha} \mid \rho^{\Psi}\right) - \left(\Omega_{\alpha} \mid \rho^{\text{ref}}\right) = \left(\Omega_{\alpha} \mid \rho^{\Psi} - \rho^{\text{ref}}\right).
\end{aligned} \tag{3.102}$$

The Lieb gradient is zero when the reference potential has been recreated.

Solving Equation (3.100) is obviously expensive, especially when the wave-function method is FCI, but it allows various approximations, such as $F_{\lambda}^{\text{B3LYP}}$ or F_{λ}^{LDA} to be compared "apples to apples" with the wave-function methods.

3.5.7 Magnetic formalisms

The magnetic field, however, has so far not been introduced, and classical DFT does not include it at all. Consequently, DFT is an exact theory only when $\mathbf{B} = 0$. If a field is to be introduced, then the theory must be expanded to accommodate it. This can be achieved in several ways, but only two formalisms will be mentioned here.

One is the BDFT formalism, which was suggested by Grayce and Harris [103, 104]. It is a handy generalization of the DFT methodology. The Hamiltonian and the variational principles in this case becomes

$$\hat{H}_\lambda [v; \mathbf{A}] = T [\mathbf{A}] + \lambda W + V_{\text{ext}}, \tag{3.103}$$

$$\begin{aligned} F_\lambda [\rho; \mathbf{A}] &= \inf_{\Psi \mapsto \rho} \left\langle \Psi \middle| \hat{H}_\lambda [0; v] \middle| \Psi \right\rangle \\ &= \sup_v \left(E [v, \mathbf{A}] - (\rho \,|\, v) \right), \end{aligned} \tag{3.104}$$

$$E [v, \mathbf{A}] = \inf_\rho \left(F_\lambda [\rho; \mathbf{A}] + (\rho \,|\, v) \right), \tag{3.105}$$

where the kinetic energy operator has been written in terms of $\hat{\boldsymbol{\pi}}$,

$$\hat{T} [\mathbf{A}] = \frac{1}{2} \sum_{j=1}^{N} \left(-\mathrm{i} \nabla_j + \mathbf{A} (\mathbf{r}_j) \right)^2, \tag{3.106}$$

as usual. In this case, F_λ depends parametrically on $\mathbf{A}$. It is therefore a *semi-universal* functional – loosely speaking, this means there is one DFT for each magnetic vector potential [105].

The other is *current density functional theory* (CDFT), which relies on a potential $u \equiv v + \frac{1}{2} A^2$ and the Hamiltonian then becomes

$$\hat{H}'_\lambda [u, \mathbf{A}] = \hat{H}'_\lambda [u] - \frac{\mathrm{i}}{2} \sum_j \left(\mathbf{A} \cdot \nabla_j + \nabla_j \cdot \mathbf{A} \right). \tag{3.107}$$

This simplifies to

$$\hat{H}'_\lambda [u, \mathbf{A}] = \hat{H}'_\lambda [u] - \mathrm{i} \sum_j \mathbf{A} \cdot \nabla_j, \tag{3.108}$$

if $\mathbf{A}$ is solenoidal, but CDFT makes no such assumptions. The potential u allows the variational principles from Equations (3.83) and (3.84) to be generalized into

$$E_\lambda [u, \mathbf{A}] = \inf_{\rho, \mathbf{j_p}} \left(F_\lambda [\rho, j_p] + (\rho \,|\, u) + (j_p \,|\, \mathbf{A}) \right) \tag{3.109}$$

and

$$F_\lambda\left[\rho, \mathbf{j_p}\right] = \sup_{u,\mathbf{A}} \left(E_\lambda\left[u, \mathbf{A}\right] - \left(u \,|\, \rho\right) + \left(j_p \,|\, \mathbf{A}\right)\right), \tag{3.110}$$

respectively. The term $\mathbf{j_p}$ is the paramagnetic current density. This is formalism is not directly related to my work, but it is one of the key actors in the magnetic DFT approaches [106, 107]. When the field is set to zero, both BDFT and CDFT become standard, field-free DFT [108, 109].

3.5.8 Approximate functionals

So far, we have seen that even in the presence of a magnetic field, there must be a semi-universal functional whose existence ensures that BDFT is an exact description of the manybody ground state. We have also seen that this functional is hard to obtain and describe.

DFT is a practical theory because of the approximate functionals. There are many, and they belong to different classes of approximations. The most intuitive approach is the *local density approximation* (LDA). Here, the exchange-correlation energy depends only on the density:

$$E_{\mathrm{XC}}^{\mathrm{LDA}}\left[\rho\right] = \int f_{\mathrm{XC}}\left(\rho\left(\mathbf{r}\right)\right) \, \mathrm{d}\mathbf{r}. \tag{3.111}$$

Then there is the *generalized gradient approximation* (GGA), which depends on both the density and the gradient

$$E_{\mathrm{XC}}^{\mathrm{GGA}}\left[\rho\right] = \int f_{\mathrm{XC}}\left(\rho\left(\mathbf{r}\right), \nabla\rho\left(\mathbf{r}\right)\right) \, \mathrm{d}\mathbf{r}, \tag{3.112}$$

and *hybrid functionals*, which is a linear combination of the Hartree-Fock exact exchange functional from Equation (3.11) and and various additional density functionals for correlation and exchange [7] usually empirically weighted, or specifically chosen for some distinct computational purpose. Finally, there are the meta-GGAs, which depends on either the Laplacian, the kinetic energy density (τ), or both. A general, field-free meta-GGA may therefore look like this:

$$E_{\mathrm{XC}}^{\mathrm{mGGA}}\left[\rho\right] = \int f_{\mathrm{XC}}\left(\rho\left(\mathbf{r}\right), \nabla\rho\left(\mathbf{r}\right), \nabla^2\rho\left(\mathbf{r}\right), \tau\left(\mathbf{r}\right)\right) \, \mathrm{d}\mathbf{r}. \tag{3.113}$$

[7] These additions to the hybrid functionals can be both LDAs or GGAs.

To complicate matters a bit, there are several possible choices of kinetic energy density. The physical kinetic energy density is

$$\tau_{\text{phys}}(\mathbf{r}) = \frac{1}{2}\sum_{l} \left|\hat{\boldsymbol{\pi}}\phi_l(\mathbf{r})\right|^2, \tag{3.114}$$

while the Dobson kinetic energy density is

$$\tau_{\text{D}}(\mathbf{r}) = \frac{1}{2}\sum_{l} \left|\hat{\mathbf{p}}\phi_l(\mathbf{r})\right|^2 - \frac{j_p(\mathbf{r})^2}{2\rho(\mathbf{r})}. \tag{3.115}$$

As a practical example, the *TPSS*-functional (Tao, Perdew, Staroverov and Scuseria) is a meta-GGA employing both the Laplacian and the kinetic energy density [110]. Of the latter, both variants may be used, and are considered flavors of the same functional – with the τ_{phys}, the functional is sometimes called aTPSS and cTPSS with τ_{D}.

Then, there is the field – the BDFT formalism includes it, but the approximations for the functionals do not. The standard, heuristic approach, is to simply use the standard DFT functionals anyway. An important note must be made at this point: There *are* "magnetic functionals" as such. For example, the Keal-Tozer functionals (KT1 and KT2) are GGAs specifically developed for computing magnetic properties such as NMR shielding constants [111]. They are fitted to experimental data and will usually provide excellent predictions of magnetic properties, but not necessarily anything else. However, the KT-family do not explicitly include the magnetic field; they are not on the form $F[\rho, \mathbf{B}]$.

In Paper I, we thoroughly investigated how the common approximations held up against the exact functional component wise.

There has been dedicated much work into better understanding the nature of the universal functional, and the quest for better approximations is neverending. This also goes for the different formalisms of DFT itself.

Part II

Results, discussion and conclusion

Chapter 4

The papers

The three papers that constitute the scientific work of the thesis all relate to the usage of wave-function methods in magnetic fields in order to solve vastly different problems. London orbitals, as discussed in Chapter 2, are used throughout.

The first paper explores the BDFT formalism. The energy and magnetic components were calculated with various approximate functionals, and with functionals of wave-function quality provided by the Lieb optimization. These were all compared against a reference, which was CCSD for small molecules and MP2 for larger molecules. Thus, wave-function methods were used to explore and calibrate a formalism of DFT where the magnetic field is explicitly included. In the second paper, molecular properties and the electronic structure of helium dimers in strong magnetic fields of arbitrary orientation was thoroughly mapped out. The behavior of fermionic matter in such intense fields has been a point of interest for a long time [112]. The final paper is of a more practical nature: The magnetic properties of water in strong magnetic fields – strong in the vernacular sense, not in the astrophysical sense! – has been disputed for decades [113, 12]. Some researchers have found "odd behavior" for the molecule, and some studies report nothing unexpected. We investigated the matter by means of MP2 theory and London orbitals, since this approach has not yet been attempted by anyone else.

4.1 Paper I

The importance of DFT for the entire field of quantum chemistry can hardly be exaggerated. Most of the time, results of adequate quality for the investigations undertaken can be produced for a fraction of the cost demanded by wave-function methods. However, as discussed at length in Section 3.5, DFT does not have the

ab initio status of wave-function methods. A universal density functional has been proven to exist, and while algorithms for producing it are available, these are prohibitively expensive. Also, none of this allows the universal functional to be spelled out in a comprehensive manner: It is not possible to "find it once" and thereafter produce a nifty expression that will see general application. Therefore, all practical approaches of DFT rely on approximate functionals whose physical justifications may be somewhat heuristic. With magnetic fields, this is more problematic than usual.

As elaborated in Section 3.5.7, the BDFT and CDFT formalisms are generalizations of DFT which includes the magnetic field – either directly (BDFT) or as a vorticity (CDFT). A major issue of practical importance is to determine how large the dependencies of the exchange-correlation energy are to either the field or the vorticity. This is an ongoing issue in the development of magnetic DFT formalisms.

As with the previous B- and CDFT studies by Reimann *et al.* [105, 114], the wave-function methods of the London program were used to generate a density to be reproduced. By decomposing the energy into Kohn-Sham (KS) components, a meaningful analysis of the magnetic properties of the functionals can be made. The motivation for doing it this way, rather than just straight comparison of energy, is rather subtle: A nonsensical result may falsify a claim about reliability or robustness, but what a about a seemingly *correct* result? Good results can be produced by fortunate error cancellation[1] or similarly unpredictable circumstances. This may be fine if this behavior is well known and understood, so that the usage of the method can be restricted to "safe systems". However, when investigating new formalisms or less known physics, it is important to know if the result is correct because the method is sound, or if it is a happy fluke. Producing the right answer for the wrong reasons may therefore be just as bad, or worse, than simply getting random garbage. The KS decomposition provides several distinct components, each of which can be compared with different methods. Getting all these terms right is substantially harder than getting a reasonable value for the energy alone. There are two reasons for this. The first is that the total energy of a molecular system does not change much as the magnetic field increases from 0 to 0.03 atomic units. The other reason is that the errors scale differently with the Lieb optimization error: The error of the total energy is quadratic, while the KS components are linear. Securing adequate numerical precision was hard.

Magnetizabilities can be computed accurately with wave-function methods, and are also experimentally available. As such, the quality and reliability of a calculation can be determined with high confidence. As introduced in Equation (2.15), the

[1] Disturbingly often, two wrongs do indeed make a right.

magnetizabilities are

$$\chi_{\alpha\beta} = -\frac{\partial^2 E(\mathbf{B})}{\partial B_\alpha \partial B_\beta}\bigg|_{\mathbf{B}=0} \tag{4.1}$$

and this property is often hard to accurately compute at the DFT level. Furthermore, for a closed shell system, the total energy is

$$E(\mathbf{B}) = E(\mathbf{0}) - \frac{1}{2}\mathbf{B}^\dagger \chi \mathbf{B} + O\left(\mathbf{B}^4\right). \tag{4.2}$$

As long as the higher order hyper magnetizabilities are small, the magnetizability contains all the magnetic field-dependence. Magnetizabilities were therefore useful properties to compare against: Good numbers are available, it is hard to reproduce them at the DFT level, and they signify that the magnetic interactions are accurately depicted. For magnetic behavior around zero field, the quality of the magnetizabilities are an excellent measure of the overall correctness of the results.

4.1.1 Background and related work

Given that no conventional GGA or hybrid functionals have an explicit dependence on either the field or the vorticity[2], it is important to clarify whether or not this is an important source of error for calculations of molecular magnetic properties.

A CDFT study by Reimann *et al.* [114] investigated the vorticity dependence of nuclear shielding constants by means of Lieb optimization, and found that vorticity corrections could be as large as 10ppm for some nuclei. It was also found that while the KT2 functional outperformed all other functionals at reproducing NMR shielding constants, it did so for the wrong reason: The error in diamagnetic term was an order of magnitude larger than for the other functionals. It was also found that TPSS was the best functional in terms of "being right for the right reasons", and that classical MP2 theory at the response level produced better NMR shielding constants than all functionals except KT2. This study of the vorticity dependence in a CDFT setting could also be interpreted as a study of magnetic field dependence in a BDFT setting, even though the BDFT and CDFT settings are different – the BDFT KS system reproduces only the density, while the CDFT KS system reproduces both the density and the paramagnetic current density $\mathbf{j}_p$. This connection was highlighted in a BDFT study of a similar vein (also by Reimann and collaborators) where they investigated some small molecules and atoms [105]. All systems had four electrons

[2]The VRG family of functionals has an explicit vorticity dependence, but these functionals are not yet considered useful for molecular calculations [115, 116]

or less, allowing for comparison with FCI results. The close relationship between BDFT and CDFT was discussed in more detail in Section 3.5.7. This latter study concentrated on the Kohn-Sham decomposition of molecules like H_2 in zero or weak fields. It was found that the correlation energy was mostly unaffected by the field, except for the beryllium atom.

4.1.2 The specifics of this study

In this paper, we continue the exploration of the BDFT formalism by means of Lieb theory, as discussed in Section 3.5.6. This is a larger and more exhaustive investigation of KS components than the previous studies. Lieb gradients at the MP2 level are now available, and larger molecules with more electrons can be investigated – which we were keen to do. Aromatic systems, for example, have interesting electronic structures, but must necessarily include a fair amount of electrons.

The magnetic field dependence of these components was determined by means of polynomial interpolation, and compared with different approximate functionals and wave-function methods. The fields investigated in this paper were up to 0.03 atomic units, similar to the two aforementioned studies. Reference magnetizabilities were produced at the CCSD(T) level. We investigated closed shell molecules of three different classes: diamagnetic, paramagnetic and aromatic. The previous studies revolved around small, diamagnetic molecules alone.

Remarkably, for small diamagnetic systems, the exchange energy is virtually constant as a function of magnetic field. For larger diamagnetic systems and for paramagnetic systems, the exchange energy does vary with magnetic field. For atoms, this is expected, since angular momentum is quantized: The wave function cannot change continuously, and remains constant with respect to field until a level cross occurs. For the single orbital systems, the explanation lies in the fact that the density constraint also fixates the exchange energy. For the remaining two systems – LiH and H_2O – the explanation is perhaps that symmetries prevent orbital mixing, so that the density constraint is somewhat restrictive.

The common, approximate functionals all behaved qualitatively well, especially for the diamagnetic molecules. The electronic structure of these molecules does not change much in the presence of an external field, and consequently all approximate functionals produced reasonable numbers – even functionals which ignores completely the field-dependence of the exchange-correlation energy. The TPSS functionals performed well for the KS decomposition, matching the accuracy of CCSD. We used two variants of this functional; aTPSS (based on the physical kinetic energy density τ_{phys}) and cTPSS (based on Dobsons energy density τ_{D}). Both variants were

comparable to CCSD. For the aromatic molecules, the only available wave-function methods were HF and MP2, and the latter was selected to be the reference. These molecules behaved much like the other diamagnetic molecules, and we found no reason to assume that magnetic properties of aromatic molecules are harder to predict in the BDFT regime than non-aromatic diamagnetic molecules.

In the paramagnetic case, the exchange-correlation energy changes with the field. Therefore, the conventional hybrid functionals performed less well, but this also holds true for the wave-function methods. However, no methods misidentified paramagnetic systems as diamagnetic or vice versa. The cTPSS functional considerably out-performed all other functionals and wave-function methods, but the exact reason for this remains elusive. From Table 2 and Figure 3 in the article, it is clear that the best overall performance is that of CCSD theory and the cTPSS functional, whereas LDA gives the poorest performance. The good performance of the cTPSS functional is striking: It is the only method that gives similar errors for the dia- and paramagnetic molecules. All other methods produce errors that are one or two orders of magnitude larger for the latter category of molecules. CCSD was slightly better than aTPSS, but both variants TPSS out-performed MP2.

Simply put, paramagnetic molecules are tricky customers, but conventional DFT functionals and wave-function methods all produced qualitatively correct results for these molecules as well.

4.1.3 Discussion and future research

The study was performed with zero-field geometries held fixed. That is, we investigated $F_{\mathrm{XC}}[\rho_{\mathbf{0}}, \mathbf{B}]$ en lieu of $F_{\mathrm{XC}}[\rho_{\mathbf{B}}, \mathbf{B}]$. The maximum field strengths employed were 0.03 atomic units, which is far too weak to perceptibly alter the molecular geometries. Furthermore, the density is prescribed as input to the optimization on the right-hand side of Equation (3.104), and the resulting optimal potential v must cancel out the external diamagnetic term if this would otherwise prevent ρ from being reproduced. Holding the geometry fixed is therefore a valid approach.

All in all, the results were encouraging, and it seems like approximate functionals are surprisingly reliable even when magnetic fields are present. Meta-GGAs, and especially the TPSS variants, are particularly promising. Unfortunately, the BDFT formalism appears to be at an impasse: It works qualitatively well, but the approximate functionals are not tailored for magnetic fields. With or without magnetic fields, reproducing the density is a notoriously difficult endeavor. An amelioration of this issue seems critical for further progress with the field-dependencies. How this should be undertaken is as of yet an open question.

4.2 Paper II

Molecules in strong magnetic fields have seen considerable attention over the years, but most work has been limited to extremely small and symmetric systems, such as atoms [117, 118, 119, 120, 121], single electron ions [122, 123, 124, 125] or linear, homoatomic molecules in a perfectly parallel field [126, 127, 128, 129, 130, 131, 132]. This is for the reasons explained in Chapter 2.2. The study of matter in strong magnetic fields is not limited to chemistry; the subject has been of interest within the domains of both semi-conductor physics and astronomy as well [112, 133].

On an overarching level, there are three regimes where different approaches of theoretical physics are valid. Low field is anything where the Coulomb forces are much stronger than magnetic interactions, and entails that $B \ll B_0$. In this regime, the effect of the magnetic field is frequently treated with response theory. However, that approach quickly becomes inadequate as the field strength increases [55, 42, 134, 135].

The strong field regime ($B \gg B_0$) is also called the Landau regime because a free article with mass m and charge Z has energies are quantized into Landau levels [29]:

$$E = \left(n_L + \frac{1}{2}\right)\hbar\omega_c \qquad\qquad n_L = 0, 1, 2... \tag{4.3}$$

where the cyclotron frequency ω_c is given by

$$\omega_c = \frac{|Z|\,B}{mc}. \tag{4.4}$$

In this regime, electrostatic repulsion and attraction are but minor perturbations to the magnetic interactions of matter, and the atoms acquire the shape of tiny needles. Fields of this intensity are found on neutron stars, particularly on magnetars. Chemistry in such extreme physical environments is alien to us [136, 137, 138].

When $|\mathbf{B}| \approx B_0$, the electrostatic and magnetic interactions are of the same order of magnitude and interesting varieties of conventional chemistry may occur. Helium clusters are one such example: Noble gas atoms do not normally bond, but this becomes possible under the influence of strong magnetic fields. The triplet state of the He_2 dimer is well known to be bonding, but the energy of this triplet state normally lies far above that of two free singlet atoms. In strong fields, however, the lowest triplet state (and the quintet, for that matter) will eventually fall below the singlet. While these fields are only attainable in the vicinity of exceedingly hot stellar objects, this does not mean that the molecules cannot form: It should be emphasized that at least the nonmagnetic H_2 molecule has been observed on white

dwarfs [139], and rather complex molecules are readily available on the Sun and other stellar entities [140]. The temperatures on the surface of various stars may be large, but so is the pressure!

The purpose of this study was to further explore the chemical bond and the electronic structure of the He_2 dimer in magnetic fields. Specifically, we wanted to clarify the role of spin and angular momentum. There has been a distinct lack of studies where the orientation of the magnetic field is not parallel to the molecular axis. The phenomenon called paramagnetic perpendicular bonding is a recent discovery, and there is still much to be clarified. Our study is more comprehensive and larger than previous works.

This paper has both theoretical and computational results. The theoretical result is a novel way of dealing with orbital angular momentum in the presence of an arbitrarily oriented magnetic field. The practical results revolves around spin states and molecular bonds of helium dimers.

4.2.1 Angular momentum: Quantized and otherwise

When tracking the development of electronic states as a function of field intensity and orientation, it is useful to sort the states by various quantum numbers. Spin and angular momenta are the two obvious choices. In the presence of a magnetic field, angular momentum becomes more problematic.

The *canonical* and *physical orbital angular momenta* around a gauge origin $\mathbf{O}$ are

$$\mathbf{L_O} = (\mathbf{r} - \mathbf{O}) \times \mathbf{p} \tag{4.5}$$

and

$$\mathbf{K_O} = (\mathbf{r} - \mathbf{O}) \times \boldsymbol{\pi} \tag{4.6}$$

respectively. The commutation relations for canonical angular momentum are simply

$$\left[\hat{L}_j, \hat{L}_k\right] = \mathrm{i} \sum_l \varepsilon_{jkl} \hat{L}_l \tag{4.7}$$

where ε_{jkl} is the Levi-Civita term as introduced in Section 3.1.1. The indices refer to Cartesian coordinates. These commutation relations allow for the construction of ladder operators,

$$\hat{L}_\pm \equiv \hat{L}_x \pm \mathrm{i}\hat{L}_y. \tag{4.8}$$

Inserting this into Equation (4.7), we get

$$\left[\hat{L}_+, \hat{L}_-\right] = 2\hat{L}_z \quad \text{and} \quad \left[\hat{L}_z, \hat{L}_\pm\right] = \pm\hat{L}_\pm. \tag{4.9}$$

Applied on an eigenstate ψ_m, they yield

$$\hat{L}_z \left|\psi_m\right\rangle = m \left|\psi_m\right\rangle \quad \text{and} \quad \hat{L}_z\hat{L}_\pm \left|\psi_m\right\rangle = (m \pm 1) \left|\psi_m\right\rangle, \tag{4.10}$$

meaning that the eigenvalues are quantized. With the physical angular momentum, these relations are less straightforward and give rise to convoluted and field-dependent commutation relations. Furthermore, the same wave function may give a different value for the physical angular momentum due to changes in the magnetic vector potential. The physical angular momentum is usually not quantized.

In order to be a good quantum number, quantization alone is insufficient: The operator in question must also commute with the Hamiltonian and all other operators used for classification of the quantum states. For atoms, all Cartesian components of $\hat{L}$ commute with $\hat{H}$. However, as seen in Equation (4.7), the Cartesian components of $\hat{L}$ do not commute with each other – there can only be one. By convention, $\hat{L}^2$ and $\hat{L}_z$ are used for classification of atomic states.

The expectation value of $\hat{L}_z$ is preserved for cylindrically symmetric systems oriented in the z direction because local symmetries and conservation laws are inextricably linked by Noether's theorem [141]. Since the orientation of a Cartesian grid can be arbitrarily chosen, $\hat{L}_z$ is a good quantum number for all linear molecules – in the absence of a magnetic field, that is. As discussed at length in Section 2.3, a magnetic field introduces a field-dependent anisotropy, and the molecule will cease to be cylindrical symmetric unless the molecular axis is parallel to the field. Atoms, being highly symmetric, always have a quantized $\hat{L}_z$.

Obviously, it is interesting to categorize quantum states for all possible orientations to the field. While exact discretization is beneficial, a reasonable approximation to a quantum number is still useful for this endeavor, and so one might be tempted to use the angular momentum as it is. Unfortunately, it exhibits a non-physical, gauge dependent quadratic divergence with the atomic distance. A novel tool for circumnavigating this bothersome issue is introduced in this paper: *Almost Quantized Angular Momentum* (AQAM). For linear, homonuclear molecules with the gauge origin $\mathbf{G}$ placed at the electronic center of mass $\mathbf{C}$, AQAM is defined as

$$\mathbf{\Lambda} = \sum_\alpha \left(\mathbf{L}_{\mathbf{C},\alpha} - \frac{1}{2} N_\alpha \left(\mathbf{C}_\alpha - \mathbf{C}\right) \times \left[\mathbf{B} \times \left(\mathbf{C} - \mathbf{C}_\alpha\right)\right] \right) \tag{4.11}$$

where N_α is the number of electrons of atom α and $\mathbf{C}_\alpha$ is the position of nucleus α. Note that in the following special cases, the second term disappears and $\mathbf{\Lambda}$ becomes exactly identical to $\mathbf{L}_z$:

1. when $\mathbf{B} = \mathbf{0}$,
2. when the system has exactly one atom, since that makes $\mathbf{C}_\alpha$ and $\mathbf{C}$ equal, and
3. when a linear molecule is parallel to the field since the cross product of parallel vectors disappears.

AQAM becomes a sum of atomic angular momenta when applicable, and is exactly quantized whenever $\hat{L}_z$ is. From a practical perspective, we are simply splitting a molecule into non-interacting atoms and subtracting their angular momenta from the overall results.

AQAM is an important theoretical contribution to our understanding of angular momentum. It also turned out to be a remarkably useful tool for modeling the evolution of molecular quantum states as a function of changes in geometry and orientation relative to the field.

For more details about the mathematical foundations upon which AQAM has been constructed, consult [142]. For more information about angular momentum in general, see [143].

4.2.2 Computational results

The electronic structure of the He_2 molecule was thoroughly described at the FCI level in magnetic fields. We developed AQAM and showed that molecular states can be separated, even when classical orbital angular momentum diverges with the field. The ground state for different spin configurations was investigated as a function of inter-atomic distance and orientation relative to the field. The electronic configuration for different fields of the molecule in the dissociation and united atom limits was clarified. Also, the field dependent behavior of basis set superposition errors was explained in detail.

Figure 4.1 shows the complexity of the field dependent FCI states of several closely related systems: the helium atom, the beryllium atom and the helium dimer in the united atom limit[3].

[3]The standard notation for atomic states has been used in Figure 4.1. This is not strictly applicable to molecules, but for the lack of a better alternative, this simple solution was elected. It is adequate for my purposes. The states found, their energy and ordering when the field is zero are in excellent agreement with the literature for the beryllium atom [144].

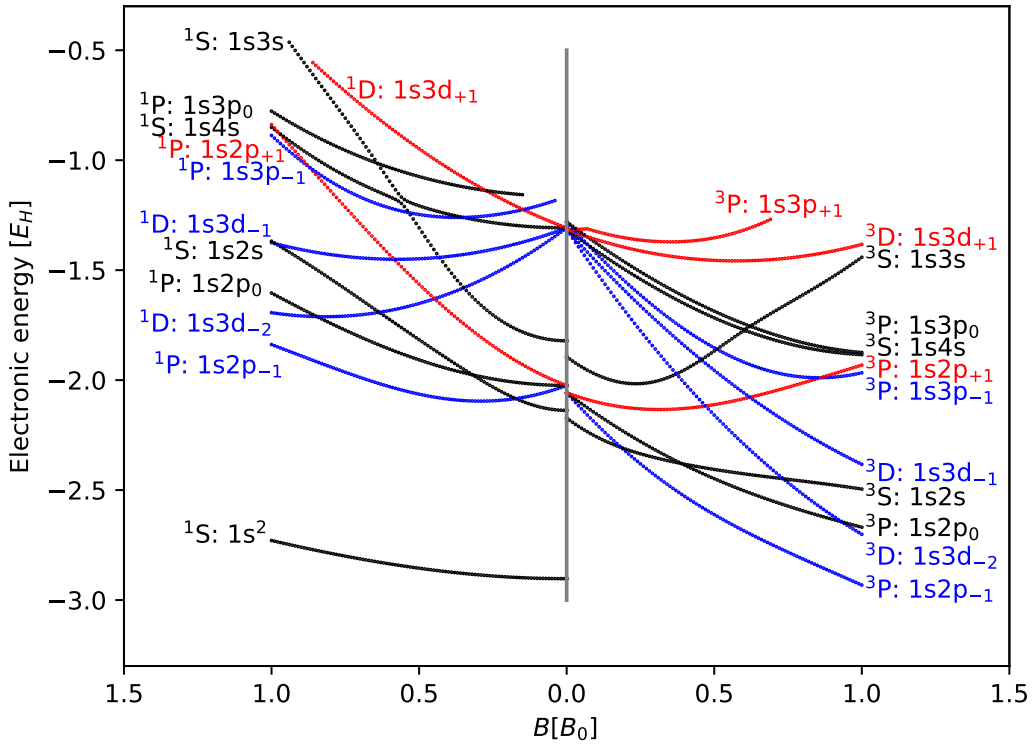

(a) *A single helium atom (`Lu-aug-cc-pVQZ`)*

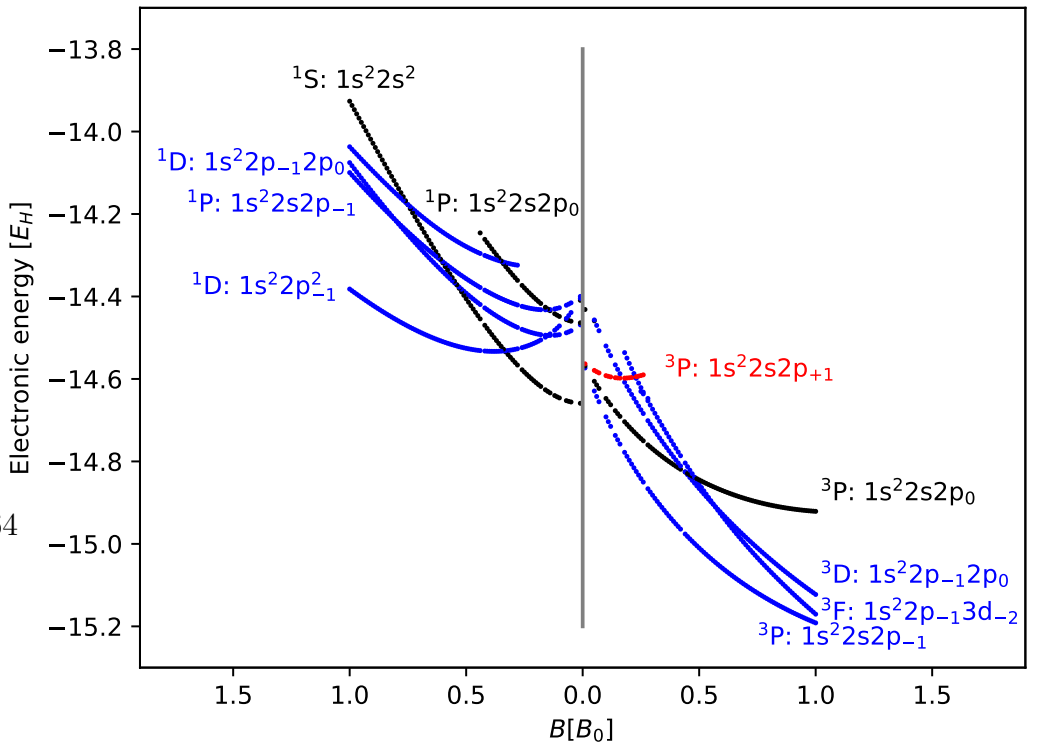

(b) *A single beryllium atom (`Lu-aug-cc-pVDZ`)*

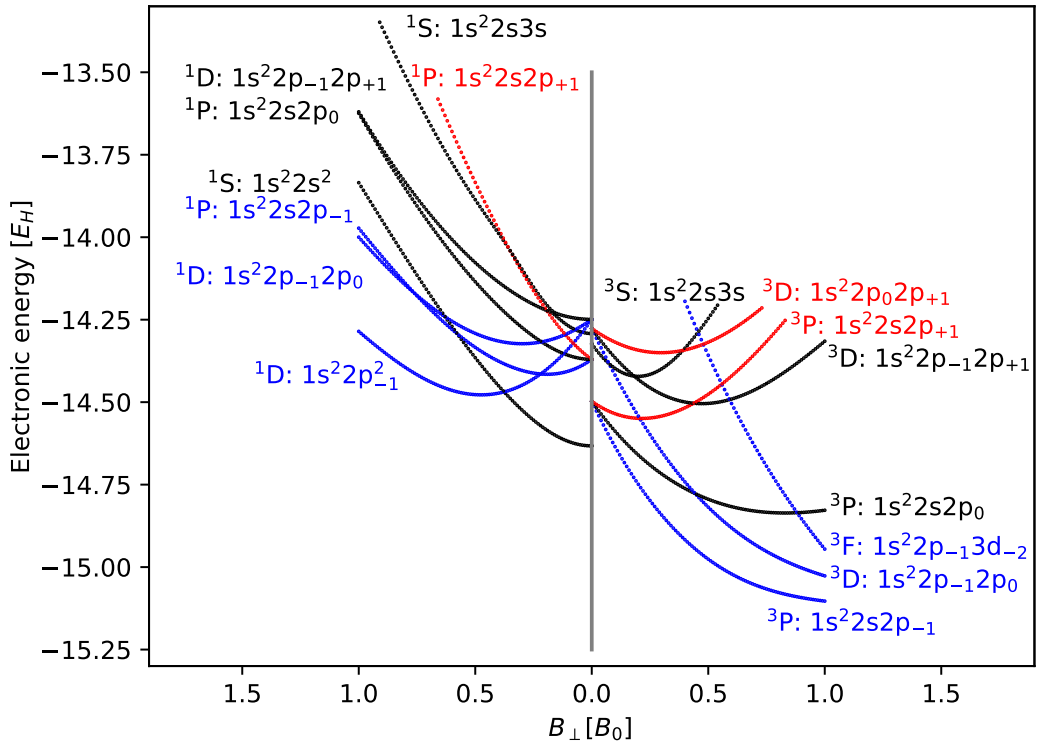

(a) *The helium dimer in the united atom limit ($R = 0.1$ millibohr), calculated with the* `Lu-aug-cc-pVTZ` *basis set*

Figure 4.1: *The FCI states of the beryllium and helium atoms, and the helium dimer in the united atom limit, calculated as a function of magnetic field intensity. Basis sets vary. In all subplots are singlet states to the left of gray line and triplets to the right. The sign of m_z determines the color of the lines: red for positive, blue for negative and black for zero.*

Evidently, the electronic structure of the helium dimer in the united atom limit greatly resembles a beryllium atom, as it should[4]. The basis sets[5] used in the three calculations are different due to computational convergence issues, but this is not really an issue: Each atom type has different exponents optimized for their specific electronic structure, and calculations such as these are therefore never truly "apples to apples". In light of this, the difference seems less pertinent. Furthermore, the computational results are in excellent qualitative agreement. We see for example that a high lying ^{3}F-state of the two four electron system is rapidly brought down by the Zeeman effect and becomes one of the lowest lying states when $B = B_0$. This is interesting for several reasons: Not only is it clear that even moderate basis sets, such as `Lu-aug-cc-pVDZ` can correctly predict the behavior of spin states with high angular momentum, it also reveals near ground state degeneracy, heralding a complex chemistry with multiple exotic transitions available.

Carpet plots are quite helpful for getting the broader picture. Typically, we kept the absolute value of the magnetic field fixed at B_0. The varied parameters were the distance between the atoms and the alignment of the molecule to the field – from parallel to perpendicular orientation. Figure 4.2 shows a FCI values for the lowest lying singlet (Figure 4.2a), triplet (Figure 4.2b), and quintet (Figure 4.2a) states of the dimer, respectively. All three tell a different story, however.

The singlet shows a small, but quite measurable, minimum. The bond strength and bond length varies smoothly with the orientation to the field, implying a stable molecule that will orient itself perpendicular to the field. Parallel to the field, a weak minimum exists. This is an artifact of dispersion: Figure 4.3 shows the BSSE corrected interaction energy of the parallel and perpendicular case at the HF and MP2 levels. Dispersion cannot be computed at the HF level, and indeed – the molecule is predicted to be completely dissociated when parallel to the field. On the other hand, MP2 predicts a subtle minimum slightly shy of 5.8 bohr. This is pure dispersion. Perpendicular to the field, the predicted molecular geometry is quite similar at both theory levels, but MP2 indicates a stronger bond than HF. This is expected.

The triplet, on the other hand, has two distinct, but still strongly binding states, one preferring a parallel orientation to the field, the other perpendicular. Disentangling these two states like this tend to be a thorny issue, but this task becomes

[4]In fact, the atoms are somewhat too close; a calculation performed at, say, 0.5 bohr would probably be more illustrative.

[5]In this case, the term *basis set*, refers to a collection of exponents to be used as input in a calculation and carrying a name, such as as `6-31G` or `aug-cc-pV5Z` etc. Two different helium atoms would have a different *set of basis functions* assigned to them, however.

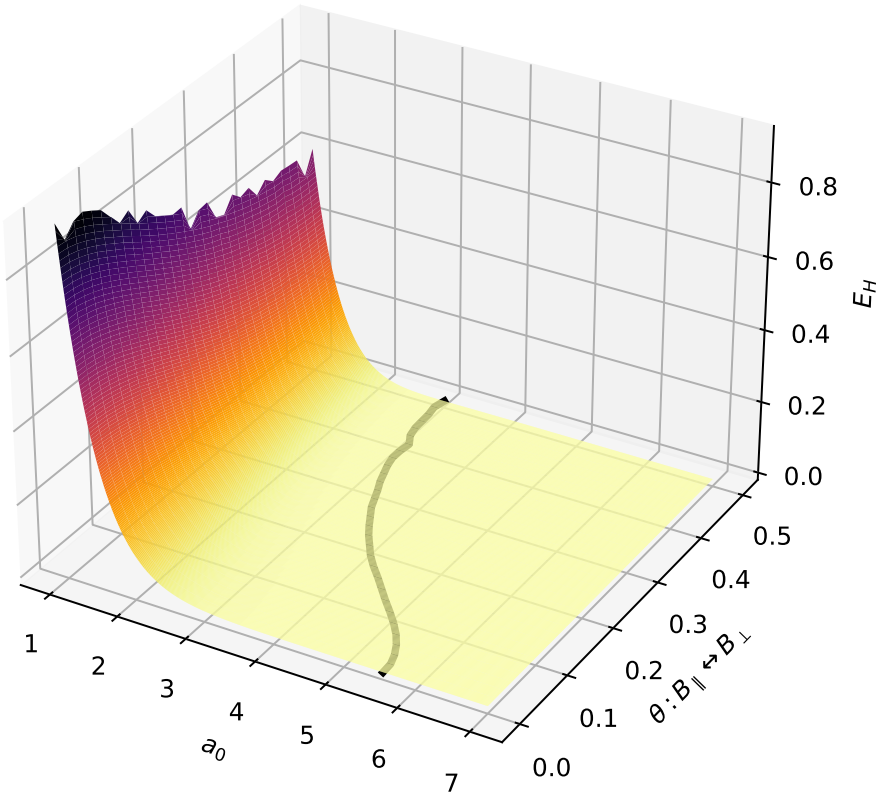

(a) *Singlet*

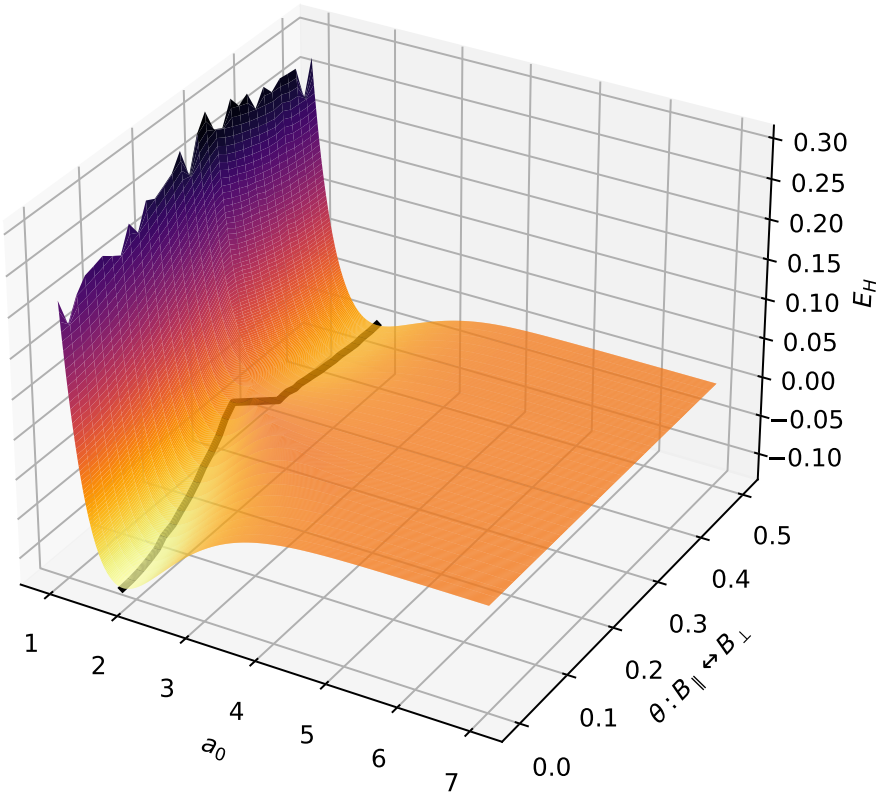

(b) *Triplet*

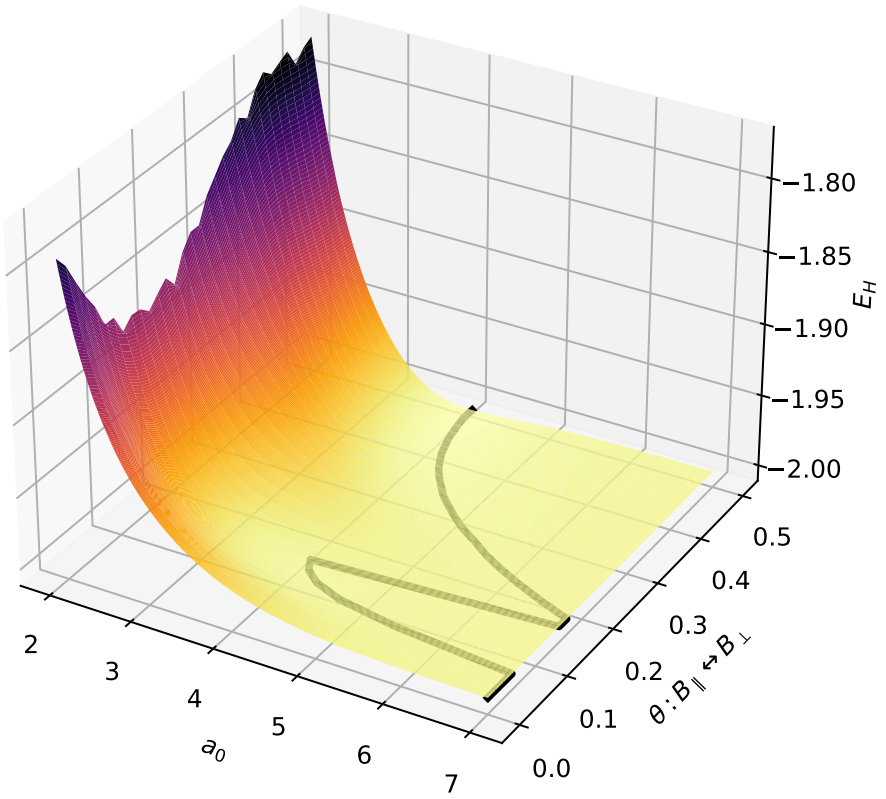

(a) *Quintet*

Figure 4.2: *FCI calculations with the* `Lu-aug-cc-pVTZ` *basis set of the* He_2 *molecule in i a field of* $|B| = B_0$*. The orientation of the molecular axis to the field is varied from parallel to perpendicular, and the distance between the atoms ranges from the united atom limit to dissociation. Spin states are singlet, triplet and quintet. All calculations are BSSE-corrected. The cragginess of the surface as atoms are brought close together is an artifact of interpolation procedure used when analyzing the data.*

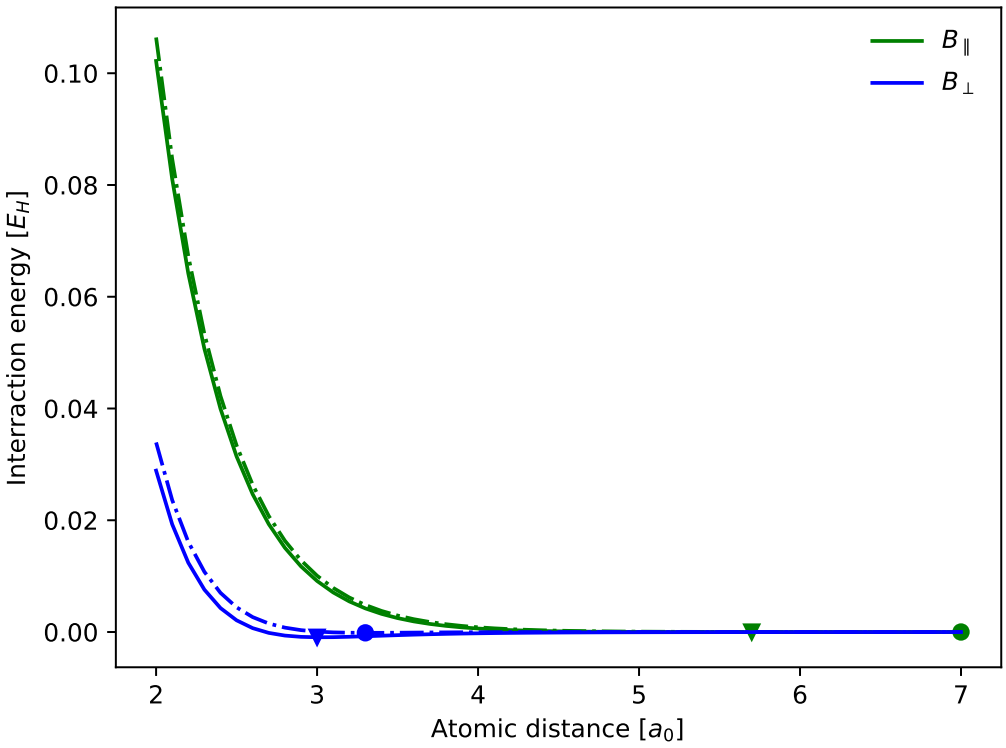

Figure 4.3: *BSSE corrected interaction energy of He_2 singlet in a parallel and perpendicular field of one atomic unit. The dashed lines denotes calculations at the Hartree-Fock level, the continuous lines are the corresponding MP2 values. The minimum energies are marked with circles for Hartree-Fock and triangles for MP2. The basis set is* `Lu-aug-cc-pVTZ`.

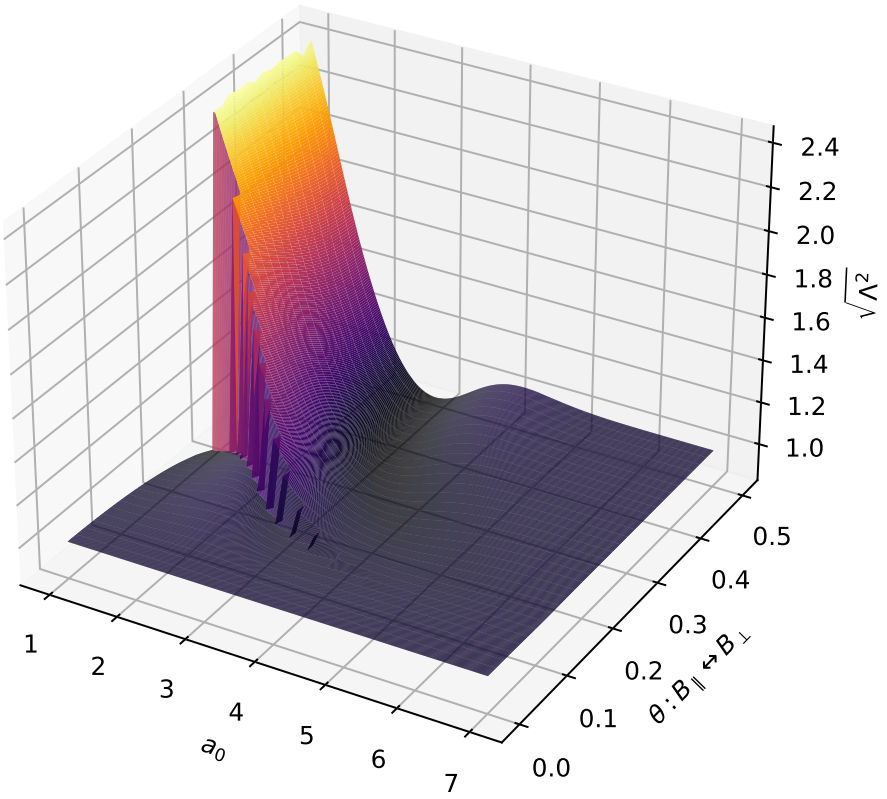

Figure 4.4: *Absolute value of AQAM for the lowest He_2 triplets, computed at the FCI/`Lu-aug-cc-pVTZ` level. Variational parameters are orientation to a static field of one atomic unit and distance between the atoms.*

trivial with AQAM. AQAM is a vector, so for making a carpet plot, similar to what has been made for interaction energies, either the absolute value or the projection must be plotted at a time. Figure 4.4 shows the absolute value of AQAM for the triplet. Clearly, there are two competing states, one which favors a perpendicular orientation, and one which favors a parallel orientation to the field. This picture cannot be properly computed at the MP2 level due to spin contamination. As an aside, this plot also shows how AQAM becomes an integer value for linear molecules parallel to the field, and in the dissociation limit, as it should.

The quintet is an odd job: The molecule appears to be completely dissociative in perpendicular configurations, and then oscillate a bit back and forth before it settles on a quite strongly bonding configuration perpendicular to the field. This effect is accentuated when the counterpoise correction is applied, and considering that the equilibrium distance is rather large, this is surprising.

All these open questions contributed to our decision to restrict ourselves to FCI calculations an fewer atoms. It seems clear, however, that the singlet states are easily modeled quite well by single-reference methods. The basis set of choice for this study was `Lu-aug-cc-pVTZ`[6]. It is common knowledge that anisotropic deformations of s-orbitals can be handled by higher lying entities to certain extent, as described in Section 3.1.2 [7]. At the double ζ level, which was used for the beryllium calculations, d-orbital states appeared – apparently from a combination of s and p orbitals. This was unexpected. A surprise, to be sure, but a welcome one. As the field increases, energy levels are shifted, and states may cross. It was also made clear that there is quite a bit more to paramagnetic bonding than what first meets the eye.

4.2.3 Other results

While making this paper, we investigated several avenues of research. We were initially most interested in the interactions between larger clusters in strong fields, but as mentioned, it soon became apparent that there were too many different spin-states involved, and that it might be best to fully understand these first. Therefore, we focused the paper on the many electronic states of the helium dimer, and how these are affected by the fields. However, some of the the results found for larger singlet state clusters were illuminating, but did not make it to the final version of the paper. They are therefore presented here instead. In the coming paragraphs, all calculations are for singlets, and the field intensity is one B_0 in the z-direction.

[6]For helium atoms, the sets `*-pVnZ` and `*-pCVnZ` are identical. For larger atoms, the latter contains extra core functions.

[7]See the discussion around Equation (3.18) for the particulars.

The first question we wanted to settle, was what kind of clusters were formed. There were earlier indications that the flakes of equilateral triangles would form perpendicular to the field. We wanted to investigate this matter more thoroughly.

First off, we found the bond length of the dimer to be 3 bohr when it was oriented perpendicularly to the field. The bond lengths increased when the molecules were disaligned from the field. This is clearly seen i Figure 4.2a. Then we found that the linear trimer (symmetry assumed) also preferred 3 bohr between the atoms, and also that the same held true for the vertices in an equilateral triangle. The dissociation curves of the latter two are seen in Figure 4.5. MP2 predictions of geometry compares well with FCI for these calculations, and BSSE is irrelevant in that regard. Then, a thorough scan of the trimer was performed at the CCSD(T)/`Lu-aug-cc-pVTZ` level to further map out the geometry and determine if an equilateral triangle perpendicular to the field truly was the correct shape of the cluster. Figure 4.6 depicts the molecule and highlights the varied parameters. The atoms A and B were kept perpendicular to the field and at the corresponding equilibrium distance of 3 bohr. I elected to *not* hold the distance R_{AC} fixed, but rather $R_{AC'}$. Therefore,

$$R_{AC} = \sqrt{R_{AC'}^2 + z_c^2}. \tag{4.12}$$

In other words, the scan was made over varied cylindrical coordinates for the position of atom C, and the energy is a function of those parameters alone. Another approach would have been to forget about C' entirely, keep the distance AC fixed, and rather vary the two angles. However, the equilibrium distance between two helium atoms smoothly increases to nearly six bohr when the dimer is rotated with respect to the field. Therefore, it seems less meaningful to insist on a fixed distance of 3 bohr for all orientations. Given this non-trivial behavior, fixation of AC seems irrelevant. The aforementioned cylindrical approach allows for dissociation to be included without imposing the need for additional variables.

The corresponding BSSE-corrected interaction energy for some specified value of z_c and γ is calculated like

$$E_{ABC}^{\text{int}} = \underbrace{E_{ABC}}_{\text{3 atoms, 0 ghosts}} \quad \underbrace{-E'_A - E'_B - E'_C}_{3\times(\text{1 atom, 2 ghosts})}, \tag{4.13}$$

where the apostrophe denotes the ghost fragments. This energy as a function of z_c and γ is plotted in Figure 4.7. There is a deep energy minimum when $z_c = 0$ and $\gamma = 60°$. This is exactly the equilateral triangle configuration oriented perpendicularly to the field, as expected. As the angle becomes more acute, while z_c is kept at zero, the energy increases due to Coulomb repulsion between B and C. For practical and

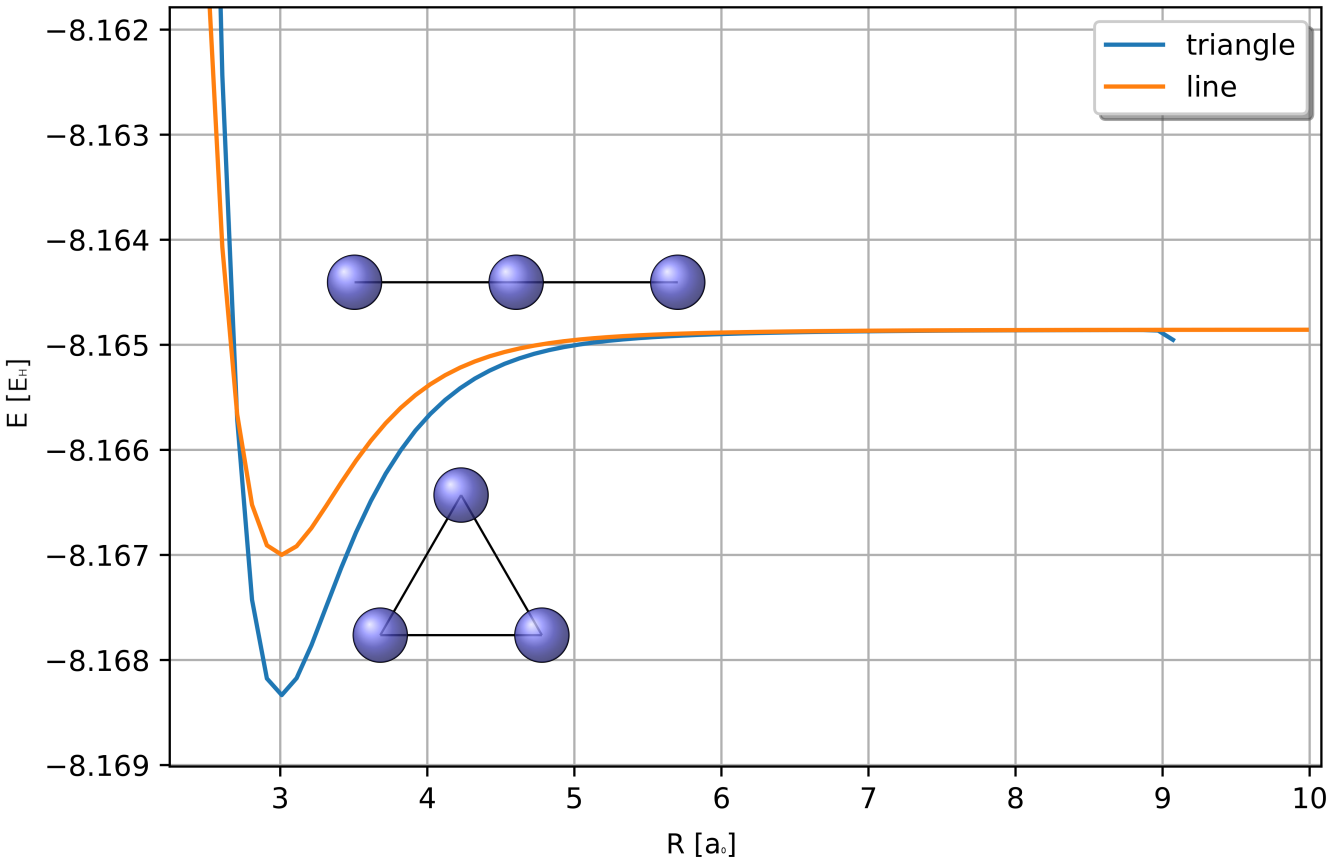

Figure 4.5: *The dissociation curves for He_3 singlet clusters in a linear and equilateral triangular configuration, oriented perpendicularly to a field of one atomic unit. Both minima occur when the atoms are three bohr apart. Interaction energy is larger for the triangular configuration.*

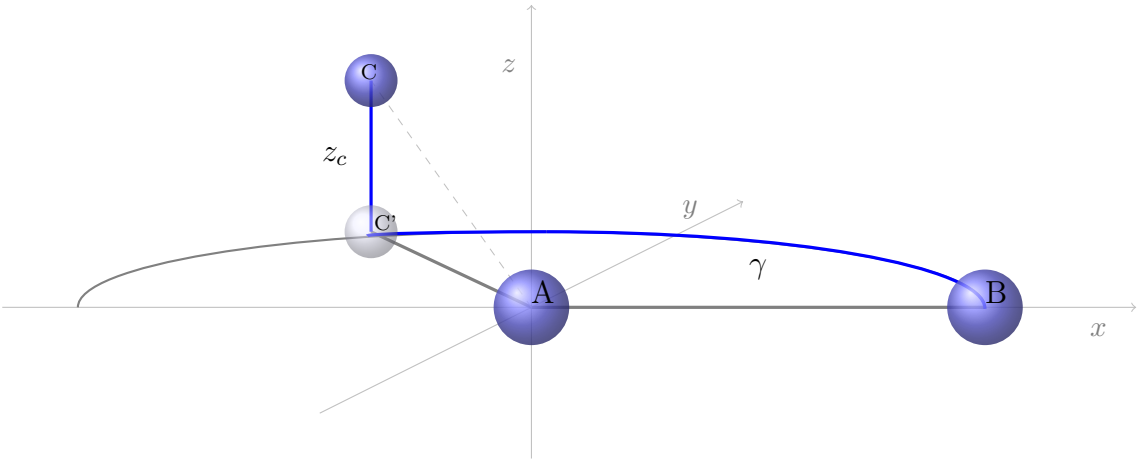

Figure 4.6: *A and B are two helium atoms fixed in place along the x-axis. C is the third atom, which is moved, and C' is the projection of this atom onto the xy-plane. The distance between C and C' is z_c, while $\gamma = \angle$ BAC'. These two variables are depicted in blue and determine the position of C. The distance between C' and A is 3 bohr, irrespective of z_c and γ.*

aesthetic reasons, the positive divergent values from this region has been set to 0. When the angle becomes larger than 60° (while still keeping z_c at zero), the energy rises, but only until around $\gamma = 110°$. After that, γ does not affect the energy at all. This angle corresponds to a distance of 4.9 bohr between B and C, and as seen in Figure 4.5, this is on the brink of dissociation. Evidently, only two interaction are relevant in this region of the energy landscape (AC and AB), while there were three closer to the triangular configuration (AB, AC and BC).

Table 4.1 holds key data underlying Figure 4.7 and some relations between these. Simply put, there are three distinct region of interest: The global minimum, and the first and second "plateau". This corresponds to 3, 2 and one interactions between the atoms, respectively. The total interaction energy, if divided with the number of interactions, lies between -1.19 and -1.27, clearly suggesting that all such interactions are quite equal.

It is also illuminating to break the plot up by fixing γ. When $\gamma \geq 60°$, classical dissociation curves as a function of z_c are seen. When the angle is more acute, however, then Coulomb repulsion between C and B causes a divergence for modest values of z_c. One might expect to see a tiny minimum even for $\gamma = 0°$, as this would correspond somewhat to field-free dispersion. However, the specimen appears to dissociate completely when C' approaches B. This is somewhat surprising, but

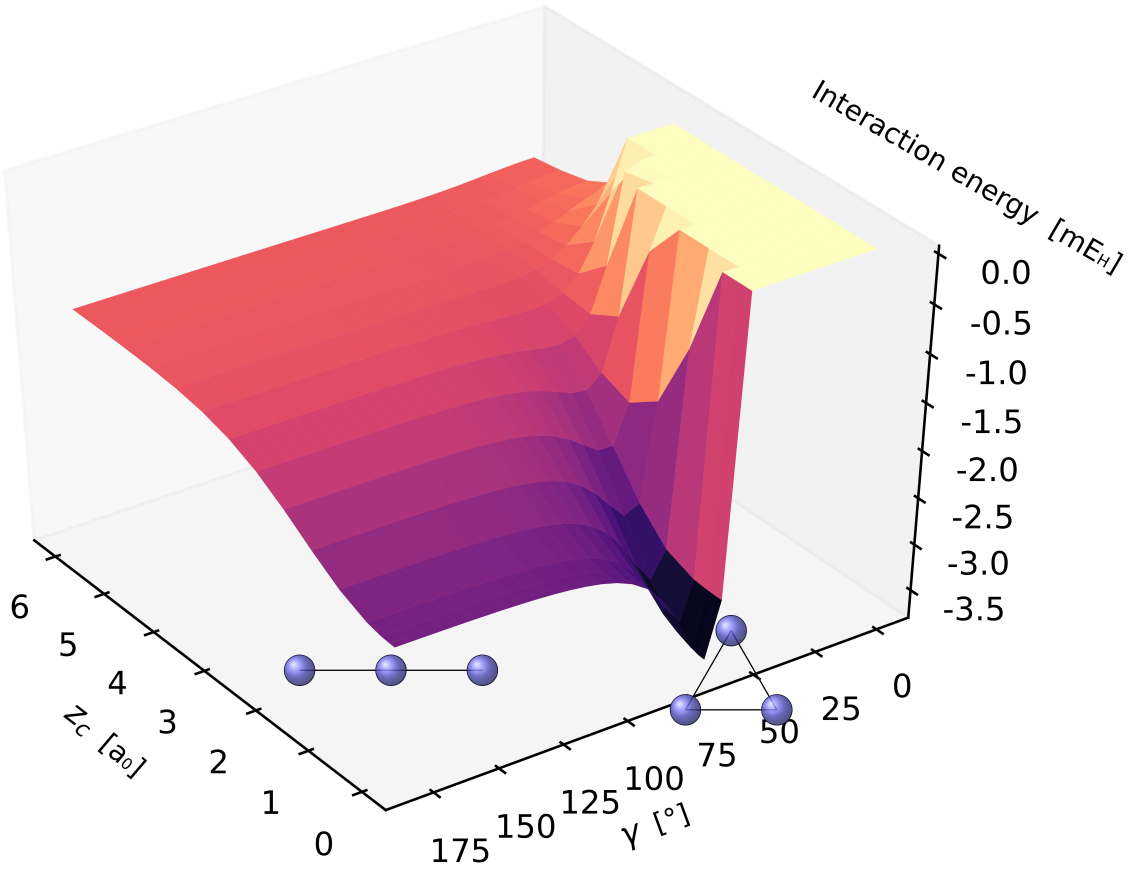

Figure 4.7: *The interaction energy for He_3 in the singlet state at $B_z = 1$. The theory level is CCSD(T)/`Lu-aug-cc-pVTZ`. For the sake of visibility, values diverging towards $+\infty$ due to Coulomb repulsion between the nuclei B and C has been set to 0. The two small clusters illustrate the molecular geometry in the region of interest, as described in Figure 4.6.*

Table 4.1: *Three selected data points from Figure 4.7 and their relationship. These are the interaction energies of the global minimum (which has three equal interactions), the first plateau (which has two) and the second plateau (which has only one non-zero interaction) between the atoms.The number n identify this number, while E_n^{int} is the total interaction energy in this region in millihartree.*

$z_c[a_0]$	γ	n	E_n^{int}	$\frac{E_n^{\text{int}}}{n}$	Description
0	$60°$	3	-3.73	-1.24	Global minimum (eq.lat. triangle)
0	$110° - 180°$	2	-2.38	-1.19	First plateau
6	$0° - 180°$	1	-1.27	-1.27	Second plateau (dissociation of C)

there might exist a subtle minimum which simply cannot be seen on this coarse grid. This effect *is* present in Figure 4.2a.

A HF study from 2012 suggests that helium atoms in the singlet state tend to prefer a planar and triangular tessellated configuration oriented perpendicularly to the field. In other words, the atoms tend to form sheets of equilateral triangles or similar [61]. The results for He_3 certainly reinforces this impression.

We also made some brief investigations of larger singlet clusters, all the way up to 20 atoms or so. Corroborating evidence for the hypothesis of equilateral triangle formation was found, but there were simply to many variables to properly investigate the matter. Also, because of different spin states, this line of research was put on ice – the current MP2 implementation only supports ground state calculations, and spin contamination is a serious issue. Singlet clusters are much easier to deal with than other spins states at the MP2 level, and when comparable, the results are both qualitatively and quantitatively close to CCSD(T) and FCI.

The feasibility of reducing complex interactions between clusters to general potentials was also briefly explored: The di- and triatomic singlet clusters behaved in a smooth and predictable manner, and it appeared that the interaction energy of larger clusters could be described as a sum of interaction energies for smaller specimens. Figure 4.8 shows a simplified example. Assuming two stable He_2 molecules in a singlet state and oriented perpendicularly to the field, how would these two molecules interact? Ideally, the question could be reduced to identifying the different twobody interactions, all of which are different points in Figure 4.2a. Parametrizing these interactions as a function of distance and angle to the field should then in theory provide all information needed to model any cluster – or even large conglomerates of

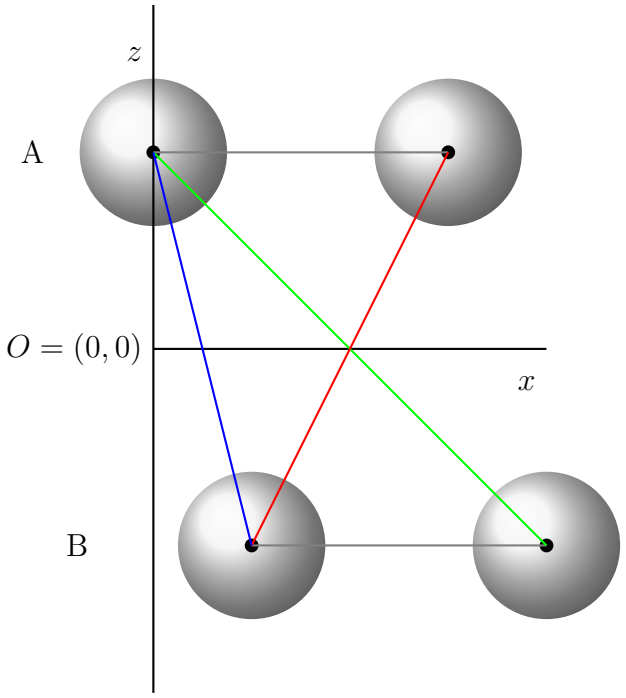

Figure 4.8: *Planar He_4 in the xz-plane. The offset between the layers is 1.0 bohr. There are four kinds of twobody interactions, labeled with different colors. Gray: Paramagnetic bonds at equilibrium distance 3.0 bohr, 2 in total. The blue line represents an interaction nearly parallel to the field between two atoms that are approximately 4.1 bohr apart. The red and the green lines represents interactions nearly diagonal to the field, between atoms that are about 4.5 bohr and 5.7 bohrs apart respectively. The magnitude of the magnetic field equals B_0, and it is oriented along the z-axis.*

clusters. However, as the ground state for such fields is most emphatically *not* a singlet, constructing methods tailored for such an artificial situation seemed premature. It also quickly became apparent that a parametrization from twobody interactions alone was unsatisfying, but the reason was not understood. Clearly, a better description of the smaller systems were essential before predictions of larger clusters could be made with confidence. It seems a worthwhile endeavour, however: Even if only the singlet state is pursued, if such an approach could work for helium atoms, it might also lend itself to larger noble gas atoms.

4.2.4 Discussion and future research

It was found that perpendicular paramagnetic bonding is a common phenomenon for several spin states as the field strength increases. It was also found that the landscape of possible energy minima is rich and complex: Depending on spin states and orientation to the field, multiple different types of bonds exist, some of them rather stable. These stable dimers are oriented either perfectly parallel or perpendicularly to the field. This was expected, as all strong-field deformations are anisotropic.

If the trends observed for the dimers – that is, the surprisingly large number of stable, field-dependent geometrical configurations – extends to larger clusters, then it would appear that a magnetic field allows multiple allotropes of helium to exist. This should be explored further.

AQAM has not been tested beyond homoatomic dimers, but the results so far are promising.

We still do not know exactly what form helium assumes as a function of magnetic fields. It is clear that the mono-atomic noble gas behavior is abandoned at some point, and that chemical bonding occurs. But exactly when does the different bonding mechanisms dominate, and how are the phase transitions? Will there be a regime of dimers in the triplet state oriented parallel to the field? And can these be reoriented perpendicularly to the field, but in a different spin state? And if so, will the transition between these states be something akin to phosphorescence? It also seems reasonable to assume that a spin polarized crystal structure will emerge if the fields are sufficiently strong, but this too remains to be demonstrated. All these open questions merit an answer.

If strong-field magnetic interactions truly can cause a noble gas to form different types of field-oriented clusters, then an entirely new branch of chemistry will emerge once the required hardware is installed. This is a bold statement, but it seems reasonable: Chemical bonds that can be turned on and off at will in specific directions as a function of an external factor which is hitherto irrelevant for chemical properties

(the magnetic field) would be a game changer. The production of sufficient field intensities appears insurmountable in a short term perspective, but there might be molecules that exhibit alien behavior in fields of less extreme magnitude.

4.3 Paper III

Given the tremendous importance water has for almost every human endeavor, even our very existence, it is one of the – if not *the most* – widely studied chemicals on Earth. The magnetic properties of water in strong fields has consequently been a matter of interest for as long as powerful magnets have been available, and spectacular results such diamagnetic levitation is readily demonstrated. One might expect that all similar oddities down that lane to be well established and described by now.

However, magnetic properties can be subtle and tricky to measure experimentally. Even when results are available, the exact processes can be difficult to understand. There has been persistent claims that well studied properties of water, such as Raman spectra, viscosity, surface-tension and the like significantly change under the influence of strong magnetic fields [145, 146, 147, 148], but the findings tend to be at odds with each other, and are still not commonly accepted in the the scientific community.

As has been hinted towards in the previous chapters, quantum chemistry in the presence of magnetic fields is a non-trivial endeavor, and reasonable doubts may be allayed towards computational results produced by conventional methods. Accordingly, the available theoretical studies are limited in scope and accuracy, for example to Monte Carlo simulations [149].

This matter has great practical importance: Any new chemical or physical properties of such an important compound *will* be useful for someone, somewhere – if only as an explanation for an experimental artifact, or as a nice opportunity to investigate something related, or for a technocratic entrepreneur to make a ton of money. If there are no strange new discoveries to be made down this alley, then perhaps a better understanding of methods which predicts otherwise may arise.

Despite any clear reason to believe that a "magnetic water treatment" could be effective, even in theory, such devices are commercially available, and have been so for decades. This is a controversial issue [12, 13].

Some of the predictions and claimed observations are refreshingly bold. For example, it has been claimed that in a field of a mere 34 T, the water dimer dissociates [150]. This is *not* a subtle effect, and should imply that bulk water more readily evaporates. Again, despite impressive experimental studies [151] of water clusters, iron clad experimental results about the magnetic properties of interest are unfortunately unavailable.

It seems clear that a better, and more definitive, understanding of whether or not magnetic fields attainable on Earth affects water at all is relevant and long overdue.

4.3.1 Layout of the study

Given the disputed nature of the claimed observations themselves, any proposed explanation must be somewhat tentative. Unfortunately, all experimental studies pertaining to magnetic water treatment are, by necessity, concerned with *impure* water. From a chemical perspective, even potable water usually has a large amount of impurities. For example, Norwegian authorities allows up to 50 milligrams per litre of nitrates [152], which drastically affect properties like conductivity.

We first restricted ourselves to water clusters utterly free of contaminants, saline or otherwise, and thus excluded a large number of practical questions. However, a reductionistic approach dictates such limitations, and it is imperative to understand the properties of the pure substance before the importance of impurities present can be determined.

Water is a truly unique chemical, and it has some unusual properties – the best example is probably the fact that the solid state has lower density than the liquid. This chemically unusual behavior, much like water's other quirks, are a result of strong hydrogen bonds. It is therefore no surprise that a hypothesis offered in response to purportedly odd observations of water revolves around hydrogen bonding to some extent. Such an effect ought to be present in a pure sample, and that is why our computational setup has great capacity for falsification. If a magnetic water treatment really do produce cleaner water, then describing the behaviour of the product in the presence of a magnetic field seems necessary.

Another candidate for any deviant behaviour would be the presence of oxygen. Water naturally contains a certain level of dissolved O_2. As discussed at length in Section 2.3, and explored in depth in Paper 1, a diamagnetic molecule has no other magnetic interactions. These are weak for attainable fields, and can be computed to high accuracy. The oxygen molecule is paramagnetic, and paramagnetic interactions in attainable fields tend to be about three orders of magnitude larger than diamagnetic interactions. As an avenue of research, it is certainly reasonable to explore. However, considering that that the amount of dissolved oxygen in water is low, any effects of importance to the clusters would have to be astoundingly overwhelming if it were to also affect bulk water.

Accurate calculations of water clusters were performed with LONDON, using the MP2 module and the `Lu-aug-cc-pCVTZ` basis set. We investigated single molecules and clusters of increasing size (1, 2, 3 and 4 water molecules). The idea was to safely

extrapolate into bulk matter. This is a reasonable approach, since a previous study by Góra et al. revealed that the interaction energy in water clusters as a function of cluster size converge quickly, even when four-body interactions are accounted for [153]. Then, a similar setup was performed for water molecules and oxygen molecules.

4.3.2 Results and discussion

The field dependence of the interaction energy of all the investigated water clusters stays below 3 ppm, even for field strengths up to 100 T. This is seen in Figure 4.9. This field dependency is expressed as

$$\frac{\Delta E_{\text{int}}}{E_{\text{int}}} = \frac{E_{\text{int}}\left(B_w\right) - E_{\text{int}}\left(0\right)}{E_{\text{int}}\left(0\right)}, \tag{4.14}$$

where B_w is a magnetic field in either x, y or z-direction and E_{int} the interaction energy. Figure 4.9 also shows that in the relevant regime of $B \leq 40\ \ T$, the field dependency of the interaction energy is less than 0.4 ppm for all clusters. This corresponds to less than half a kcal/mol. For all practical purposes, the field dependency of the interaction energy is zero.

Furthermore, even the if errors due to the reduced cluster size were as much as 100%, none of the above would change; one kcal/mol is also a rather modes amount. The conclusion is therefore simple: None of the aforementioned molecular properties of water are measurably affected by relevant magnetic fields. This holds true for both the pure water clusters and the combinations of water molecules and oxygen.

4.3.3 Future work

The chemistry was not affected at all by the fields we studied, but at some point *it will be*. We do not yet know when exactly this will occur, nor what exactly will happen. From previous studies, and particularly from the work related to noble gas clusters, ample evidence for bold conjectures about the intricate spin states of noble gas clusters are available. Why should water be any different in that regard? There is no reason to assume that other atoms and molecules will not experience as of yet uncharacterized transitions into new and exotic states of matter. A detailed study of different molecules in increasing fields seems to be the obvious continuation of this research. The tools are available.

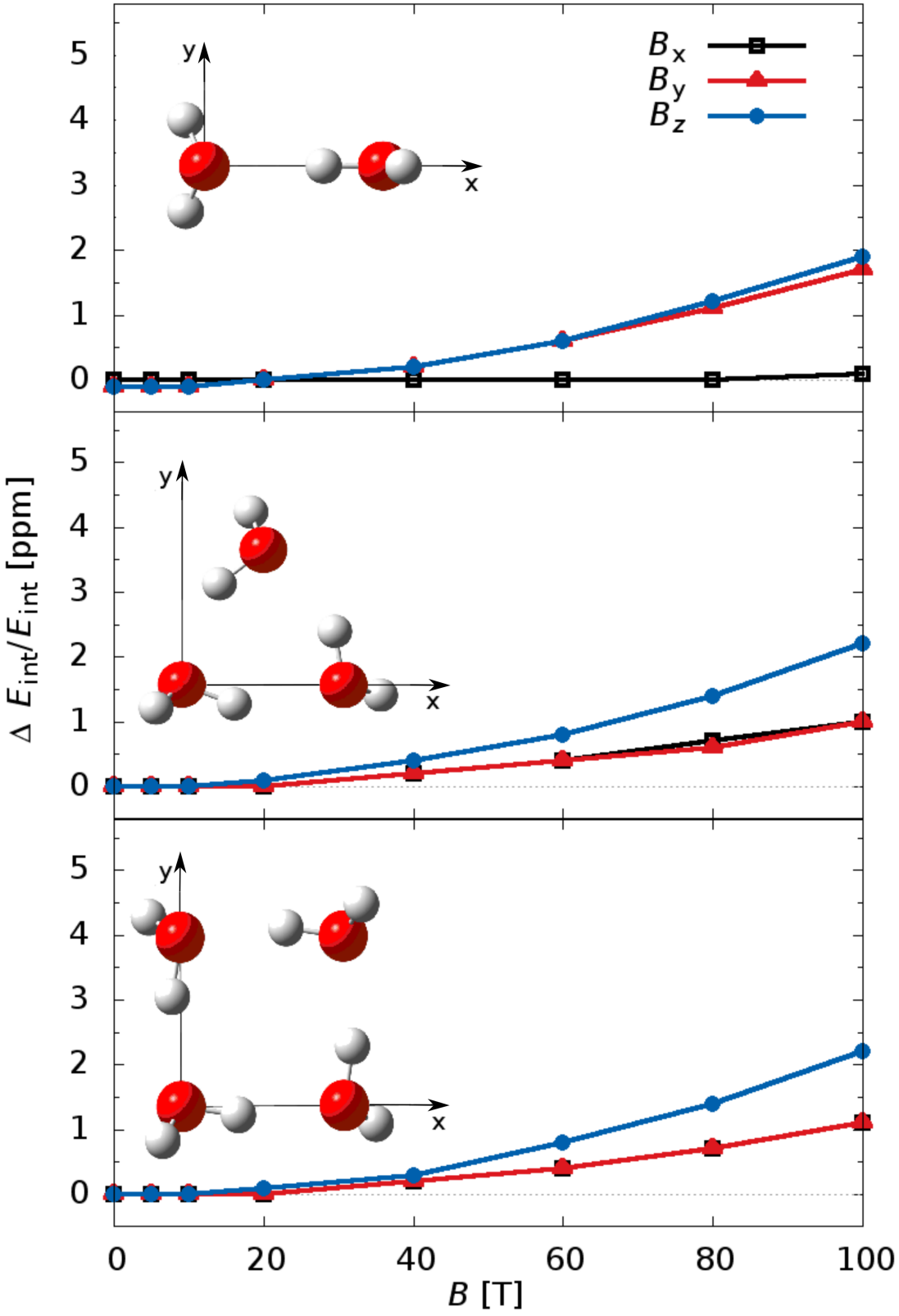

Figure 4.9: *Field dependence of interaction energy for clusters of 2, 3 and 4 water molecules. This image is used in the article (Figure 1).*

Chapter 5

Concluding remarks

The gist of this thesis has been the implementation of quantum chemistry methods in the gauge origin independent formalism, applied on a varied set of interesting problems. The underlying ambition has been twofold: First, to better understand the vast and curious nature of molecules in magnetic field. Second, to create versatile and useful software for quantum chemistry calculations that can handle magnetic fields in a consistent, predictable and accurate manner.

5.1 Summary

The three papers each cover different theory levels and different abstraction levels: The first paper was about the proper inclusion of magnetic fields in DFT. Wavefunction methods were used to create densities, and by means of the Lieb optimization, the behavior of the functional itself was studied. This paper did not investigate new properties of molecules, but rather why certain methods produce the results they do.

The second paper was conceptually less abstract: The electronic structure of helium clusters in magnetic fields was investigated at the FCI level. But the molecular specimens in question, and the stellar objects on which they might be found, were of a far more arcane nature! For the first time, the molecular properties of such exotic species, existing only in magnetic fields unattainable on Earth, was properly clarified at this theory level. In this study, the necessity of methods proven to be accurate from first principles was essential, since the results cannot be compared with experiment.

The final paper was in every way more down to Earth: An important contribution to our understanding of the nature of water was made. This final paper also high-

lights the necessity of having trustworthy quantum chemistry methods for magnetic systems, even for practical, everyday chemistry. This points back to the first article; properly understanding DFT in general, and creating a reliable DFT for magnetic fields in particular seems a highly relevant task. For tiny water clusters, MP2 was adequate, but should more complex systems be investigated, more computationally efficient methods must be employed. BDFT can match, or even surpass MP2, but bold conclusions rely on certain results. Hopefully, our investigations in the matter has illuminated some of the unresolved conundrums.

The London orbital formalism is a key component of our approach to doing quantum chemistry in the presence of finite magnetic fields. This approach has proven to be versatile and efficient for vastly different scientific inquiries. None of the results would have been sufficiently reliable without gauge origin-independent wave functions. On a thematic level, the works runs the gamut from highly abstract method development and calibration, via obscure astrochemistry, and back to earthly chemistry – thus forming a full circle.

5.2 The future

It is not uncommon for theoretical endeavors to lie far beyond experimental capabilities for a while. The Higgs boson is a stellar example; prediction preceded discovery with five decades. On a similar note: London orbitals are octogenarians by now, but applications in computational quantum chemistry has so far been restricted to response theory. Employing London atomic orbitals at finite fields is a fairly recent achievement. In turn, bold claims have been made about strong field chemistry. Practical production of the the magnetic fields required is pure science fiction as of now.

This is a common pattern in science. It is, generally speaking, easier to design an experiment based on a good hypothesis than shooting blindly for data[1]. However, all theories are eventually thoroughly tested if they are still deemed relevant when the experimental capabilities are up the challenge. Now that the realm of exotic magnetic chemistry becomes rapidly more well established, and new phenomena predicted, it seems reasonable to assume that experimental work will soon be turned in this direction. As technology progresses, stronger magnets are bound to be made, and detection limits and times will be reduced. This latter point means that more experimental work can be performed with pulsed fields, and pulsed fields have been

[1]It's also easier to get funding for expensive equipment if there are good reasons to assume interesting results will be found.

available in the kilotesla regime for decades. I certainly hope to see demonstrations of perpendicular paramagnetic bonding and similar oddball mechanisms – or even better, experimental falsification! – within my lifetime.

Maybe exotic magnetic properties will even see practical applications in technology and chemistry, not just as an interesting demonstration of unusual physical properties, but as a useful and relevant part of the modern chemists tool box? Time will tell.

5.3 Final note

This thesis has a rather broad scope, reflecting the multi headed nature of magnetic quantum chemistry. Overall, high quality quantum chemistry calculations in magnetic fields are important for numerous theoretical and experimental endeavors. As experimental designs becomes more sophisticated, and theoretical predictions provides new hypothesis to be tested, this avenue of scientific work will become more important. Easy access to accurate and amply tested, well established methods for computations is a prerequisite in that regard. Hopefully, this work has contributed to making accurate strong-field quantum chemistry more available to the masses.

Part III

Bibliography and articles

Bibliography

[1] S. Reimann, A. Borgoo, J. Austad, E. I. Tellgren, A. M. Teale, T. Helgaker, and S. Stopkowicz, "Kohn–Sham energy decomposition for molecules in a magnetic field," *Mol. Phys.*, vol. 117, no. 1, pp. 97–109, 2019.

[2] W. Heitler and F. London, "Wechselwirkung neutraler atome und homöopolare bindung nach der quantenmechanik," *Z. Phys.*, vol. 44, no. 6, pp. 455–472, 1927.

[3] E. A. Hylleraas, "Neue berechnung der energie des heliums im grundzus ande, sowie des tiefsten terms von ortho-helium," *Z. Phys.*, vol. 54, no. 5, pp. 347–366, 1929.

[4] E. A. Hylleraas, "The Schrödinger two-electron atomic problem," in *The Schrödinger Two-Electron Atomic Problem* (P.-O. Löwdin, ed.), vol. 1 of *Advances in Quantum Chemistry*, pp. 1 – 33, Academic Press, 1964.

[5] O.-A. Al-Hujaj and P. Schmelcher, "Ground and excited states of the hydrogen negative ion in strong magnetic fields," *Phys. Rev. A*, vol. 61, no. 6, p. 063413, 2000.

[6] F. London, "Théorie quantique des courants interatomiques dans les combinaisons aromatiques," *J. Phys. Radium*, vol. 8, no. 10, pp. 397–409, 1937.

[7] T. Helgaker and P. Jørgensen, "An electronic hamiltonian for origin independent calculations of magnetic properties," *J. Chem. Phys.*, vol. 95, no. 4, pp. 2595–2601, 1991.

[8] E. I. Tellgren, T. Helgaker, A. Soncini, K. K. Lange, A. M. Teale, U. Ekström, S. Stopkowicz, J. Austad, and S. Sen, "LONDON, a quantum-chemistry program for plane-wave/GTO hybrid basis sets and finite magnetic field calculations. See londonprogram.org for more information.."

[9] E. I. Tellgren, *Quantum-chemical method developement for extended and magnetic systems*. PhD thesis, University of Oslo, 2009.

[10] S. Jordan, P. Schmelcher, and W. Becken, "Stationary components of He I in strong magnetic fields - a tool to identify magnetic DB white dwarfs," *Astron. Astrophys.*, vol. 376, no. 2, pp. 614–620, 2001.

[11] S. Jordan, P. Schmelcher, W. Becken, and W. Schweizer, "Evidence for helium in the magnetic white dwarf GD 229," *Astron. Astrophys.*, vol. 336, no. 2, pp. L33–36, 1998.

[12] J. S. Baker and S. J. Judd, "Magnetic amelioration of scale formation," *Wat. Res*, vol. 30, no. 2, pp. 247 – 260, 1996.

[13] D. Hasson and D. Bramson, "Effectiveness of magnetic water treatment in suppressing calcium carbonate scale deposition," *Ind. Eng. Chem. Proc. DD*, vol. 24, no. 3, pp. 588–592, 1985.

[14] P. M. Colletti, "Size "H" oxygen cylinder: Accidental MR projectile at 1.5 tesla," *J. Mag. Res Img.*, vol. 19, pp. 141–143, 2004.

[15] M. V. Berry and A. K. Geim, "Of flying frogs and levitrons," *Eur. J. Phys.*, vol. 18, pp. 307–313, 1997.

[16] J. R. Miller, M. D. Bird, S. Bole, A. Bonito-Oliva, Y. Eyssa, W. J. Kenney, T. A. Painter, H. . Schneider-Muntau, L. T. Summers, S. W. van Sciver, S. Welton, R. J. Wood, J. E. C. Williams, S. Bobrov, Y. Iwasa, M. Leupold, V. Stejskal, and R. Weggel, "An overview of the 45 T hybrid magnet system for the new national high magnetic field laboratory," *IEEE T. Mag.*, vol. 30, no. 4, pp. 1563–1571, 1994.

[17] J. W. T. Hessels, S. M. Ransom, I. H. Stairs, P. C. C. Freire, V. M. Kaspi, and F. a. Camilo, "A radio pulsar spinning at 716 Hz," *Science*, vol. 311, no. 5769, pp. 1901–1904, 2006.

[18] S. K. Range, "GRAVITY PROBE B: Examining Einstein's Spacetime with Gyroscopes," tech. rep., NASA, 2004.

[19] M. Lockwood, R. Stamper, and M. N. Wild, "A doubling of the sun's coronal magnetic field during the past 100 years," *Nature*, vol. 399, pp. 437–439, 1999.

[20] A. Chulliat, S. Macmillan, P. Alken, C. Beggan, M. Nair, B. Hamilton, A. Woods, V. Ridley, S. Maus, and A. Thomson, "The US/UK World Magnetic Model for 2015-2020," tech. rep., National Geophysical Data Center, 2015.

[21] M. Motokawa, "Physics in high magnetic fields," *Rep. Prog. Phys.*, vol. 67, no. 11, pp. 1995–2052, 2004.

[22] DOE/Los Alamos National Laboratory, "World-record pulsed magnetic field achieved; lab moves closer to 100-tesla mark." www.sciencedaily.com/releases/2011/08/110823134929.htm. Accesed: 2019-04-25.

[23] D. Nakamura, A. Ikeda, H. Sawabe, Y. H. Matsuda, and S. Takeyama, "Record indoor magnetic field of 1200 T generated by electromagnetic flux-compression," *Rev. Sci. Instrum.*, vol. 89, no. 9, p. 095106, 2018.

[24] D. Nakamura, H. Sawabe, Y. H. Matsuda, and S. Takeyama, "Precise measurement of a magnetic field generated by the electromagnetic flux compression technique," *Rev. Sci. Instrum.*, vol. 84, no. 4, p. 044702, 2013.

[25] A. I. Bykov, M. I. Dolotenko, N. P. Kolokolchikov, S. V. D., and O. M. Tatsenko, "VNIIEF achievements on ultra-high magnetic fields generation," *Physica B*, vol. 274-275, pp. 574–578, 2001.

[26] B. A. Boyko, A. I. Bykov, M. I. Dolotenko, N. P. Kolokolchikov, I. M. Markevtsev, O. M. Tatsenko, and K. Shuvalov, "With record magnetic fields to the 21st century," in *Pulsed Power Conference, 1999. Digest of Technical Papers. 12th IEEE International*, vol. 2, pp. 746–749, 1999.

[27] D. Koester and G. Chanmugam, "Physics of white dwarf stars," *Rep. Prog. Phys.*, vol. 53, no. 7, pp. 837–915, 1990.

[28] A. Reisenegger, "Origin and evolution of neutron star magnetic fields," *arXiv e-prints*, pp. astro–ph/0307133, 2003.

[29] D. Lai, "Matter in strong magnetic fields," *Rev. Mod. Phys.*, vol. 73, no. 3, pp. 629–662, 2001.

[30] V. M. Kaspi and A. M. Beloborodov, "Magnetars," *Annu. Rev. Astron. Astr.*, vol. 55, no. 1, pp. 261–301, 2017.

[31] J. Schwinger, "On gauge invariance and vacuum polarization," *Phys. Rev.*, vol. 82, pp. 664–679, Jun 1951.

[32] E. Bavarsad, S. P. Kim, C. Stahl, and S.-S. Xue, "Effect of a magnetic field on schwinger mechanism in de sitter spacetime," *Phys. Rev. D*, vol. 97, p. 025017, Jan 2018.

[33] G. Zavattini, U. Gastaldi, R. Pengo, G. Ruoso, F. D. Valle, and E. Milotti, "Measuring the magnetic birefringence of vacuum: The pvlas experiment," *Int. J Mod. Phys. A*, vol. 27, no. 15, p. 1260017, 2012.

[34] K. L. Litvinenko, M. Pang, J. Li, E. Bowyer, H. Engelkamp, V. B. Shuman, L. M. Portsel, A. N. Lodygin, Y. A. Astrov, S. G. Pavlov, H.-W. Hübers, C. R. Pidgeon, and B. N. Murdin, "High-field impurity magneto-optics of Si:Se," *Phys. Rev. B*, vol. 90, p. 115204, 2014.

[35] B. N. Murdin, J. Li, M. L. Y. Pang, E. T. Bowyer, K. L. Litvinenko, S. K. Clowes, H. Engelkamp, C. R. Pidgeon, I. Galbraith, N. V. Abrosimov, H. Riemann, S. G. Pavlov, H.-W. Hübers, and P. G. Murdin, "Si:P as a laboratory analogue for hydrogen on high magnetic field white dwarf stars," *Nature Comm.*, vol. 4, p. 1469, 2013.

[36] A. V. Korolev and M. A. Lieberman, "Binding energy and singlet-triplet splitting for the hydrogen molecule in ultrahigh magnetic fields," *Phys. Rev. A*, vol. 45, no. 3, pp. 1762–1766, 1992.

[37] K. K. Lange, E. I. Tellgren, M. R. Hoffmann, and T. Helgaker, "A paramagnetic bonding mechanism for diatomics in strong magnetic fields," *Science*, vol. 337, no. 6092, pp. 327–331, 2012.

[38] S. Stopkowicz, "Perspective: Coupled cluster theory for atoms and molecules in strong magnetic fields," *Int. J. Quantum Chem.*, vol. 118, no. 1, p. e25391, 2018.

[39] E. I. Tellgren, T. Helgaker, and A. Soncini, "Non-perturbative magnetic phenomena in closed-shell paramagnetic molecules," *Phys. Chem. Chem. Phys.*, vol. 11, no. 26, pp. 5489–5498, 2009.

[40] G. I. Pagola, S. Pelloni, M. C. Caputo, M. B. Ferraro, and P. Lazzeretti, "Fourth-rank hypermagnetizability of medium-size planar conjugated molecules and fullerene," *Phys. Rev. A*, vol. 72, no. 3, p. 033401, 2005.

[41] G. I. Pagola, M. B. Ferraro, and P. Lazzeretti, "Can induced orbital paramagnetism be controlled by strong magnetic fields?," *J. Chem. Theor. Comp.*, vol. 5, no. 11, pp. 3049–3059, 2009.

[42] M. C. Caputo and P. Lazzeretti, "Geometry distortion of the benzene molecule in a strong magnetic field," *Int. J. Quantum Chem.*, vol. 111, no. 4, pp. 772–779, 2011.

[43] M. Žaucer and A. Ažman, "Molecules in strong magnetic fields," *Phys. Rev. A*, vol. 18, no. 3, pp. 1320–1321, 1978.

[44] Y. E. Lozovik and A. V. Klyuchnik, "Change of binding type and dissociation of molecules and biexcitons in a strong magnetic field," *Phys. Lett. A*, vol. 66, no. 4, pp. 282–284, 1978.

[45] S. Basile, F. Trombetta, and G. Ferrante, "The hydrogen molecule in an arbitrarily oriented magnetic field," *Il Nuovo Cimento*, vol. 9, no. 5, pp. 457–472, 1987.

[46] J. Avron, I. Herbst, and B. Simon, "Formation of negative ions in magnetic fields," *Phys. Rev. Lett.*, vol. 39, pp. 1068–1070, 1977.

[47] H. F. Hameka, "On the nuclear magnetic shielding in the hydrogen molecule," *Mol. Phys.*, vol. 1, no. 3, pp. 203–215, 1958.

[48] D. F. Styer, M. S. Balkin, K. M. Becker, M. R. Burns, C. E. Dudley, S. T. Forth, J. S. Gaumer, M. A. Kramer, D. C. Oertel, L. H. Park, M. T. Rinkoski, C. T. Smith, and T. D. Wotherspoon, "Nine formulations of quantum mechanics," *Am. J. Phys.*, vol. 70, no. 3, pp. 288–297, 2002.

[49] M. Born and R. Oppenheimer, "Zur Quantentheorie der Molekeln," *Ann. der Phys.*, vol. 389, no. 20, pp. 457–484, 1927.

[50] R. G. Woolley and B. T. Sutcliffe, "Molecular structure and the Born–Oppenheimer approximation," *Chem. Phys. Lett.*, vol. 45, no. 2, pp. 393 – 398, 1977.

[51] M. Vincke and D. Baye, "Centre-of-mass effects on the hydrogen atom in a magnetic field," *J. Phys. B: At. Mol. Opt. Phys.*, vol. 21, no. 13, pp. 2407–2424, 1988.

[52] D. Baye and M. Vincke, "Center-of-mass problem in a magnetic field: Unified treatment of charged and neutral systems," *Phys. Rev. A*, vol. 42, no. 1, pp. 391–396, 1990.

[53] P. Schmelcher, L. S. Cederbaum, and H.-D. Meyer, "On the validity of the born-oppenheimer approximation in magnetic fields," *J. Phys. B: At. Mol. Opt. Phys.*, vol. 21, no. 15, pp. L445–450, 1988.

[54] T. U. Helgaker and J. Almlöf, "A second-quantization approach to the analytical evaluation of response properties for perturbation-dependent basis sets," *Int. J. Quantum Chem.*, vol. 26, no. 2, pp. 275–291, 1984.

[55] G. I. Pagola, M. C. Caputo, M. B. Ferraro, and P. Lazzeretti, "Calculation of the fourth–rank molecular hypermagnetizability of some small molecules," *J. Chem. Phys.*, vol. 120, no. 20, pp. 9556–9560, 2004.

[56] T. Helgaker, P. Jørgensen, and J. Olsen, *Molecular Electronic-Structure Theory*. John Wiley & Sons, Ltd, 2000.

[57] A. Szabo and N. S. Ostlund, *Modern Quantum Chemistry: Introduction to Advanced Electronic Structure Theory*. Dover Publications, Inc, 1996.

[58] J. D. Jackson, *Classical electrodynamics*. New York, NY: Wiley, 2. ed., 1975.

[59] W.-M. Sun, X.-S. Chen, X.-F. Lü, and F. Wang, "Gauge-invariant hydrogen-atom Hamiltonian," *Phys. Rev. A*, vol. 82, p. 012107, 2010.

[60] E. I. Tellgren and H. Fliegl, "Non-perturbative treatment of molecules in linear magnetic fields: Calculation of anapole susceptibilities," *J. Chem. Phys.*, vol. 139, no. 16, p. 164118, 2013.

[61] E. I. Tellgren, S. S. Reine, and T. Helgaker, "Analytical GIAO and hybrid-basis integral derivatives: application to geometry optimization of molecules in strong magnetic fields," *Phys. Chem. Chem. Phys.*, vol. 14, no. 26, pp. 9492–9499, 2012.

[62] E. I. Tellgren, A. Soncini, and T. Helgaker, "Non-perturbative ab initio calculations in strong magnetic fields using London orbitals," *J. Chem. Phys.*, vol. 129, no. 15, p. 154114, 2008.

[63] T. J. P. Irons, J. Zemen, and A. M. Teale, "Efficient calculation of molecular integrals over london atomic orbitals," *J. Chem. Theory Comput.*, vol. 13, no. 8, pp. 3636–3649, 2017.

[64] S. Stopkowicz, J. Gauss, K. K. Lange, E. I. Tellgren, and T. Helgaker, "Coupled-cluster theory for atoms and molecules in strong magnetic fields," *J. Chem. Phys.*, vol. 143, no. 7, p. 074110, 2015.

[65] R. D. Reynolds and T. Shiozaki, "Fully relativistic self-consistent field under a magnetic field," *Phys. Chem. Chem. Phys.*, vol. 17, pp. 14280–14283, 2015.

[66] G. I. Pagola, M. C. Caputo, M. B. Ferraro, and P. Lazzeretti, "Effects of strong magnetic fields on the electron distribution and magnetisability of rare gas atoms," *Chem. Phys. Lett.*, vol. 400, no. 1-3, pp. 133–138, 2004.

[67] R. McWeeny, *Methods of Molecular Quantum Mechanics*. Academic Press, 2 ed., 1992.

[68] D. R. Hartree, "The wave mechanics of an atom with a non-coulomb central field. part ii. some results and discussion," *Proc. Cambridge Philos. Soc.*, vol. 24, no. 1, pp. 111–132, 1928.

[69] S. Høst, J. Olsen, B. Jansík, L. Thøgersen, P. Jørgensen, and T. Helgaker, "The augmented Roothaan–Hall method for optimizing Hartree–Fock and Kohn–Sham density matrices," *J. Chem. Phys.*, vol. 129, no. 12, p. 124106, 2008.

[70] P. Echenique and J. L. Alonso, "A mathematical and computational review of Hartree–Fock SCF methods in quantum chemistry," *Mol. Phys.*, vol. 105, no. 23-24, pp. 3057–3098, 2007.

[71] P.-O. Löwdin, "Expansion theorems for the total wave function and extended Hartree–Fock schemes," *Rev. Mod. Phys.*, vol. 32, pp. 328–334, 1960.

[72] T. Kato, "On the eigenfunctions of many-particle systems in quantum mechanics," *Commun.Pur.Appl.Math*, vol. 10, no. 2, pp. 151–177, 1957.

[73] N. H. March, "Spatially dependent generalization of kato's theorem for atomic closed shells in a bare coulomb field," *Phys. Rev. A*, vol. 33, pp. 88–89, 1986.

[74] U. Kappes and P. Schmelcher, "Atomic orbital basis set optimization for ab initio calculations of molecules with hydrogen atoms in strong magnetic fields," *J. Chem. Phys.*, vol. 100, no. 4, pp. 2878–2887, 1994.

[75] A. Kubo, "The hydrogen molecule in strong magnetic fields: Optimizations of anisotropic Gaussian basis sets," *J. Phys. Chem. A*, vol. 111, no. 25, pp. 5572–5581, 2007.

[76] T. Detmer, P. Schmelcher, and L. S. Cederbaum, "Ab initio calculations with a nonspherical Gaussian basis set: Excited states of the hydrogen molecule," *J. Chem. Phys.*, vol. 109, no. 22, pp. 9694–9700, 1998.

[77] Y. P. Kravchenko, M. A. Lieberman, and B. Johansson, "Exact solution for a hydrogen atom in a magnetic field of arbitrary strength," *Phys. Rev. A*, vol. 54, no. 1, pp. 287–305, 1996.

[78] T. H. Dunning, "Gaussian basis sets for use in correlated molecular calculations. i. the atoms boron through neon and hydrogen," *J. Chem. Phys.*, vol. 90, no. 2, pp. 1007–1023, 1989.

[79] D. E. Woon and T. H. Dunning, "Gaussian basis sets for use in correlated molecular calculations. iii. the atoms aluminum through argon," *The Journal of Chemical Physics*, vol. 98, no. 2, pp. 1358–1371, 1993.

[80] R. A. Kendall, T. H. Dunning, and R. J. Harrison, "Electron affinities of the first-row atoms revisited. Systematic basis sets and wave functions," *J. Chem. Phys.*, vol. 96, no. 9, pp. 6796–6806, 1992.

[81] P. Schmelcher and L. S. Cederbaum, "Crossings of potential-energy surfaces in a magnetic field," *Phys. Rev. A*, vol. 41, no. 9, pp. 4936–4943, 1990.

[82] R. Bast and P.-O. Widmark, eds., *European Summerschool in quantum chemistry 2013*. ESQC committee, 2013.

[83] I. Shavitt and R. J. Bartlett, *Many-Body Methods in Chemistry and Physics: MBPT and Coupled-Cluster Theory*. Cambridge Molecular Science, Cambridge University Press, 2009.

[84] R. J. Bartlett and I. Shavitt, "Determination of the size-consistency error in the single and double excitation configuration interaction model," *Int. J. Quantum Chem.*, vol. 12, no. S11, pp. 165–173, 1977.

[85] A. Meunier and B. Levy, "Difficulties in the computation of physical observables due to a truncated CI," *Int. J. Quantum Chem.*, vol. 16, no. 5, pp. 955–972, 1979.

[86] F. Jensen, *Introduction to Computational Chemistry*. John Wiley & Sons Ltd., 2003.

[87] C. J. Cramer, *Essentials of Computational Chemistry*. John Wiley & Sons, Ltd, second ed., 2004.

[88] W. Silvert, "Comparison of Rayleigh–Schrödinger and Brillouin–Wigner perturbation theories," *Am. J. Phys.*, vol. 40, no. 4, pp. 557–561, 1972.

[89] M. J. Frisch, M. Head-Gordon, and J. A. Pople, "A direct MP2 gradient method," *Chem. Phys. Lett.*, vol. 166, no. 3, pp. 275–280, 1990.

[90] T. Helgaker, P. Jørgensen, and N. C. Handy, "A numerically stable procedure for calculating møller-plesset energy derivatives, derived using the theory of lagrangians," *Theor. Chim. Acta*, vol. 76, no. 4, pp. 227–245, 1989.

[91] E. S. Kryachko and E. V. Ludeña, "Density functional theory: Foundations reviewed," *Phys. Rep.*, vol. 544, no. 2, pp. 123–239, 2014.

[92] N. Pieniazek, F. ando R. Clemente, and K. N. Houk, "Sources of error in DFT computations of C–C bond formation thermochemistries: $\pi-\sigma$ transformations and error cancellation by DFT methods," *Angew. Chem. Int. Ed.*, vol. 47, no. 40, pp. 7746–7749, 2008.

[93] D. R. B. Brittain, C. Y. Lin, A. T. B. Gilbert, E. I. Izgorodina, P. M. W. Gill, and M. L. Coote, "The role of exchange in systematic DFT errors for some organic reactions," *Phys. Chem. Chem. Phys.*, vol. 11, pp. 1138–1142, 2009.

[94] P. Hohenberg and W. Kohn, "Inhomogeneous electron gas," *Phys. Rev.*, vol. 136, pp. B864–B871, Nov 1964.

[95] J. K. Percus, "The role of model systems in the few-body reduction of the n-fermion problem," *Int. J. Quantum Chem.*, vol. 13, no. 1, pp. 89–124, 1978.

[96] M. Levy, "Universal variational functionals of electron densities, first-order density matrices, and natural spin-orbitals and solution of the v-representability problem," *Proc. Natl. Acad. Sci. USA*, vol. 76, no. 12, pp. 6062–6065, 1979.

[97] E. H. Lieb, "Density functionals for Coulomb-systems," *Int. J. Quantum Chem.*, vol. 24, no. 3, pp. 243–277, 1983.

[98] M. Levy, "Electron densities in search of hamiltonians," *Phys. Rev. A*, vol. 26, pp. 1200–1208, Sep 1982.

[99] S. Reimann, *Treatment of Magnetic Fields in Density-Functional Theory*. PhD thesis, University of Oslo, 2018.

[100] M. Ernzerhof, "Construction of the adiabatic connection," *Chem. Phys. Lett.*, vol. 263, no. 3, pp. 499–506, 1996.

[101] C. Adamo and V. Barone, "Toward reliable adiabatic connection models free from adjustable parameters," *Chem. Phys. Lett.*, vol. 274, no. 1, pp. 242–250, 1997.

[102] Q. Wu and W. Yang, "A direct optimization method for calculating density functionals and exchange-correlation potentials from electron densities," *J. Chem. Phys.*, vol. 118, no. 6, pp. 2498–2509, 2003.

[103] R. A. Harris and F. R. Salsbury Jr., "The exchange energy functional in a weak magnetic field," *J. Chem. Phys.*, vol. 109, no. 7, pp. 2609–2613, 1998.

[104] C. J. Grayce and R. A. Harris, "Magnetic-field density-functional theory," *Phys. Rev. A*, vol. 50, no. 4, pp. 3089–3095, 1994.

[105] S. Reimann, A. Borgoo, E. I. Tellgren, A. M. Teale, and T. Helgaker, "Magnetic-field density-functional theory (BDFT): Lessons from the adiabatic connection," *J. Chem. Theory Comput.*, vol. 13, pp. 4089–4100, 2017.

[106] E. I. Tellgren, A. M. Teale, J. W. Furness, K. K. Lange, U. Ekström, and T. Helgaker, "Non-perturbative calculation of molecular magnetic properties within current-density functional theory," *J. Chem. Phys.*, vol. 140, no. 3, p. 034101, 2014.

[107] J. W. Furness, J. Verbeke, E. I. Tellgren, S. Stopkowicz, U. Ekström, T. Helgaker, and A. M. Teale, "Current density functional theory using meta-generalized gradient exchange-correlation functionals," *J. Chem. Theory Comput.*, vol. 11, no. 9, pp. 4169–4181, 2015.

[108] A. Laestadius, "Density functionals in the presence of magnetic field," *Int. J. Quantum Chem.*, vol. 114, no. 21, pp. 1445–1456, 2014.

[109] O. B. Lutnæs, A. M. Teale, T. Helgaker, D. J. Tozer, K. Ruud, and J. Gauss, "Benchmarking density-functional-theory calculations of rotational g tensors and magnetizabilities using accurate coupled-cluster calculations," *J. Chem. Phys.*, vol. 131, no. 14, p. 144104, 2009.

[110] J. Tao, J. P. Perdew, V. N. Staroverov, and G. E. Scuseria, "Climbing the density functional ladder: Nonempirical meta–generalized gradient approximation designed for molecules and solids," *Phys. Rev. Lett.*, vol. 91, p. 146401, 2003.

[111] M. J. Allen, T. W. Keal, and D. J. Tozer, "Improved NMR chemical shifts in density functional theory," *Chem. Phys. Lett.*, vol. 380, no. 1, pp. 70 – 77, 2003.

[112] R. H. Garstang, "Atoms in high magnetic fields (white dwarfs)," *Rep. Prog. Phys.*, vol. 40, no. 2, pp. 105–154, 1977.

[113] R. Eliassen, R. T. Skrinde, and W. B. Davis, "Experimental performance of 'miracle' water conditioners," *J. AWWA*, vol. 50, no. 10, pp. 1371–1385, 1958.

[114] S. Reimann, U. Ekström, S. Stopkowicz, A. M. Teale, A. Borgoo, and T. Helgaker, "The importance of current contributions to shielding constants in density-functional theory," *Phys. Chem. Chem. Phys.*, vol. 17, pp. 18834–18842, 2015.

[115] A. M. Lee, N. C. andy, and S. M. Colwell, "The density functional calculation of nuclear shielding constants using London atomic orbitals," *J. Chem. Phys.*, vol. 103, no. 23, pp. 10095–10109, 1995.

[116] W. Zhu, L. Zhang, and S. B. Trickey, "Comparative studies of density-functional approximations for light atoms in strong magnetic fields," *Phys. Rev. A*, vol. 90, p. 022504, 2014.

[117] M. D. Jones, G. Ortiz, and D. M. Ceperley, "Spectrum of neutral helium in strong magnetic fields," *Phys. Rev. A*, vol. 59, no. 4, pp. 2875–2885, 1999.

[118] W. Becken and P. Schmelcher, "Electromagnetic transitions of the helium atom in a strong magnetic field," *Phys. Rev. A*, vol. 65, no. 3, p. 033416, 2002.

[119] O.-A. a. Al-Hujaj and P. Schmelcher, "Beryllium in strong magnetic fields," *Phys. Rev. A*, vol. 70, no. 2, p. 023411, 2004.

[120] M. V. Ivanov and P. Schmelcher, "Ground state of the carbon atom in strong magnetic fields," *Phys. Rev. A*, vol. 60, no. 5, pp. 3558–3568, 1999.

[121] M. V. Ivanov and P. Schmelcher, "Ground states of H, He, ..., Ne, and their singly positive ions in strong magnetic fields: The high-field regime," *Phys. Rev. A*, vol. 61, no. 2, p. 022505, 2000.

[122] U. Kappes and P. Schmelcher, "On the topology of the adiabatic potential energy surfaces of the H_2^+-ion in a strong magnetic field," *Phys. Lett. A*, vol. 210, no. 6, pp. 409–415, 1996.

[123] U. Kappes and P. Schmelcher, "Adiabatic potential-energy surfaces for higher excited states of the H_2^+ ion in a strong magnetic field," *Phys. Rev. A*, vol. 54, no. 2, pp. 1313–1317, 1996.

[124] U. Kappes and P. Schmelcher, "Adiabatic potential-energy surfaces of the H_2^+ ion in a strong magnetic field," *Phys. Rev. A*, vol. 53, no. 6, pp. 3869–3883, 1996.

[125] U. Kappes, P. Schmelcher, and T. Pacher, "Influence of a strong magnetic field on the chemical bond of the excited H_2^+ ion," *Phys. Rev. A*, vol. 50, no. 5, pp. 3775–3781, 1994.

[126] A. V. Turbiner and N. L. Guevara, "The HeH^+ molecular ion in a magnetic field," *J. Phys. B: At. Mol. Opt. Phys.*, vol. 40, no. 16, pp. 3249–3257, 2007.

[127] A. V. Turbiner and N. L. Guevara, "He_2^{2+} molecular ion can exist in a magnetic field," *Phys. Rev. A*, vol. 74, no. 6, p. 063419, 2006.

[128] J. Ozaki, "The change in character of the even z-parity states from antibonding to bonding in the H_2^+ ion by strong magnetic fields," *Chem. Phys. Lett.*, vol. 203, no. 2-3, pp. 184–188, 1993.

[129] D. Lai and E. E. Salpeter, "Motion and ionization equilibrium of hydrogen atoms in a superstrong magnetic field," *Phys. Rev. A*, vol. 52, pp. 2611–2623, 1995.

[130] T. Detmer, P. Schmelcher, and L. S. Cederbaum, "Hydrogen molecule in a magnetic field: The lowest states of the π manifold and the global ground state of the parallel configuration," *Phys. Rev. A*, vol. 57, no. 3, pp. 1767–1777, 1998.

[131] A. Ishikawa, H. Nakashima, and H. Nakatsuji, "Accurate solutions of the Schrödinger and Dirac equations of H_2^+, HD^+, and HT^+: With and without Born–Oppenheimer approximation and under magnetic field," *Chem. Phys.*, vol. 401, pp. 62–72, 2012.

[132] H. Nakashima and H. Nakatsuji, "Solving the Schrödinger and Dirac equations for a hydrogen atom in the universe's strongest magnetic fields with the free complement method," *Astrophys. J.*, vol. 725, no. 1, pp. 528–533, 2010.

[133] A. V. Turbiner and J. C. Vieyra, "One-electron molecular systems in a strong magnetic field," *Phys. Rep.*, vol. 424, no. 6, pp. 309–396, 2006.

[134] J. Vaara, P. Manninen, and J. Lounila, "Magnetic field dependence of nuclear magnetic shielding in closed-shell atomic systems," *Chem. Phys. Lett.*, vol. 372, no. 5-6, pp. 750–757, 2003.

[135] P. Manninen and J. Vaara, "Magnetic-field dependence of Co-59 nuclear magnetic shielding in Co(III) complexes," *Phys. Rev. A*, vol. 69, no. 2, p. 022503, 2004.

[136] A. Thirumalai, , and J. S. Heyl, "Two-dimensional pseudospectral Hartree–Fock method for low-z atoms in intense magnetic fields," *Phys. Rev. A*, vol. 89, p. 052522, 2014.

[137] A. Thirumalai, , S. J. Desch, and P. Young, "Carbon atom in intense magnetic fields," *Phys. Rev. A*, vol. 90, p. 052501, 2014.

[138] A. Thirumalai, , and J. S. Heyl, "Hydrogen and helium atoms in strong magnetic fields," *Phys. Rev. A*, vol. 79, p. 012514, 2009.

[139] S. Xu, M. Jura, D. Koester, B. Klein, and B. Zuckerman, "Discovery of molecular hydrogen in white dwarf atmospheres," *Astrophys. J.*, vol. 766, no. 2, p. L18, 2013.

[140] B. Gustafsson and N. Olander, "The effects of molecules on the structure of stellar atmospheres," *Phys. Scripta*, vol. 20, no. 5-6, pp. 570–574, 1979.

[141] C. R. Greenshields, R. L. Stamps, S. Franke-Arnold, and S. M. Barnett, "Is the angular momentum of an electron conserved in a uniform magnetic field?," *Phys. Rev. Lett.*, vol. 113, p. 240404, 2014.

[142] E. I. Tellgren, A. L., T. Helgaker, S. Kvaal, and A. M. Teale, "Uniform magnetic fields in density-functional theory," *J. Chem. Phys.*, vol. 148, p. 024101, 2018.

[143] B. R. Johnson, J. O. Hirschfelder, and K.-H. Yang, "Interaction of atoms, molecules, and ions with constant electric and magnetic fields," *Rev. Mod. Phys.*, vol. 55, no. 1, pp. 109–153, 1983.

[144] J. S. Sims and S. Hagstrom, "Combined configuration-interaction—Hylleraas-type wave-function study of the ground state of the beryllium atom," *Phys. Rev. A*, vol. 4, pp. 908–916, Sep 1971.

[145] X.-F. Pang and B. Deng, "The changes of macroscopic features and microscopic structures of water under influence of magnetic field," *Physica B*, vol. 403, no. 19-20, pp. 3571–3577, 2008.

[146] S. A. Ghauri and M. S. Ansari, "Increase of water viscosity under the influence of magnetic field," *J. Appl. Phys.*, vol. 100, no. 6, p. 066101, 2006.

[147] H. Hosoda, H. Mori, N. Sogoshi, A. Nagasawa, and S. Nakabayashi, "Refractive indices of water and aqueous electrolyte solutions under high magnetic fields," *J. Phys. Chem. A*, vol. 108, no. 9, pp. 1461–1464, 2004.

[148] H. Inaba, T. Saitou, K.-i. Tozaki, and H. Hayashi, "Effect of the magnetic field on the melting transition of H_2O and D_2O measured by a high resolution and supersensitive differential scanning calorimeter," *J. Appl. Phys*, vol. 96, no. 11, pp. 6127–6132, 2004.

[149] K. X. Zhou, G. W. Lu, Q. C. Zhou, J. H. Song, S. T. Jiang, and H. R. Xia, "Monte carlo simulation of liquid water in a magnetic field," *J. Appl. Phys.*, vol. 88, no. 4, pp. 1802–1805, 2000.

[150] E. J. Toledo, T. C. Ramalho, and Z. M. Magriotis, "Influence of magnetic field on physical–chemical properties of the liquid water: Insights from experimental and theoretical models," *J. Mol. Struct.*, vol. 888, no. 1, pp. 409 – 415, 2008.

[151] F. N. Keutsch, L. B. Braly, M. G. Brown, H. A. Harker, P. B. Petersen, C. Leforestier, and R. J. Saykally, "Water dimer hydrogen bond stretch, donor torsion overtone, and "in-plane bend" vibrations," *J. Chem. Phys.*, vol. 119, no. 17, pp. 8927–8937, 2003.

[152] Ministry of Health and Care Services, "Forskrift om vannforsyning og drikkevann (2016-12-22-1868)." §5, first sentence, letter a, attachment 1.

[153] U. Góra, R. Podeszwa, W. Cencek, and K. Szalewicz, "Interaction energies of large clusters from many-body expansion," *J. Chem. Phys.*, vol. 135, no. 22, p. 224102, 2011.

Paper I

Kohn–Sham energy decomposition for molecules in a magnetic field

Sarah Reimann, Alex Borgoo, Jon Austad, Erik I. Tellgren, Andrew M. Teale, Trygve U. Helgaker and Stella Stopkowicz.
Molecular Physics, 2019, **volume 117**, No. 1, pages 97 to 109.

Paper II

Bonding in strong magnetic fields: role of spin and angular momentum

Jon Austad, Alex Borgoo, Erik I. Tellgren and Trygve Helgaker.
Submitted for publication in PCCP

II

Bonding in the helium dimer in strong magnetic fields: the role of spin and angular momentum

Jon Austad,[1] Alex Borgoo,[1] Erik I. Tellgren,[1,*] and Trygve Helgaker[1,†]

[1] *Hylleraas Centre for Quantum Molecular Sciences, Department of Chemistry, University of Oslo, P.O. Box 1033 Blindern, N-0315 Oslo, Norway*

We investigate the helium dimer in strong magnetic fields, focusing on the spectrum of low-lying electronic states and their dissociation curves, at the full configuration-interaction level of theory. To address the loss of cylindrical symmetry and angular momentum as a good quantum number for nontrivial angles between the bond axis and magnetic field, we introduce the almost quantized angular momentum (AQAM) and show that it provides useful information about states in arbitrary orientations. In general, strong magnetic fields dramatically rearrange the spectrum, with the orbital Zeeman effect bringing down states of higher angular momentum below the states with pure σ character as the field strength increases. In addition, the spin Zeeman effect pushes triplet states below the lowest singlet; in particular, a field of one atomic unit is strong enough to push a quintet state below the triplets. In general, the angle between the bond axis and the magnetic field also continuously modulates the degree of σ, π, and δ character of bonds and the previously identified perpendicular paramagnetic bonding mechanism is found to be common among excited states. Electronic states with preferred skew field orientations are identified and rationalized in terms of permanent and induced electronic currents.

I. INTRODUCTION

It has long been known that strong magnetic fields dramatically affect the physics and chemistry of molecules [1, 2]. In the atmospheres of neutron stars, intense magnetic fields, orders of magnitudes stronger than one atomic unit $B_0 = 235\,\mathrm{kT}$, dominate the electrostatic forces, resulting in highly prolate, or even needle-like, charge distributions around atoms. In such ultrastrong magnetic fields, matter is expected to consist of long chains of atoms, oriented parallel to the magnetic field vector. The strong field regime $0.1B_0 < B < B_0$ is interesting as the direct magnetic effects and electrostatic forces in small molecules are on the same order of magnitude, leading to novel and complicated bonding mechanisms. This regime corresponds to the upper range of magnetic field strengths encountered in magnetic white dwarf (MWD) stars.

In the strong and ultrastrong field regimes, atomic spectra and chemical bonding become modified. Calculated helium spectra have assisted the interpretation of observed spectra from the atmosphere of MWDs [3, 4], supplementing the well-established use of hydrogen lines to analyse MWDs. The magnetic field dependence of energy levels in hydrogen [5], hydrogen anions [6], helium [7–9], and other small atoms [10–13] have been subject to several studies. Even one-electron molecular ions exhibit a rich phenomenology to explore [14]. Many otherwise unstable few-electron ions, such as He^-, HeH^+, and He_2^{2+}, become stabilized in external magnetic fields [15–17]. Several studies have focused on potential-energy surfaces and the modification of bonding in H_2^+ and H_2 subject to strong fields [18–22]. Most studies have been restricted to the parallel orientation as this is by far the easiest to study. However, a few studies of varying accuracy have found that the H_2 triplet state becomes stabilized in a perpendicular magnetic field [23–27], subsequently explained based on high-quality quantum-chemical calculations as an orientation-dependent stabilization of the antibonding σ-orbital [28]. This effect, termed perpendicular paramagnetic bonding, is also seen in singlet helium clusters and other diatomic molecules [29, 30].

While the highest field strengths available in the laboratory are two to three orders of magnitude below B_0 [31–34], quasiparticles in semiconductors can have effective masses much below that of a bare electron and exhibit analogous effects at lower field strengths. Notably, quasiparticle analogues to perpendicular paramagnetic bonding have already been reported [35, 36]. Rydberg states, which are sensitive to magnetic fields due to their diffuseness and high angular momenta [37, 38], are another promising candidate for analogous effects.

In what follows, we report a computational study of the chemical bonding of the helium dimer. Potential-energy surfaces are mapped for low-lying states of singlet, triplet, and quintet total spin, subject to strong magnetic fields of arbitrary orientation. We use a finite-field approach, where the magnetic-field effects are incorporated directly without perturbative approximations. Although higher-order perturbation theory is sometimes an alternative to probe high-field effects [39–44], a nonperturbative approach is needed to study reliably potential-energy surfaces and level crossings in a strong field. To handle the gauge-origin problem and ensure faster basis-set convergence, we employ London atomic orbitals [45–48]. Without a solution the gauge-origin problem, potential-energy surfaces suffer from a spurious parabolic distance dependence and become qualitatively wrong in a magnetic field. Unlike perturbative approaches, the

* erik.tellgren@kjemi.uio.no
† t.u.helgaker@kjemi.uio.no

present non-perturbative approach necessitates an unconventional integral evaluation scheme, such as the one reported for the LONDON program package [49, 50] or the subsequent approaches in the BAGEL [51], QUEST [52], and CHRONUSQ [53, 54] packages. For the smallest systems, the extremely accurate free-complement method is also an option [55, 56].

The outline of this article is as follows. First, in Sec. II, we specify the electronic Hamiltonian and the quantum-chemical model. We also introduce a new way to classify electronic states and discuss perpendicular paramagnetic bonding involving higher-angular-momentum states. Moreover, we discuss a simple analytical model that gives insight into bonding in strong fields. In Sec. III, we present results for singlet, triplet, and quintet states of the helium dimer in a strong magnetic field. Finally, we summarize the conclusions in Sec. V.

II. THEORY

In the presence of a uniform magnetic field $\mathbf{B}$, the standard nonrelativistic Hamiltonian for N electrons is in SI-based atomic units given by

$$\hat{H} = \frac{1}{2}\sum_{j=1}^{N}\hat{\pi}_j^2 + \sum_{j=1}^{N}\mathbf{B}\cdot\hat{\mathbf{S}}_j + \sum_{j=1}^{N}v(\mathbf{r}_j) + \sum_{j<l}\frac{1}{r_{jl}}. \quad (1)$$

where $\hat{\mathbf{S}}_j$ is the spin operator for the jth electron, $v(\mathbf{r}_j)$ is the electrostatic potential from the nuclei at the position of the jth electron, $\hat{\boldsymbol{\pi}}_j = -\mathrm{i}\nabla_j + \mathbf{A}(\mathbf{r}_j)$ is the mechanical momentum operator, to be distinguished from the canonical momentum operator $\hat{\mathbf{p}}_j = -i\nabla_j$, and $\mathbf{A}(\mathbf{r}_j)$ is the magnetic vector potential at $\mathbf{r}_j$. Restriction of the vector potential to the linear form $\mathbf{A}(\mathbf{r}) = \frac{1}{2}\mathbf{B}\times(\mathbf{r}-\mathbf{G})$ reduces the gauge freedom to the position of the gauge origin $\mathbf{G}$.

An efficient way to handle this gauge-origin freedom is to use London atomic orbitals [45–48], leading to gauge-origin invariant results and faster basis-set convergence; see Ref. [57] for a more general perspective. Given a Gaussian-type orbital $\chi(\mathbf{r})$ centred at $\mathbf{C}$, the corresponding London atomic orbital is $\omega(\mathbf{r}) = \mathrm{e}^{-\mathrm{i}\mathbf{A}(\mathbf{C})\cdot\mathbf{r}}\chi(\mathbf{r})$. Hence, ω is product of a Gaussian and a plane wave with wave vector $\mathbf{q} = \mathbf{A}(\mathbf{C})$. The resulting nonstandard integrals, including the two-electron four-centre Coulomb integrals, are evaluated using the LONDON program [49, 50]. This program package also contains a number of electronic structure models [28, 30, 58–60]. We here use the full configuration-interaction (FCI) model [28] to be able to handle exact degeneracies and quasidegeneracies that inevitably arise when parameters such as bond distances and external magnetic fields are varied over large intervals.

A. Classification of states using an approximately quantized angular momentum

In the present section, we shall not be concerned with the spin contribution to angular momentum. For a given state Ψ, the gauge-invariant, physical angular momentum relative to a point $\mathbf{D}$ may then be defined as $\mathbf{J}_\mathbf{D} = \langle\Psi|\sum_j(\mathbf{r}_j-\mathbf{D})\times\hat{\boldsymbol{\pi}}_j|\Psi\rangle$. In fact, since $\langle\Psi|\sum_j\hat{\boldsymbol{\pi}}_j|\Psi\rangle$ vanishes in the complete basis-set limit for any variationally optimized state, the physical angular momentum is independent of the reference point. The gauge-dependent, canonical angular momentum is likewise given by the expectation value $\mathbf{L}_\mathbf{D} = \langle\Psi|\sum_j(\mathbf{r}_j-\mathbf{D})\times\hat{\mathbf{p}}|\Psi\rangle$. Introducing the density and paramagnetic current density,

$$\rho(\mathbf{r}) = \sum_{j=1}^{N}\langle\Psi|\delta(\mathbf{r}-\mathbf{r}_j)|\Psi\rangle, \quad (2)$$

$$\mathbf{j}_\mathrm{p}(\mathbf{r}) = \frac{1}{2}\sum_{j=1}^{N}\langle\Psi|\delta(\mathbf{r}-\mathbf{r}_j)\hat{\mathbf{p}}_j + \hat{\mathbf{p}}_j\delta(\mathbf{r}-\mathbf{r}_j)|\Psi\rangle, \quad (3)$$

the canonical momentum can also be calculated as $\mathbf{L}_\mathbf{D} = \int(\mathbf{r}-\mathbf{D})\times\mathbf{j}_\mathrm{p}\mathrm{d}\mathbf{r}$. Under a gauge transformation with gauge function f, we have $\mathbf{A}\mapsto\mathbf{A}+\nabla f$, $\mathbf{j}_\mathrm{p}\mapsto\mathbf{j}_\mathrm{p}-\rho\nabla f$, and $\mathbf{L}_\mathbf{D}\mapsto\mathbf{L}_\mathbf{D}-\int(\mathbf{r}-\mathbf{D})\times\rho\nabla f\mathrm{d}\mathbf{r}$. Despite its gauge dependence, the canonical angular momentum is sometimes useful for classifying states.

When both the electrostatic potential and the magnetic vector potential are cylindrically symmetric, the component of $\mathbf{L}_\mathbf{G}$ parallel to the symmetry axis is a good quantum number. In general, for a diatomic molecule in a non-parallel magnetic field, canonical momentum ceases to be a good quantum number—also the dissociation limit, since the total system is not cylindrically symmetric even though cylindrical symmetry is restored for the individual subsystems (dissociated atoms). Unlike the physical angular momentum, the canonical momentum depends on a global reference position. To restore quantization in the dissociation limit, the angular momentum of a subsystem instead needs to be evaluated with respect to the symmetry centre of that subsystem, and the wave function must be gauge transformed to correspond to what is obtained in a calculation with gauge origin adapted to the subsystem.

We now consider the idealized case where each isolated subsystem α is cylindrically symmetric about its electronic centre of mass $\mathbf{C}_\alpha$. In a calculation of the isolated system, with the gauge origin placed at $\mathbf{C}_\alpha$, the resulting density ρ_α and paramagnetic current density $\mathbf{j}'_{\mathrm{p};\alpha}$ are cylindrically symmetric too. Moreover, the canonical angular momentum relative to $\mathbf{C}_\alpha$ is

$$\mathbf{L}'_\alpha = \int(\mathbf{r}-\mathbf{C}_\alpha)\times\mathbf{j}'_{\mathrm{p};\alpha}(\mathbf{r})\,\mathrm{d}\mathbf{r}, \quad (4)$$

and the component parallel to $\mathbf{B}$ is quantized. In the limit of a complete basis, the mechanical linear momentum must vanish for any energy eigenstate. Using the

fact that $\mathbf{C}_\alpha$ is the subsystem centre of mass, we see that the paramagnetic and diamagnetic contributions must vanish separately,

$$\begin{aligned}\boldsymbol{\pi}_\alpha &= \int \big(\mathbf{j}'_{\mathrm{p};\alpha}(\mathbf{r}) + \frac{1}{2}\rho_\alpha(\mathbf{r})\,\mathbf{B}\times(\mathbf{r}-\mathbf{C}_\alpha)\big)\mathrm{d}\mathbf{r} \\ &= \int \mathbf{j}'_{\mathrm{p};\alpha}(\mathbf{r})\,\mathrm{d}\mathbf{r} = \mathbf{0}. \end{aligned} \tag{5}$$

Next, consider the total system. The gauge origin $\mathbf{G}$ cannot coincide with all subsystem centres $\mathbf{C}_\alpha$. Hence, the subsystem paramagnetic current densities obtained from a calculation on the total systems are gauge transformed according to

$$\mathbf{j}_{\mathrm{p};\alpha}(\mathbf{r}) = \mathbf{j}'_{\mathrm{p};\alpha}(\mathbf{r}) + \frac{1}{2}\rho_\alpha(\mathbf{r})\,\mathbf{B}\times(\mathbf{G}-\mathbf{C}_\alpha). \tag{6}$$

The subsystem contribution to the total angular momentum about a global reference point $\mathbf{D}$ thus becomes

$$\mathbf{L}_{\mathbf{D},\alpha} = \int (\mathbf{r}-\mathbf{D})\times\mathbf{j}_{\mathrm{p};\alpha}(\mathbf{r})\,\mathrm{d}\mathbf{r}, \tag{7}$$

or, using the relations established above,

$$\begin{aligned}\mathbf{L}_{\mathbf{D},\alpha} = \int\Big((\mathbf{r}-\mathbf{D})\times\mathbf{j}'_{\mathrm{p};\alpha}(\mathbf{r}) \\ +\frac{1}{2}\rho_\alpha(\mathbf{r})\,(\mathbf{r}-\mathbf{D})\times(\mathbf{B}\times(\mathbf{G}-\mathbf{C}_\alpha))\Big)\,\mathrm{d}\mathbf{r}.\end{aligned} \tag{8}$$

Writing $N_\alpha = \int\rho_\alpha(\mathbf{r})\mathrm{d}\mathbf{r}$ for the number of electrons in a subsystem and using Eq. (5), we obtain in the basis-set limit

$$\mathbf{L}_{\mathbf{D},\alpha} = \mathbf{L}'_\alpha + \frac{N_\alpha}{2}(\mathbf{C}_\alpha-\mathbf{D})\times(\mathbf{B}\times(\mathbf{G}-\mathbf{C}_\alpha)). \tag{9}$$

Whereas the total canonical angular momentum

$$\mathbf{L}_\mathbf{D} = \sum_\alpha \mathbf{L}_{\mathbf{D},\alpha} \tag{10}$$

exhibits a gauge-dependent quadratic growth with the distances $|\mathbf{C}_\alpha-\mathbf{C}_\beta|^2$ between different subsystems, we can now subtract the quadratic terms to obtain

$$\begin{aligned}\boldsymbol{\Lambda} &= \sum_\alpha\Big(\mathbf{L}_{\mathbf{D},\alpha} - \frac{N_\alpha}{2}(\mathbf{C}_\alpha-\mathbf{D})\times(\mathbf{B}\times(\mathbf{G}-\mathbf{C}_\alpha))\Big) \\ &= \sum_\alpha \mathbf{L}'_\alpha. \end{aligned} \tag{11}$$

We term $\boldsymbol{\Lambda}$ the *approximately quantized angular momentum* (AQAM) since, for a diatomic molecule, its projection $\Lambda_\mathbf{B} = \mathbf{e}_\mathbf{B}\cdot\boldsymbol{\Lambda}$ onto the field direction $\mathbf{e}_\mathbf{B} = \mathbf{B}/|\mathbf{B}|$ exhibits exact quantization for all parallel orientations as well as in the dissociation limit. In other cases, $\Lambda_\mathbf{B}$ is often approximately quantized, despite the presence of interactions between subsystems. This quantity therefore provides a useful generalization of the atomic quantum number m_l for classifying the states of a diatomic molecule. A closely related quantity was considered for a different purpose (and with different notation) in a formal density-functional context in Sec. IV.C of Ref. [61].

Finally, we remark that some care is required when interpreting $\frac{1}{2}\mathbf{B}\cdot\boldsymbol{\Lambda}$ as an energy. The physical angular momentum is a sum of two terms: the canonical angular momentum and the diamagnetic contribution. However, the gauge invariant kinetic energy is a sum of three terms: the canonical kinetic energy, the orbital Zeeman term, and the diamagnetic term. Only one of these terms (and the sum of the other two) can be modified to have a well-defined dissociation limit, not all three simultaneously.

TABLE I. Symmetries and bonding properties of molecular orbitals of homonuclear diatomic molecule in a magnetic field. The symbol $\angle$ here indicates an intermediate angle.

$\mathrm{D}_{\infty\mathrm{h}}$ $B=0$	$\mathrm{C}_{\infty\mathrm{h}}$ $B_\parallel$	$\mathrm{C}_{2\mathrm{h}}$ $B_\perp$	C_i $B_\angle$	united-atom limit	preferred orientation	chemical bonding
σ_g^+	σ_g	$\mathrm{a_g}$	$\mathrm{a_g}$	s	$\parallel$	covalent
σ_u^+	σ_u	$\mathrm{b_u}$	$\mathrm{a_u}$	p_0	$\perp$	magnetic
π_u	π_u	$\mathrm{a_u}+\mathrm{b_u}$	$\mathrm{a_u}$	$\mathrm{p}_{\pm1}$	$\parallel$	covalent
π_g	π_g	$\mathrm{a_g}+\mathrm{b_g}$	$\mathrm{a_g}$	$\mathrm{d}_{\pm1}$	$\angle$	magnetic
δ_g	δ_g	$\mathrm{a_g}+\mathrm{b_g}$	$\mathrm{a_g}$	$\mathrm{d}_{\pm2}$	$\parallel$	covalent
δ_u	δ_u	$\mathrm{a_u}+\mathrm{b_u}$	$\mathrm{a_u}$	$\mathrm{f}_{\pm2}$	$\angle$	magnetic

B. Symmetry properties of molecular orbitals

In a magnetic field, the point-group symmetry of He_2 is lower than the symmetry $\mathrm{D}_{\infty\mathrm{h}}$ of the molecule in the absence of a field. In all field orientations, inversion symmetry exists and the molecule therefore belongs to the $\mathrm{C_i}$ point group with the irreps $\mathrm{A_g}$ and $\mathrm{A_u}$. In the parallel and perpendicular field orientations additional symmetry operations exist. In the parallel orientation, rotation about the molecular axis give rise to the $\mathrm{C}_{\infty\mathrm{h}}$ point group with the one-dimensional irreps Σ_g and Σ_u and the two-dimensional irreps Π_g, Π_u, Δ_g, Δ_u,.... The $\mathrm{C}_{\infty\mathrm{h}}$ symmetry group (which does not occur for molecules in the absence of a magnetic field) differs from $\mathrm{D}_{\infty\mathrm{h}}$ by the absence of vertical mirror planes and two-fold perpendicular axes. Finally, in the perpendicular field orientation, we have in addition to inversion symmetry a two-fold symmetry axis along the field direction, giving rise to the $\mathrm{C_{2h}}$ symmetry group with the $\mathrm{A_g}$, $\mathrm{A_u}$, $\mathrm{B_g}$ and $\mathrm{B_u}$ irreps.

In Table I, we compare the symmetries of the molecular orbitals in the field orientations and also with the atomic orbitals in the united atoms limit.

C. Perpendicular paramagnetic bonding

Strong magnetic fields can lead to new exotic bonding mechanisms. Previous work has established that the normally unbound lowest triplet state of the H_2 becomes

bound in a perpendicular magnetic field of strength on the order of $B \sim B_0$. Also the lowest singlet state of the He_2 molecule becomes substantially stabilized and the equilibrium bond length substantially compressed in a perpendicular field. The underlying bonding mechanism, termed *perpendicular paramagnetic bonding*, is that the antibonding σ_u^* orbital develops an angular momentum, which leads to an energetic stabilization by the orbital Zeeman effect [28]. This is true even in a minimal basis of only s orbitals, provided that they are equipped with London gauge factors. The magnitude of the angular momentum of σ_u^* vanishes in the parallel orientation and the net energetic effect is largest in the perpendicular orientation at intermediate bond lengths. By contrast, the bonding σ_g orbital does not develop an angular momentum and is not stabilized by this mechanism.

The above considerations generalize and apply in a somewhat stronger form to higher angular-momentum states. In the parallel orientation, a linear combination of atomic orbitals with atomic quantum numbers $|m_l| \leq M$ can never lead to an angular momentum exceeding M. By contrast, this becomes possible in nonparallel orientations. For example, the cc-pVDZ basis has two s orbitals and three p orbitals for each helium atom. In a dimer with the helium atoms placed on the x axis at $(\pm 1, 0, 0)$ bohr, one finds by diagonalizing the canonical angular-momentum operator (relative to the mid-bond position) that the largest perpendicular components are $L_{\mathbf{0};z} = \pm 1.83\hbar$. If we omit the 1s orbitals, the 2s orbitals, and both the 1s and 2s orbitals on the two atoms, we obtain $L_{\mathbf{0};z} = \pm 1.35\hbar$, $L_{\mathbf{0};z} = \pm 1.06\hbar$ and $L_{\mathbf{0};z} = \pm 1.03\hbar$, respectively. With London gauge factors and a perpendicular field $\mathbf{B} = 0.5\hbar\mathbf{e}_z$, the most negative eigenvalue becomes $L_{\mathbf{0};z} = -2.08\hbar$. Hence, some combination of s and p orbitals acquires a d-orbital character when the orientation is changed from parallel to perpendicular, leading to a lower orbital Zeeman energy, which competes with the diamagnetic energy.

In light of the visual similarity of antisymmetric combinations of *real-valued* p orbitals to real valued d orbitals, it may be surprising that s functions play such a large role in the above example—for example, an antisymmetric linear combination of two p_y orbitals centred at different points on the x axis resembles a d_{xy} orbital. We remark, however, that the canonical angular momentum vanishes for all real valued orbitals and the s functions are needed to produce complex-valued orbitals of the right form to represent an angular momentum of about $\pm 2\hbar$.

A simple analytical model provides further insight into magnetic-field effects on bonding and antibonding orbitals in homonuclear diatomic molecules. Let $G_{\ell m}(\mathbf{r}, \alpha, \mathbf{K}, \mathbf{B})$ denote a solid-harmonic Gaussian orbital of exponent α centred at $\mathbf{K}$ and equipped with a London phase factor for the magnetic field $\mathbf{B}$:

$$\begin{aligned} G_{\ell m}(\mathbf{r}, \alpha, \mathbf{K}, \mathbf{B}) =& c_{\ell,m}(\alpha) \exp\left(-\mathrm{i}(\tfrac{1}{2}\mathbf{B} \times \mathbf{K}) \cdot \mathbf{r}\right) \\ & \times S_{\ell m}(\mathbf{r}_K) \exp\left(-\alpha |\mathbf{r}|_K^2\right). \end{aligned} \tag{12}$$

Here $c_{\ell,m}(\alpha)$ is a normalization constant and $S_{\ell m}(\mathbf{r}_K)$ with $\mathbf{r}_K = \mathbf{r} - \mathbf{K}$ is a solid-harmonic function centred at $\mathbf{K}$ of angular-momentum quantum numbers ℓ and m about the z axis.

Consider now the normalized bonding and antibonding orbitals along the z axis:

$$\begin{aligned} & g^{\pm}_{\ell m}(\mathbf{r}, \alpha, \delta, \mathbf{B}) = C_{\ell m}(\delta, \alpha) \times \\ & \times \left(G_{\ell m}(\mathbf{r}, \alpha, (0,0,+\delta), \mathbf{B}) \pm G_{\ell m}(\mathbf{r}, \alpha, (0,0,-\delta), \mathbf{B})\right), \end{aligned} \tag{13}$$

where $C_{\ell m}(\delta, \alpha)$ is a normalization constant. We are interested in the united-atom limits of these orbitals,

$$G^{\pm}_{\ell m}(\mathbf{r}, \alpha, \mathbf{B}) = \lim_{\delta \to 0^+} g^{\pm}_{\ell m}(\mathbf{r}, \alpha, \delta, \mathbf{B}). \tag{14}$$

Clearly, for the bonding orbitals, we have the field-free standard Gaussian orbital positioned at the origin,

$$G^{+}_{\ell m}(\mathbf{r}, \alpha, \mathbf{B}) = G_{\ell m}(\mathbf{r}, \alpha), \tag{15}$$

in the notation $G_{\ell m}(\mathbf{r}, \alpha) = G_{\ell m}(\mathbf{r}, \alpha, \mathbf{0}, \mathbf{0})$. For the antibonding orbitals, the limit is less trivial. To illustrate, we consider the special case when the magnetic field is oriented perpendicular to the bonding and antibonding orbitals $\mathbf{B}_x = (B, 0, 0)$. We furthermore set the Gaussian exponent equal to the optimal exponent of a free electron in uniform magnetic field, $\alpha_B = B/4$. For $\ell \leq 1$, we then find

$$G^{-}_{0,0}(\mathbf{r}, \alpha_B, \mathbf{B}_x) = \sqrt{\tfrac{B}{2}}(y - \mathrm{i}z) G_{0,0}(\mathbf{r}, \alpha_B), \tag{16}$$

$$G^{-}_{1,\pm 1}(\mathbf{r}, \alpha_B, \mathbf{B}_x) = \sqrt{\tfrac{B}{3}}(y - \mathrm{i}z) G_{1,\pm 1}(\mathbf{r}, \alpha_B), \tag{17}$$

$$\begin{aligned} G^{-}_{1,0}(\mathbf{r}, \alpha_B, \mathbf{B}_x) = & \sqrt{\tfrac{B}{4}}(y - \mathrm{i}z) G_{1,0}(\mathbf{r}, \alpha_B) \\ & - G_{0,0}(\mathbf{r}, \alpha_B). \end{aligned} \tag{18}$$

Noting that $[L_x, y - \mathrm{i}z] = -\hbar(y - \mathrm{i}z)$ we conclude that a magnetic field perpendicular to the antibonding orbital induces a component of the angular momentum about the field axis and perpendicular to the angular momentum about the bond axis. To first order, this will reduce the energy of the antibonding orbital in the united-atom limit relative to the dissociation limit. It is a reasonable assumption that this stabilization of antibonding orbitals occurs at all atomic separations but is stronger the closer the two atoms are to each other—that is, to the united-atom limit.

The total kinetic energy and angular momentum of bonding and antibonding atomic orbitals in the united-atom limit with $\alpha = 1$ are given by

$$T_{\ell m}(\mathbf{B}) = \int G^{\pm}_{\ell m}(\mathbf{r}, 1, \mathbf{B})^* \tfrac{1}{2}\pi_{\mathbf{B}}^2 \, G^{\pm}_{\ell m}(\mathbf{r}, 1, \mathbf{B}) \, \mathrm{d}\mathbf{r}, \tag{19}$$

$$\mathbf{L}_{\ell m}(\mathbf{B}) = \int G^{\pm}_{\ell m}(\mathbf{r}, 1, \mathbf{B})^* \, \mathbf{L} \, G^{\pm}_{\ell m}(\mathbf{r}, 1, \mathbf{B}) \, \mathrm{d}\mathbf{r}, \tag{20}$$

where $\frac{1}{2}\pi_{\mathbf{B}}^2$ is the kinetic-energy operator in the magnetic field and $\mathbf{L}$ the canonical angular-momentum operator. For a fixed Gaussian exponent $\alpha = 1$, we have in Table II

TABLE II. Kinetic energy and angular momentum of bonding and antibonding atomic orbitals in the united-atom limit $G^{\pm}_{\ell,m}$ in a zero magnetic field $\mathbf{B} = \mathbf{0}$ and in the minimizing magnetic field $\mathbf{B} = \mathbf{B}_{\ell m}$. Here $\Delta T_{\ell m}(\mathbf{B}_{\ell m}) = T_{\ell m}(\mathbf{B}_{\ell m}) - T_{\ell m}(\mathbf{0})$ and the components of the angular momentum not listed are zero. Units are E_h for energy, $\hbar$ for angular momentum, and B_0 for magnetic field strength.

	$T_{\ell m}(\mathbf{0})$	$L^z_{\ell m}(\mathbf{0})$	$\Delta T_{\ell m}(\mathbf{B}_{\ell m})$	$L^x_{\ell m}(\mathbf{B}_{\ell m})$	$B_{\ell m}$	$\theta_{\ell m}$
$G^+_{0,0}$	3/2	0	0	0	0	✓
$G^+_{1,\pm1}$	5/2	±1	$-\frac{1}{2}$	0	2	$(90 \pm 90)^\circ$
$G^+_{1,0}$	5/2	0	0	0	0	✓
$G^+_{2,\pm2}$	7/2	±2	$-\frac{4}{3}$	0	$\frac{8}{3}$	$(90 \pm 90)^\circ$
$G^+_{2,\pm1}$	7/2	±1	$-\frac{1}{2}$	0	2	$(90 \pm 90)^\circ$
$G^+_{2,0}$	7/2	0	0	0	0	✓
$G^-_{0,0}$	5/2	0	−0.3	−0.9	2.6	90°
$G^-_{1,\pm1}$	7/2	±1	−1.2	−1.0	2.9	$(90 \pm 35)^\circ$
$G^-_{1,0}$	7/2	0	−0.2	−0.8	2.7	90°
$G^-_{2,\pm2}$	9/2	±2	−2.1	−1.1	3.1	$(90 \pm 48)^\circ$
$G^-_{2,\pm1}$	9/2	±1	−1.2	−1.2	3.4	$(90 \pm 32)^\circ$
$G^-_{2,0}$	9/2	0	−0.7	−1.4	3.2	90°

calculated the kinetic energy and angular momentum of the bonding and antibonding orbitals in the united-atom limit for zero field $\mathbf{B} = \mathbf{0}$ and for the magnetic field $\mathbf{B} = \mathbf{B}_\mathrm{min}$ that minimizes the kinetic energy for $\alpha = 1$:

$$\mathbf{B}_{\ell m} = \underset{\mathbf{B}}{\operatorname{argmin}}\, T_{\ell m}(\mathbf{B}). \tag{21}$$

In the table, we have also listed $B_{\ell m} = |\mathbf{B}_{\ell m}|$ and the angle $\theta_{\ell m}$ of $\mathbf{B}_{\ell m}$ with the z axis (bond axis). We note that, for a free electron in a magnetic field, the optimal Gaussian exponent is $B/4$; for an electron in an atom or molecule up to field strengths of about B_0, the electronic wave function responds less directly to the magnetic field strength. In Fig. 1, we have plotted the kinetic energy of the bonding and antibonding orbitals in the united-atom limit in the xz plane.

The first two columns in Table II contains information about the energies and angular momentum in the absence of a magnetic field. The kinetic energy is $(\ell + 3/2)E_\mathrm{h}$ and $(\ell + 5/2)E_\mathrm{h}$ for bonding and antibonding orbitals, respectively, the higher energy of the antibonding arising from the presence of an additional nodal plane in the orbital.

Turning our attention to the orbitals in the minimizing magnetic field $\mathbf{B}_{\ell m}$, we note that

$$\Delta T_{\ell m}(\mathbf{B}_{\ell m}) = T_{\ell m}(\mathbf{B}_{\ell m}) - T_{\ell m}(\mathbf{0}) \tag{22}$$

is zero or negative. Furthermore, the only orbitals whose global energy minimum occurs at zero field are the bonding orbitals with $m = 0$. For bonding orbitals with $m < 0$, the energy is lowered by applying a field parallel with the quantization axis (bond axis); if $m > 0$, the same minimum energy is obtained by applying a magnetic field of the same magnitude but in the opposite direction. As expected, the energy minimum becomes deeper and the minimizing field stronger with increasing value of $|m|$. We note that the energy minimization of the bonding orbitals is the same in the united-atom and dissociation limits, being associated with the permanent angular momentum in the system. We also note that, in a sufficiently strong field, the energy of the orbitals will increase diamagnetically, for all field orientations

For antibonding orbitals in the united-atom limit, the energy is in all cases reduced by the magnetic field and in all cases significantly more than for the corresponding bonding orbitals. At the same time, an angular momentum is induced in the direction of the magnetic field, as predicted from Eqs. (16)–(18). The resulting total angular momentum is then no longer parallel to the bond axis and the minimizing magnetic field is no longer parallel or antiparallel to the z axis. Indeed, for orbitals with $m = 0$, the preferred field orientation is perpendicular to the bond axis, while for orbitals with $m \neq 0$, the preferred field orientation is skewed relative to the bond axis. We note that the energy lowering arising from the induced angular momentum vanishes in the dissociation limit, unlike the energy lowering arising from the permanent angular momentum.

III. RESULTS

The spectrum of He_2 depends on the bond length R, the strength of the magnetic field B, and the angle θ between the field and the bond axis. We have employed the LONDON program [49, 50] to map out the spectrum as a function of these parameters. Basis sets are denoted by standard notation amended by prefixes 'L' and 'u' to indicate London gauge factors and uncontracted functions, respectively. The calculations have been carried out at the FCI/Lu-aug-cc-pVTZ level unless otherwise indicated. All bond distances are reported in units of $a_0 = 1$ bohr.

A. Dissociation limit: helium atom

In the limit of an infinite bond distance, the helium dimer becomes two isolated helium atoms. The atomic spectrum, calculated at the FCI/Lu-aug-cc-pVQZ level, is shown in Fig. 2, with singlet- and triplet-state energies plotted along the negative and positive axes, respectively.

While the diamagnetic $^1\Sigma_\mathrm{g}(1\mathrm{s}^2)$ singlet state is the lowest singlet in the plotted field interval (and also the ground state up to about $0.8B_0$), the remaining singlets in the plot undergo several level crossings. In particular, due to the orbital Zeeman interaction, the $^1\Pi_\mathrm{u}(1\mathrm{s}2\mathrm{p}_{-1})$ state crosses the $^1\Sigma_\mathrm{g}(1\mathrm{s}2\mathrm{s})$ state to become the first excited singlet state at about $0.1B_0$. At a magnetic field strength of about $1B_0$, the paramagnetic $^1\Delta_\mathrm{g}(1\mathrm{s}3\mathrm{d}_{-2})$ state has been sufficiently stabilized to become the second excited singlet state, having crossed in turn the four dia-

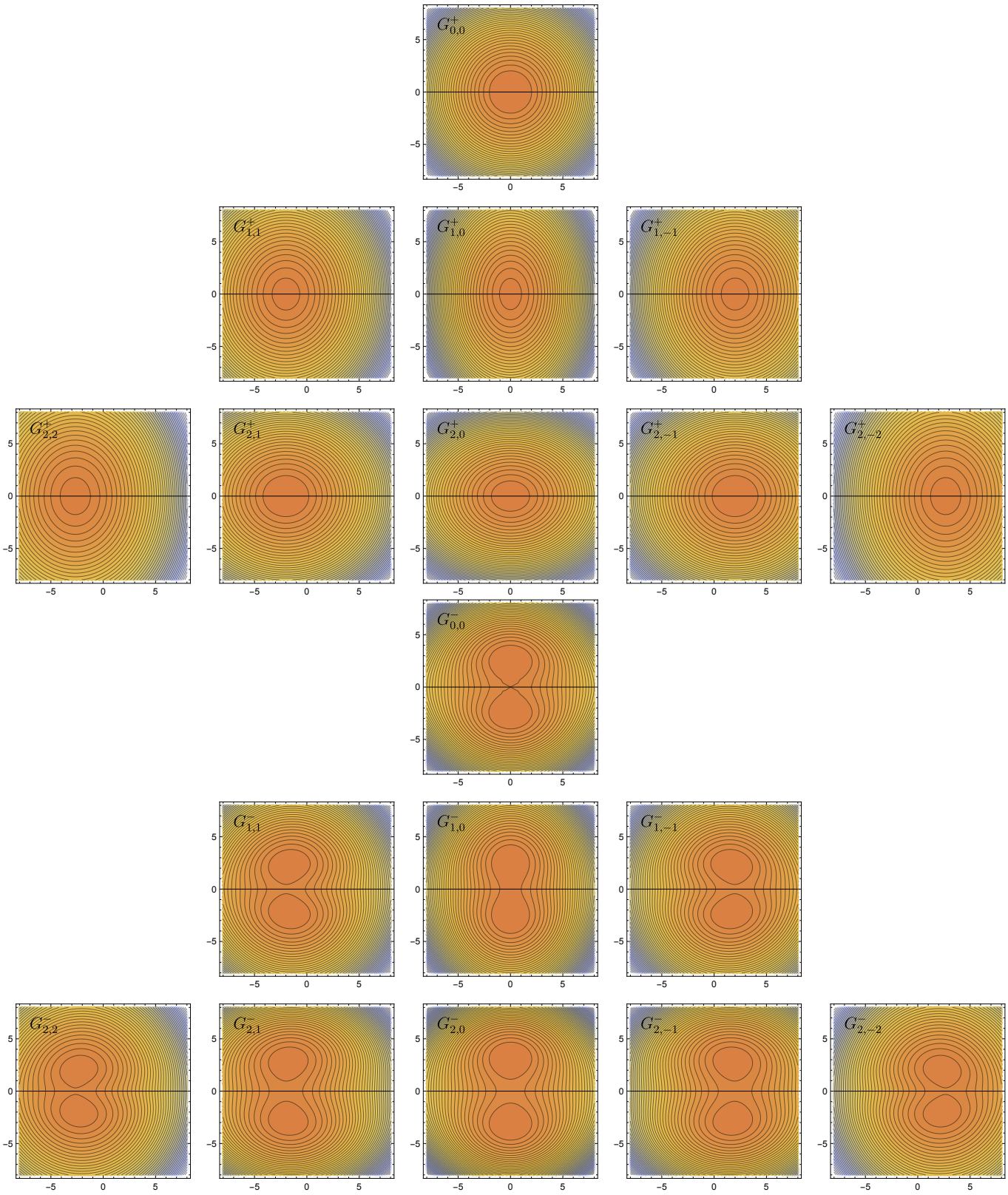

FIG. 1. Contour plots of the kinetic energy of bonding and antibonding orbitals in the united-atom limit as a function of magnetic field strength **B** in the zx plane; with the z axis marked by a horizontal line. For bonding orbitals, the minimum is located on the z axis; for the antibonding orbitals, the minima are located away from the z axis, symmetrically on each side.

magnetic states $^1\Sigma_g(1s3s)$, $^1\Pi_u(1s2p_{+1})$, $^1\Sigma_g(1s2s)$, and $^1\Sigma_u(1s2p_0)$ with increasing field strength.

Most singlet states have analogues in the triplet spectrum. However, because of the the spin Zeeman interaction, the triplet states are split, the $m_s = -1$ components (with two spin-down electrons) being stabilized more than the corresponding singlet states. Additional stabilization may be provided by the orbital Zeeman interaction. Thus, while the lowest triplet state is $^3\Sigma_g(1s\,2s)$ in weak magnetic fields, the $^3\Pi_u(1s\,2p_{-1})$ state becomes the lowest triplet at $0.2B_0$ and the ground state at about $0.8B_0$. In even stronger fields, the ground state becomes $^3\Delta_g(1s\,3d_{-2})$, and so on.

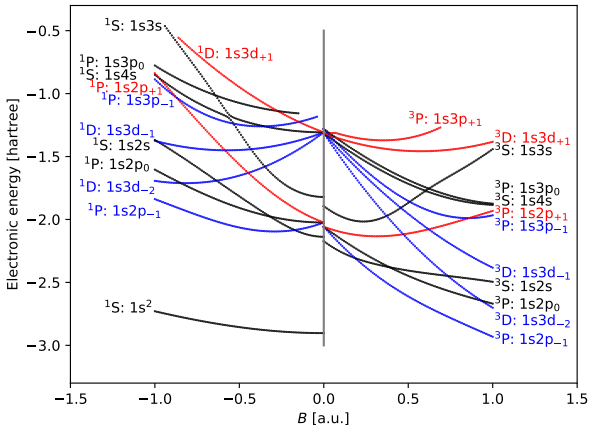

FIG. 2. Spectrum of the helium atom as a function of magnetic field strength. Singlet states are shown along the negative horizontal axis and triplet states along the positive axis.

B. United-atom limit: beryllium atom

It is also instructive to consider the united-atom limit, in which the helium dimer becomes the beryllium atom. The corresponding spectrum, obtained at the FCI/Lucc-pVDZ level of theory, is shown in Fig. 3. Again, the Zeeman interactions result in a reordering of the spectrum. As the zero-field singlet ground state $^1\Sigma_g(1s^2 2s^2)$ is increasingly destabilized by the magnetic field, the $^1\Delta_g(1s^2 2p^2_{-1})$ state becomes the lowest singlet in the strongest fields plotted.

However, because of the spin Zeeman interaction, the $m_s = -1$ triplet components are stabilized even faster. Indeed, already at about $0.05B_0$, the ground state is $^3\Pi_u(1s^2 2s\,2p_{-1})$. For the strongest field strengths shown, the first excited state is $^3\Phi_u(1s^2 2p_{-1} 3d_{-2})$, which appears to become the ground state at a field strength slightly stronger than one atomic unit.

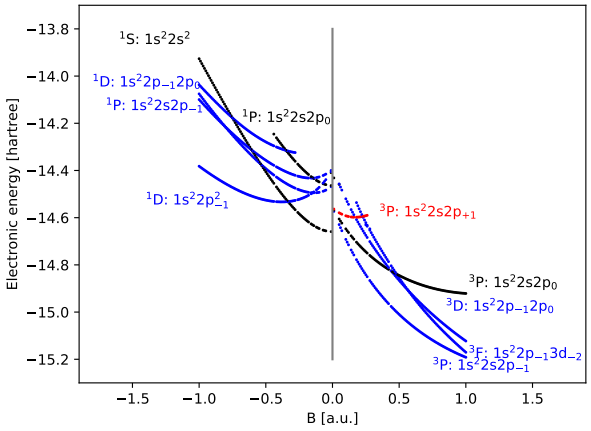

FIG. 3. Spectrum of the beryllium atom as a function of magnetic field strength. Singlet and triplet states are shown along the negative and positive horizontal axes, respectively.

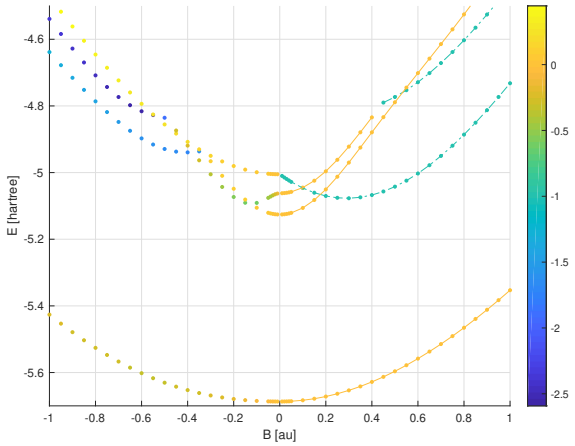

FIG. 4. Singlet spectrum as a function of magnetic field for the He_2 molecule, with fixed bond distance $R = 2a_0$. Perpendicular (parallel) magnetic fields have been mapped to the negative (positive) half of the horizontal axis.

C. States of He_2 at a fixed bond distance $R = 2a_0$

As several interesting minima in the dissociation curves appear at a He–He bond distance of about $R = 2a_0$ (see below), it is instructive to consider the field dependence of the electronic spectrum at this fixed bond length. In the following, we consider the singlet and triplet spectra of He_2 separately. The energies of singlet and triplet states are plotted in Fig. 4 and Fig. 5, respectively, with the energies in the parallel and perpendicular field orientations plotted along the positive and negative axes, respectively.

1. *Singlet states of He_2 at $R = 2a_0$*

In a parallel field, the four lowest singlet states at $R = 2a_0$ are $^1\Sigma_g(\sigma_{1s}^2\sigma_{1s}^{*2})$, $^1\Sigma_u(\sigma_{1s}^2\sigma_{1s}^*\sigma_{2s})$, and $^1\Sigma_g(\sigma_{1s}^2\sigma_{1s}^*\sigma_{2s}^*)$ with $\Lambda_\mathbf{B} = 0$ and $^1\Pi_g(\sigma_{1s}^2\sigma_{1s}^*\pi_{-1})$ with $\Lambda_\mathbf{B} = -1$, whose energies are plotted against the field strength along the positive axis in Fig. 4. While the three sigma states are destabilized diamagnetically in the field, the pi state is stabilized and becomes the second singlet state at $B = 0.18B_0$. In fields stronger than about $0.6B_0$, the third singlet is $^1\Pi_u(\sigma_{1s}^2\sigma_{1s}^*\pi_{-1}^*)$, having crossed the two highest sigma states. At this field strength, however, the ground state is no longer a singlet but a triplet, as discussed below.

In the perpendicular field orientation, where the molecular point group is C_{2h} rather than $C_{\infty h}$, the loss of cylindrical spatial symmetry manifests itself in more avoided crossings as seen in Fig. 4, where the energies of the lowest electronic states are plotted against the field strength along the negative axis.

In a weak perpendicular magnetic field, the ground state is $^1A_g(1a_g^21b_u^2)$, while the lowest excited states are $^1B_u(1a_g^21b_u2a_g)$, $^1A_g(1a_g^21b_u2b_u)$, and $^1B_g(1a_g^21b_u1a_u)$. These states originate from the same field-free states as do the lowest states in parallel field orientation except that the third excited state correlates with $^1\Pi_g(\sigma_{1s}^2\sigma_{1s}^*\pi_{||})$, which contains a singly occupied $\pi_{||} = (\pi_+ + \pi_-)/\sqrt{2}$ orbital of a_u symmetry rather than a singly occupied π_{-1} orbital of $a_u + b_u$ symmetry in the C_{2h} point group. Hence, $^1B_g(1a_g^21b_u1a_u)$ is diamagnetic rather than paramagnetic.

Here and in the following, $\pi_{||}$ denotes the π component of symmetry a_u parallel to the magnetic field, whereas $\pi_\perp$ denotes the π component of symmetry b_u perpendicular to the field and bond axes. We likewise use the notation $\pi_{||}^*$ for the π component of symmetry b_g parallel to the magnetic field, whereas $\pi_\perp^*$ denotes the component of symmetry a_g perpendicular to the field and bond axes.

In a perpendicular magnetic field of about $B = 0.15B_0$, $^1A_g(1a_g^21b_u2b_u)$ crosses $^1B_u(1a_g^21b_u2a_g)$ to become the lowest excited state, stabilized by the antibonding 2s orbital in the magnetic field by the paramagnetic bonding mechanism. At a field strength of about $B = 0.35B_0$, the state $^1B_u(1a_g^21b_u3a_g)$, which originates from the high-lying zero-field state $^1\Pi(\sigma_{1s}^2\sigma_{1s}^*\pi_\perp^*)$ with a singly occupied $\pi_\perp^*$ orbital of a_g symmetry, goes through a narrowly avoided crossing with the second lowest excited state $^1B_u(1a_g^21b_u2a_g)$. Around this avoided crossing, the $2a_g$ orbital changes character from σ_{2s} to $\pi_\perp^*$, pushing the second excited state $^1B_u(1a_g^21b_u2a_g)$ further down to recross $^1A_g(1a_g^21b_u2b_u)$, becoming again the first excited state, but with a HOMO of $\pi_\perp^*$ rather than σ_{2s} character.

To summarize, the HOMO of the first excited state in the perpendicular field orientation is σ_{2s} from zero field to $0.15B_0$, then becomes σ_{2s}^* followed by $\pi_\perp^*$ at $0.35B_0$. This progression may be understood in terms of paramagnetic stabilization of the orbitals, noting that the three orbitals have zero, one, and two nodal planes, respectively, parallel to the magnetic field vector; see Table II.

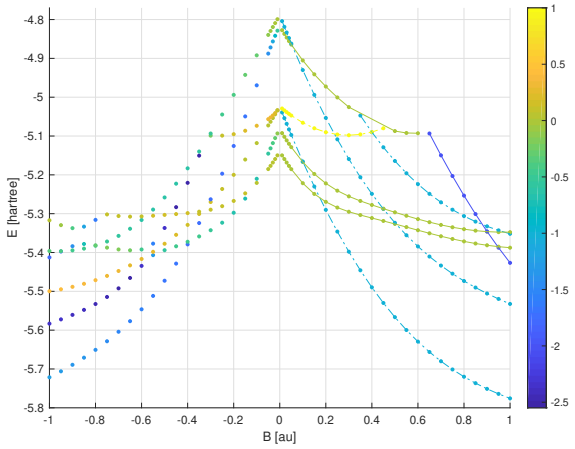

FIG. 5. Triplet spectrum as a function of magnetic field for the He_2 molecule, with fixed bond distance $R = 2a_0$. Perpendicular (parallel) magnetic fields have been mapped to the negative (positive) half of the horizontal axis.

2. *Triplet states of He_2 at $R = 2a_0$*

The behaviour of the triplet states in parallel and perpendicular fields are plotted along the positive and negative axes of Figure 5, respectively. The triplet states behave in a similar way to the corresponding open-shell singlets except that the spin Zeeman interaction splits the triplet states into three m_s components, the $m_s = -1$ and $m_s = +1$ components tilted downwards and upwards, respectively. We here consider the lowest-energy $m_s = -1$ components only.

Because of the spin Zeeman interaction, the ground state is the singlet $^1\Sigma_g(\sigma_{1s}^2\sigma_{1s}^{*2})$ only up to a field strength of about $0.55B_0$ in the parallel field orientation and about $0.65B_0$ in the perpendicular orientation, where the triplet states $^3\Pi_g(\sigma_{1s}^2\sigma_{1s}^*\pi_{-1})$ and $^3A_u(1a_g^21b_u1b_g)$, respectively, become the ground states, the latter originating from $^3\Pi_u(\sigma_{1s}^2\sigma_{1s}^*\pi_\perp^*)$.

In a weak parallel field, with $B \lesssim 0.1B_0$, the two lowest triplet states are $^3\Sigma_u(\sigma_{1s}^2\sigma_{1s}^*\sigma_{2s})$ and $^3\Sigma_g(\sigma_{1s}^2\sigma_{1s}^*\sigma_{2s}^*)$, with $\Lambda_\mathbf{B} = 0$. The next two states are $^3\Pi_g(\sigma_{1s}^2\sigma_{1s}^*\pi_{-1})$ and $^3\Pi_g(\sigma_{1s}^2\sigma_{1s}^*\pi_{+1})$, which diverge with increasing field strength due to the orbital Zeeman interaction with opposite signs of $\Lambda_\mathbf{B} = \pm 1$. In fields stronger than about $0.5B_0$, the lowest states are completely reordered by the spin and orbital Zeeman interactions. The lowest triplet is now $^3\Pi_g(\sigma_{1s}^2\sigma_{1s}^*\pi_{-1})$, which is also the electronic ground state of the system, while the first excited state is $^3\Pi_u(\sigma_{1s}^2\sigma_{1s}^*\pi_{-1}^*, \sigma_{1s}^{*2}\sigma_{1s}\pi_{-1})$. At one-atomic unit field strength B_0, the second excited state is $^3\Delta_u(\sigma_{1s}^2\sigma_{1s}^*\delta_{-2})$.

In a weak perpendicular field, the three lowest electronic triplet states are predominantly $^3B_u(1a_g^21b_u2a_g)$,

TABLE III. The lowest minima on dissociation curves for He_2 in a magnetic field $B = 0.2B_0$. The quantity $R_{\rm grid}$ is the bond distance for which the electron configuration, while other quantities are interpolated between grid points on the dissociation curve. All quantities are in atomic units.

spin	θ	n	$E_{\rm min}$	$R_{\rm eq}$	$\Lambda_{\mathbf{B}}$	E_∞	$E_{\rm dis}$	state	$R_{\rm grid}$
singlet	0°	0	−5.786650	5.733	0.00	−5.786619	0.000031	$^1\Sigma_g(0.98\,\sigma_{1s}^2\sigma_{1s}^{*2})$	5.800
		1	−5.070304	1.972	−1.00	−4.934970	0.135334	$^1\Pi_g(0.95\,\sigma_{1s}^2\sigma_{1s}^*\pi_{-1})$	2.000
		2	−5.051661	1.917	0.00	−4.960160	0.091501	$^1\Sigma_u(0.92\,\sigma_{1s}^2\sigma_{1s}^*\sigma_{2s})$	1.900
		3	−4.996800	2.079	0.00	−4.960157	0.036643	$^1\Sigma_g(0.93\,\sigma_{1s}^2\sigma_{1s}^*\sigma_{2s}^*)$	2.100
	90°	0	−5.786667	5.271	−0.00	−5.786618	0.000049	$^1A_g(0.98\ 1a_g^21b_u^2)$	5.200
		1	−5.073291	2.021	−0.57	−4.959465	0.113826	$^1A_g(0.88\ 1a_g^21b_u2b_u)$	2.000
		2	−5.050287	1.896	0.07	−4.959458	0.090829	$^1B_u(0.92\ 1a_g^21b_u2a_g)$	1.900
		3	−4.980790	1.946	0.07	unknown	unknown	$^1B_g(0.95\ 1a_g^21b_u1a_u)$	1.900
triplet	0°	0	−5.290267	1.966	−1.00	−5.182528	0.107739	$^3\Pi_g(0.95\,\sigma_{1s}^2\sigma_{1s}^*\pi_{-1})$	2.000
		1	−5.270141	1.937	0.00	−5.206973	0.063168	$^3\Sigma_u(0.89\,\sigma_{1s}^2\sigma_{1s}^*\sigma_{2s})$	1.900
		2	−5.222877	2.103	0.00	−5.206972	0.015905	$^3\Sigma_g(0.88\,\sigma_{1s}^2\sigma_{1s}^*\sigma_{2s}^*)$	2.100
	90°	0	−5.297553	2.006	−0.68	−5.206769	0.090784	$^3A_g(0.84\ 1a_g^21b_u2b_u)$	2.000
		1	−5.268197	1.918	0.07	−5.206769	0.061428	$^3B_u(0.89\ 1a_g^21b_u2a_g)$	1.900
		2	−5.200512	1.941	0.07	−5.094688	0.105824	$^3B_g(0.95\ 1a_g^21b_u1a_u)$	1.900
quintet	0°	0	−4.652235	4.141	−1.00	−4.604572	0.047663	$^5\Pi_g(0.68\,\sigma_{1s}\sigma_{1s}^*\sigma_{2s}\pi_{-1})$	4.600
		1	−4.627960	6.052	0.00	−4.626512	0.001448	$^5\Sigma_g(0.73\,\sigma_{1s}\sigma_{1s}^*\sigma_{2s}\sigma_{2s}^*)$	6.200
	90°	0	−4.686660	4.560	−0.67	−4.627365	0.059295	$^5A_g(0.44\ 1a_g1b_u2b_u3a_g, 0.32\ 1a_g1b_u2b_u2a_g)$	4.600
		1	−4.632662	5.074	−0.59	−4.603487	0.029175	$^5B_u(0.82\ 1a_g1b_u2a_g3a_g)$	5.000
		2	−4.609599	5.648	−0.90	−4.602014	0.007585	$^5A_g(0.43\ 1a_g1b_u2b_u3a_g, 0.26\ 1a_g1b_u2b_u2a_g)$	5.800

$^3A_g(1a_g^21b_u2b_u)$, and $^3B_g(1a_g^21b_u1a_u)$, originating from the field-free states $^3\Sigma_u^+(\sigma_{1s}^2\sigma_{1s}^*\sigma_{2s})$, $^3\Sigma_g^+(\sigma_{1s}^2\sigma_{1s}^*\sigma_{2s}^*)$, and $^3\Pi_g(\sigma_{1s}^2\sigma_{1s}^*\pi_\perp)$. At $0.2B_0$, the lowest two triplet states have crossed and the lowest state is now $^3A_g(1a_g^21b_u2b_u)$; see Table III. In the strongest field plotted in Fig. 5, the ground state is $^3B_u(1a_g^21b_u1a_g)$, originating from the field-free state $^3\Pi_u(\sigma_{1s}^2\sigma_{1s}^*\pi_\perp^*)$. As the field increases from zero, this highly-excited state drops below all other triplet states, including the ^3B_g state that originates from $^3\Pi_g(\sigma_{1s}^2\sigma_{1s}^*\pi_{||})$. In the process, the ^3B_u state acquires a substantial negative AQAM value from the occupied antibonding σ_{1s}^* and $\pi_\perp^*$ orbitals. Decreasing from 0.50 at field strength $0.01B_0$ to $= -1.42$ at $0.05B_0$, it reaches a minimum value of $\Lambda_{\mathbf{B}} = -1.75$ at $0.25B_0$, after which it increases again to -1.24 at field strength B_0. We note that the evolution of the lowest triplet state in the perpendicular orientation parallels that of the lowest singlet state, the HOMO changing character first from σ_{2s} to σ_{2s}^* and then from σ_{2s}^* and to $\pi_\perp^*$.

D. Potential-energy curves of He_2

Next, we explore how the energy spectrum varies with the bond distance R and the field orientation θ. For visualization purposes, energy curves for perpendicular (parallel) orientations will in all cases be plotted with a negative (positive) bond distance. The lowest minima on these dissociation curves are summarized in Table III and IV, for $B = 0.2B_0$ and $B = B_0$, respectively.

At small bond distances, the dissociation curves are dominated by the nuclear electrostatic repulsion energy, obscuring the united-atom limit. We therefore select a cut-off distance R_c, marked with vertical grey dash–dot lines in each figure. In the region $R < R_c$, we replace the actual energy $E(R)$ by a shifted energy

$$E'(R) = E(R) + \frac{Z^2}{R_c} - \frac{Z^2}{R} - a(R-R_c)^3 - b(R-R_c)^2 - c(R-R_c), \quad (23)$$

more suited to the united-atom limit. The second and third terms remove the singular nuclear repulsion energy, while the polynomial in $R - R_c$ aligns the energy scale. The shift is state independent; it vanishes but introduces nondifferentiable kinks and cusps at the cut-off distance $R = R_c$.

In the united-atom limit, as $R \to 0$, the molecular orbital basis set becomes linearly dependent, spanning only an orbital space of half the dimension. To avoid spurious results from near linear dependence in this region, we therefore avoid very short bond distances in the dissociation curves.

Finally, we remark that the common notions of bonding and antibonding orbitals, associated with symmetry and antisymmetry with respect to mirror reflection $\sigma_{\rm midbond}$ in the midbond plane, become more complicated and not well defined in the presence of a magnetic field. While this symmetry remains exact in a parallel field, a nonparallel magnetic fields breaks it. As a result, orbitals become superpositions $\phi = a\phi_+ + b\phi_-$ with $|a|^2 + |b|^2 = 1$ of symmetric and antisymmetric components. The expectation value of the mirror reflection op-

TABLE IV. The lowest minima on dissociation curves for He_2 in a magnetic field $B = B_0$. The quantity R_{grid} is the bond distance for which the electron configuration, while other quantities are interpolated between grid points on the dissociation curve. All quantities are in atomic units.

spin	θ	n	E_{min}	R_{eq}	$\Lambda_{\mathbf{B}}$	E_∞	E_{dis}	state	R_{grid}
singlet	0°	0	−5.454327	4.747	0.00	−5.453984	0.000343	$^1\Sigma_g(0.99\,\sigma_{1s}^2\sigma_{1s}^{*2})$	4.700
		1	−4.739260	1.800	−1.00	−4.555238	0.184022	$^1\Pi_g(0.96\,\sigma_{1s}^2\sigma_{1s}^{*}\pi_{-1})$	1.800
		2	−4.554578	4.420	−1.00	−4.554309	0.000269	$^1\Pi_u(0.64\,\sigma_{1s}^{*2}\sigma_{1s}\pi_{-1})$	4.600
		3	−4.423187	1.893	−2.00	unknown	unknown	$^1\Delta_g(0.96\,\sigma_{1s}^{*2}\sigma_{1s}\delta_{-2})$	1.900
	90°	0	−5.455252	3.012	−0.00	−5.453983	0.001269	$^1A_g(0.99\ 1a_g^2 1b_u^2)$	3.000
		1	−4.638450	2.009	−1.27	−4.555000	0.083450	$^1B_u(0.95\ 1a_g^2 1b_u 2a_g)$	2.000
		2	−4.570580	3.136	−1.07	−4.554542	0.016038	$^1A_g(0.76\ 1b_u^2 1a_g 2a_g)$	3.200
		3	−4.503213	1.617	0.24	unknown	unknown	$^1B_g(0.95\ 1a_g^2 1a_u 1b_u)$	1.600
triplet	0°	0	−5.782268	1.805	−1.00	−5.644685	0.137583	$^3\Pi_g(0.95\,\sigma_{1s}^2\sigma_{1s}^{*}\pi_{-1})$	1.800
		2	−5.428475	1.889	−2.00	unknown	unknown	$^3\Delta_g(0.96\,\sigma_{1s}^2\sigma_{1s}^{*}\delta_{-2})$	1.900
		2	−5.404984	2.613	−1.00	−5.256417	0.148567	$^3\Pi_u(0.61\,\sigma_{1s}^2\sigma_{1s}^{*}\pi_{-1}^{*}, 0.34\,\sigma_{1s}^{*2}\sigma_{1s}\pi_{-1})$	2.600
		2	−5.406632	5.518	0.00	−5.393051	0.013581	$^3\Sigma_u(0.75\,\sigma_{1s}^2\sigma_{1s}^{*}\sigma_{2s})$	5.400
	90°	0	−5.721430	1.991	−1.25	−5.644682	0.076748	$^3B_u(0.94\ 1a_g^2 1b_u 2a_g)$	2.000
		1	−5.658760	3.245	−1.10	−5.644682	0.014078	$^3A_g(0.70\ 1b_u^2 1a_g 2a_g, 0.25\ 1a_g^2 1b_u 2b_u)$	3.200
		2	−5.530958	1.611	0.22	−5.393015	0.137943	$^3B_g(0.95\ 1a_g^2 1b_u 1a_u)$	1.600
		2	−5.460260	2.416	−1.77	−5.256414	0.203846	$^3A_g(0.58\ 1a_g^2 1b_u 2b_u, 0.35\ 1b_u^2 1a_g 2a_g)$	2.400
quintet	0°	0	−5.835333	∞	−2.00	−5.835333	0	$^5\Delta_g(0.92\,\sigma_{1s}\sigma_{1s}^{*}\pi_{-1}\pi_{-1}^{*})$	10.000
		1	−5.645344	2.396	−3.00	−5.448259	0.197085	$^5\Phi_u(0.93\,\sigma_{1s}\sigma_{1s}^{*}\pi_{-1}\delta_{-2})$	2.400
		1	−5.650264	4.085	−1.00	−5.583994	0.066270	$^5\Pi_g(0.86\,\sigma_{1s}\sigma_{1s}^{*}\pi_{-1}\sigma_{2s})$	4.200
	90°	0	−5.855142	3.620	−2.21	−5.835368	0.019774	$^5A_g(0.91\ 1a_g 1b_u 2a_g 2b_u)$	3.800
		1	−5.677227	2.660	−0.44	−5.583805	0.093422	$^5B_g(0.89\ 1a_g 1b_u 2a_g 1a_u)$	2.600
		2	−5.618470	3.092	−0.82	−5.583719	0.034751	$^5A_u(0.83\ 1a_g 1b_u 2a_g 1b_g)$	3.000
		3	−5.577629	3.523	−2.83	−5.447773	0.129856	$^5B_u(0.87\ 1a_g 1b_u 2a_g 3a_g)$	3.400

TABLE V. Orbital expectation values s of reflection in the mid-bond plane Eq. (24) for the lowest eight RHF orbitals in He_2 in a perpendicular field of strength $B_\perp$. A value of $s = +1$ implies perfect symmetry and is associated with bonding properties, while a value of $s = -1$ implies perfect antisymmetry and is associated with a nodal plane and antibonding properties. Due to field-induced symmetry breaking, intermediate values are typical, indicating mixing of bonding and antibonding properties. The last row contains the mean absolute s value of the eight listed RHF orbitals for a given bond distance and field strength.

$B_\perp = 0.2B_0$								$B_\perp = 1.0B_0$											
$R = 2.0a_0$		$R = 3.8a_0$		$R = 5.0a_0$		$R = 5.8a_0$		$R = 1.8a_0$		$R = 2.0a_0$		$R = 2.5a_0$		$R = 3.0a_0$		$R = 3.2a_0$		$R = 3.8a_0$	
$1a_g$	1.00	$1a_g$	0.98	$1a_g$	0.96	$1a_g$	0.94	$1a_g$	0.96	$1a_g$	0.93	$1a_g$	0.86	$1a_g$	0.77	$1a_g$	0.73	$1a_g$	0.62
$1b_u$	−0.97	$1b_u$	−0.97	$1b_u$	−0.95	$1b_u$	−0.94	$1b_u$	−0.70	$1b_u$	−0.71	$1b_u$	−0.71	$1b_u$	−0.67	$1b_u$	−0.65	$1b_u$	−0.59
$2b_u$	0.12	$2b_u$	0.17	$2b_u$	0.23	$2b_u$	0.26	$2a_g$	0.08	$2a_g$	0.12	$2a_g$	0.25	$2a_g$	0.37	$2a_g$	0.40	$2a_g$	0.42
$2a_g$	0.99	$2a_g$	0.89	$2a_g$	0.73	$2a_g$	0.61	$2b_u$	0.00	$2b_u$	0.00	$2b_u$	0.01	$2b_u$	0.03	$2b_u$	0.03	$2b_u$	0.04
$1a_u$	0.99	$3a_g$	0.14	$3a_g$	0.28	$3a_g$	0.30	$1a_u$	0.90	$1a_u$	0.85	$1a_u$	0.70	$1a_u$	0.54	$1a_u$	0.47	$1a_u$	0.31
$3a_g$	−0.11	$1a_u$	0.95	$1a_u$	0.88	$3b_u$	0.06	$1b_g$	0.14	$1b_g$	0.13	$1b_g$	0.12	$1b_g$	0.12	$1b_g$	0.12	$1b_g$	0.10
$3b_u$	0.78	$3b_u$	0.62	$3b_u$	0.30	$1a_u$	0.82	$3a_g$	0.83	$3b_u$	0.26	$3b_u$	0.32	$3a_g$	0.12	$3a_g$	0.11	$3a_g$	0.18
$4b_u$	−0.61	$1b_g$	−0.84	$1b_g$	−0.81	$1b_g$	−0.78	$3b_u$	0.23	$3a_g$	0.78	$3a_g$	0.46	$3b_u$	0.34	$3b_u$	0.33	$3b_u$	0.25
	0.70		0.70		0.64		0.59		0.48		0.47		0.43		0.37		0.36		0.31

erator,

$$s = \langle\phi|\sigma_{\text{midbond}}|\phi\rangle = |a|^2 - |b|^2, \tag{24}$$

provides a measure of this mixing. In general, a fraction $|a|^2 = \frac{1}{2}(1+s)$ of ϕ is symmetric and bonding, whereas a fraction $|b|^2 = \frac{1}{2}(1-s)$ is antisymmetric and antibonding. In Table V, this expectation value is given for several bond distances R and perpendicular field strengths $B_\perp$ for the reference restricted Hartree–Fock (RHF) orbitals employed in the FCI calculations. Note that the triplet and quintet states were also calculated using RHF orbitals.

The perpendicular paramagnetic bonding mechanism, which increases the magnitude of the angular momentum of antibonding orbitals, can also be viewed as a mixing of bonding and antibonding orbitals. This is seen in Table V, where, for example, the orbital $1b_u$, which corresponds to the antibonding 1s orbital σ_{1s}^* in the parallel orientation, acquires increasingly strong bonding character in stronger fields and at longer bond distances. From the listed mean absolute s values in Table V, we note that the s values decrease with increasing field strength and increasing bond distance. Indeed, strong magnetic fields compress the orbitals and change the relevant length

scale, so that the dissociation limit is reached earlier.

1. *Singlet potential-energy curves at $B = 0.2B_0$*

Singlet dissociation curves at field strength $B = 0.2B_0$ are shown in Fig. 6 with information given in Table III. In the parallel orientation at $R = 2a_0$, the lowest singlet is dominated by the electron configuration $^1\Sigma_g(\sigma_{1s}^2\sigma_{1s}^{*2})$. The first excited state is $^1\Pi_g(\sigma_{1s}^2\sigma_{1s}^*\pi_{-1})$ with $\Lambda_\mathbf{B} = -1$, while second and third states are $^1\Pi_u(\sigma_{1s}^2\sigma_{1s}^*\sigma_{2s})$ and $^1\Sigma_g(\sigma_{1s}^2\sigma_{1s}^*\sigma_{2s}^*)$ with $\Lambda_\mathbf{B} = 0$ and the same dissociation limits. All three excited states are covalently bound with approximately the same equilibrium distance of about $2a_0$, whereas the ground state has a shallow minimum at $5.7a_0$.

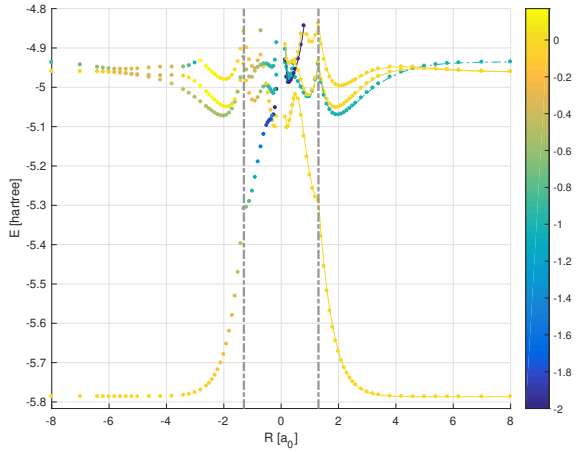

FIG. 6. Dissociation curves for singlet states in perpendicular (negative half) and parallel (positive half) magnetic field $B = 0.2B_0$. In the region between grey dashed lines, the curve is shifted by the nuclear repulsion energy and an additional quadratic fit to align the united atom limit to the same energy scale. Plot markers are coloured based on the AQAM value $\Lambda_\mathbf{B}$; scale indicated on the right.

The perpendicular orientation gives rise to dissociation curves that are visually similar. However, the identification of the states requires care since broken symmetries allow mixing of states that are distinct in the parallel case. Moreover, viewed as hypersurfaces that depend on (R, θ, B), states can be continuously deformed into each other in a way that is sometimes path dependent due to the presence of conical intersections.

At $R = 2a_0$ in the perpendicular orientation, the ground state is $^1\mathrm{A_g}(1\mathrm{a_g^2 1b_u^2})$ and the lowest three singlet excited states are $^1\mathrm{A_g}(1\mathrm{a_g^2 1b_u 2b_u})$, $^1\mathrm{B_u}(1\mathrm{a_g^2 1b_u 2a_g})$ and $^1\mathrm{B_g}(1\mathrm{a_g^2 1b_u 1a_u})$, the latter state being replaced by $^1\mathrm{B_u}(1\mathrm{a_g^2 1b_u 3a_g})$ at greater bond distances. The ground state has the same parallel and perpendicular dissociation limits but different parallel and perpendicular united-atom limits, tending to the $1s^2 2s^2$ beryllium configuration with $\Lambda_\mathbf{B} = 0$ in the parallel orientation but to $1s^2 2p_{-1}^2$ with $\Lambda_\mathbf{B} = -2$ in the perpendicular orientation. The first excited state in the perpendicular orientation has $\Lambda_\mathbf{B} = -0.6$ arising from the antibonding orbital $1\mathrm{b_u}$ and the intermediate orbital $2\mathrm{b_u}$, slightly less than the $\Lambda_\mathbf{B} = -1.0$ of the first excited state in the parallel orientation (for short bond distances), arising from the singly occupied π_{-1} orbital.

However, as seen in Fig. 7, for a fixed $R = 2$ bohr, the first excited states in the parallel configuration smoothly turn into the corresponding perpendicular states as the angle θ is varied. In particular, the antibonding orbital σ_{2s}^* transforms smoothly into π_{-1}, both being of $\mathrm{a_u}$ symmetry in skew orientations. We note that the first excited state has a minimum at $\theta \approx 40°$, which happens since the state a skew angles involves from $^1\Pi_g(\sigma_{1s}^2\sigma_{1s}^*\pi_{-1})$, where σ_{1s}^* and π_{-1} prefer perpendicular and parallel orientations, respectively.

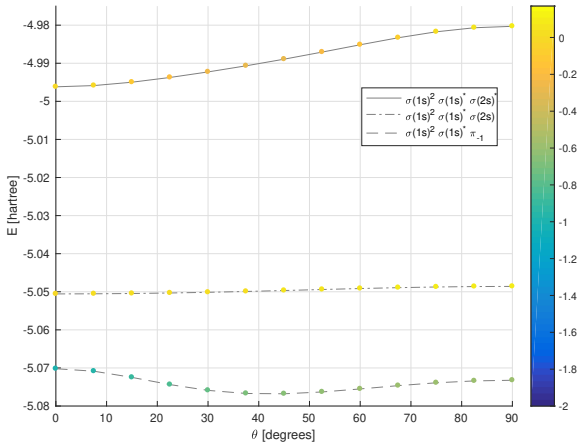

FIG. 7. Energies of singlet excited states as a function of angle θ between the bond axis and magnetic field, with magnitudes fixed at $R = 2a_0$ and $B = 0.2B_0$, respectively.

The second and third excited state have $\Lambda_\mathbf{B} \approx 0.1$ in the perpendicular orientation. The second excited state also retains the same radial dissociation limit as the corresponding parallel state, while the third excited state acquires a different dissociation limit due to symmetry breaking and orbital mixing. Globally, this indicates conical intersections on the energy surfaces.

In the given basis set, the ground state is bound by about 50 microhartree in the perpendicular configuration and 30 microhartree in the parallel orientation. Hence, at this field strength, perpendicular paramagnetic bonding is negligible in the ground state. In the first excited state, the energy is lowered by 3 millihartree from parallel to perpendicular orientation. However, the dissociation limit is lowered too, leading to a reduction in radial binding energy from 0.14 hartree to 0.11 hartree. By contrast, the second excited state is is essentially unchanged and the third excited state is higher by 16 millihartree in the

perpendicular orientation.

2. *Singlet potential-energy curves at $B = B_0$*

Potential-energy curves for singlet states at $B = B_0$ are shown in Fig. 8. In the parallel orientation, the weakly bound ground state is dominated by the $^1\Sigma_g(\sigma_{1s}^2\sigma_{1s}^{*2})$ configuration at all bond distances, just as for field strength $B = 0.2B_0$. Because of the orbital Zeeman effect, the first and second excited states have substantial π character with $\Lambda_{\mathbf{B}} = -1$, being predominantly $^1\Pi_g(\sigma_{1s}^2\sigma_{1s}^*\pi_{-1})$ and $^1\Pi_u(\sigma_{1s}^{*2}\sigma_{1s}\pi_{-1})$, respectively. The latter state is obtained from the former by promoting one electron from the σ_{1s} bonding orbital to σ_{1s}^* antibonding orbital. The two states therefore dissociate to the same limit but bind in different ways. The first state is covalently bound with a deep energy minimum at $R = 1.80a_0$, while the second is weakly bound with a shallow minimum at $R = 4.42a_0$. The third excited state has δ character, being predominantly $^1\Delta_g(\sigma_{1s}^{*2}\sigma_{1s}\delta_{-2})$ with $\Lambda_{\mathbf{B}} = -2$ and a minimum at $R = 1.89a_0$. We note that the $^1\Sigma_u(\sigma_{1s}^2\sigma_{1s}^*\sigma_{2s})$ and $^1\Sigma_g(\sigma_{1s}^2\sigma_{1s}^*\sigma_{2s}^*)$ states, which were the second and third excited states at $B = 0.2B_0$, are not stabilized by the orbital Zeeman interaction and have therefore been pushed high up in the spectrum by its diamagnetic interaction with the magnetic field.

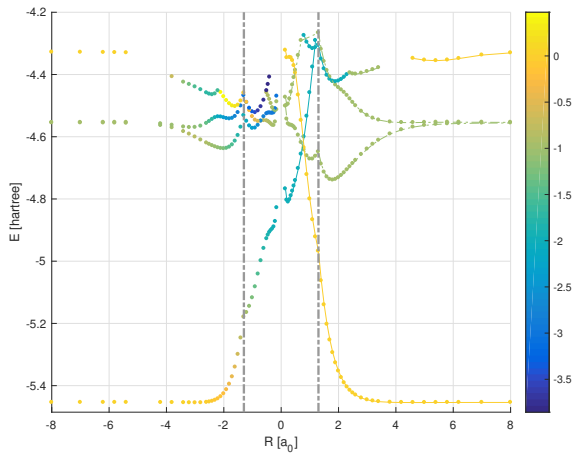

FIG. 8. Dissociation curves for singlet states in perpendicular (negative half) and parallel (positive half) magnetic field $B = B_0$.

The dissociation curves in the perpendicular field orientation are substantially different from those in the parallel orientation. However, since the dissociation limits are identical in the two orientations, the curves become increasingly similar with increasing bond distance. The ground state $^1A_g(1a_g^2 1b_u^2)$, originating from the field-free state $^1\Sigma_g^+(\sigma_{1s}^2\sigma_{1s}^{*2})$, is stabilized by perpendicular paramagnetic bonding by about 1 millihartree, with equilibrium bond distance $R = 3.01$ bohr, which is 1.4 bohr shorter than the bond distance in the parallel field orientation. While the parallel and perpendicular ground states share the same dissociation limit, they tend to different states in the united atom limit—the parallel state becomes $^1\Sigma_g(1s^2 2s^2)$, while the perpendicular state becomes $^1\Sigma_g(1s^2 2p_{-1}^2)$.

In the perpendicular orientation, the lowest three singlet excited states are $^1B_u(1a_g^2 1b_u 2a_g)$, $^1A_g(1a_g^2 1b_u 2b_u)$, and $^1B_g(1a_g^2 1b_u 1a_u)$ at $R = 1.8a_0$; at $R = 3a_0$, the lowest states are $^1B_u(1a_g^2 1b_u 2a_g)$, $^1A_g(1b_u^2 1a_g 2a_g)$, and $^1B_g(1a_g^2 1b_u 2b_u)$. Thus, while the first excited state retains its overall symmetry and orbital occupation at all distances beyond $R = 1.8$ bohr, the second state retains the overall symmetry but changes orbital character and the third state undergoes a level crossing with a state of different symmetry.

It is interesting to compare the first exited states in the two orientations. In the parallel orientation, the first excited state is predominantly $^1\Pi_g(\sigma_{1s}^2\sigma_{1s}^*\pi_{-1})$ of bond order one and a half and a deep minimum at $R = 1.80a_0$. In the perpendicular orientation, the $^1B_u(1a_g^2 1b_u 2a_g)$ is best described as having orbital configuration $\sigma_{1s}^2\sigma_{1s}^*\pi_\perp^*$, with an antibonding HOMO orbital $\pi_\perp^*$ replacing π_{-1}. Whereas the orbital Zeeman interaction favours π_{-1} in the parallel field orientation, it favours $\pi_\perp^*$ in the perpendicular orientation, by the same mechanism that generates paramagnetic bonding. The reduced bond order of one in the perpendicular orientation gives a shallower minimum at a longer bond length $2.01a_0$ compared with the parallel orientation. We note that the first excited state has $\Lambda_{\mathbf{B}} = -1.3$ at the energy minimum, indicating that it has acquired some δ character. In the united-atom limit, the perpendicular state acquires even more δ character, as shown by the colour coding in Fig. 8.

The second excited state has a double minimum in the perpendicular orientation. The global minimum occurs at $R = 3.14a_0$ with $\Lambda_{\mathbf{B}} = -1.1$, indicating some δ character. The orbital occupation in this region of the dissociation curve is $\sigma_{1s}^{*2}\sigma_{1s}\pi_\perp^*$, with a negative bond order and a strong paramagnetic bonding (more than an order of magnitude stronger than in the ground state) generated by three electrons occupying antibonding orbitals.

The local minimum in the second excited state occurs at the shorter distance of $R = 1.81a_0$ and has $\Lambda = -2.5$, indicating a substantial increase in δ character. Compared with the second excited state in the parallel orientation, the energy is much lower (by $0.1E_h$ at $R = 2a_0$). Hence, the perpendicular paramagnetic bonding effect is orders of magnitude stronger than in the ground state.

The global picture of the singlet energy surfaces is complicated by level crossings at intermediate bond distances. Rotation of the first and second excited states at a fixed bond distance of $R = 2a_0$ leads to a crossing at roughly 45°, even though the resulting perpendicular states share the same dissociation limit. Hence, at this bond distance, the strongly bound parallel state $\sigma_{1s}^2\sigma_{1s}^*\pi_{-1}$ is rotated into a state near the higher minimum on the second excited perpendicular dissociation

curve. The very weakly bound second excited state, with $\sigma_{1s}^{*2}\sigma_{1s}\pi_{-1}$ character, in the parallel orientation is consequently rotated into the more strongly bound first excited state in the perpendicular orientation.

3. *Triplet potential-energy curves at $B = 0.2B_0$*

The lowest triplet states at $B = 0.2B_0$ are shown in Fig. 9. As in the field-free case, the triplet He_2 dissociation curves display many features that are analogous to the singlet curves. Equilibrium bond distances are roughly 2 bohr. Moreover, there are again conical intersections connecting low-lying states.

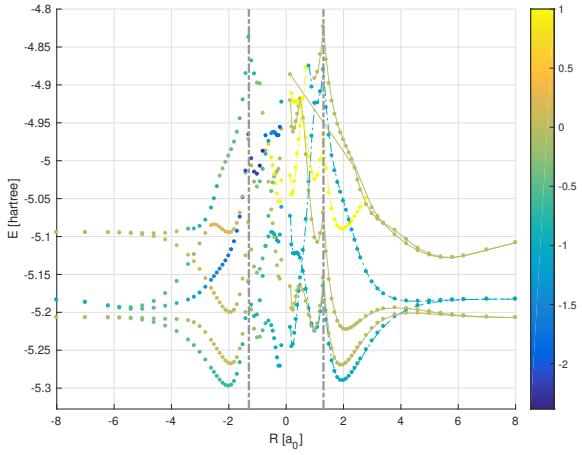

FIG. 9. Dissociation curves for triplet states in perpendicular (negative half) and parallel (positive half) magnetic field $B = 0.2B_0$. In the region between grey dashed lines, the curve is shifted by the nuclear repulsion energy and an additional quadratic fit to align the united atom limit to the same energy scale. Plot markers are coloured based on the AQAM value $\Lambda_{\mathbf{B}}$; scale indicated on the right.

In the parallel orientation at $R = 2a_0$, the lowest triplet is predominantly ${}^3\Pi_g(\sigma_{1s}^2\sigma_{1s}^*\pi_{-1})$ with $\Lambda_{\mathbf{B}} = -1$. The second and third triplet states have $\Lambda_{\mathbf{B}} = 0$ and pure σ character, with configurations predominantly $\sigma_{1s}^2\sigma_{1s}^*\sigma_{2s}$ and $\sigma_{1s}^2\sigma_{1s}^*\sigma_{2s}^*$, respectively. The fourth triplet state at $R = 2a_0$ is related to the first triplet by reversed sign of the angular momentum, having $\Lambda_{\mathbf{B}} = +1$ and an electron configuration dominated by $\sigma_{1s}^2\sigma_{1s}^*\pi_{+1}$. However, at slightly longer bond distances, the fourth triplet state is instead one with $\Lambda_{\mathbf{B}} = -1$ and configuration $\sigma_{1s}^2\sigma_{1s}^*\pi_{-1}^*$, which shares the same dissociation limit as the triplet ground state at $R = 2a_0$.

Fixing the bond distance at $R = 2a_0$ (close to the equilibrium bond distances of the lowest triplet states in all field orientations) and plotting the energies as function of the angle θ between the bond axis and the field vectors, we obtain the curves in Fig. 10. In the perpendicular orientation at this bond distance, the lowest triplet is predominantly ${}^3A_g(1a_g^2 1b_u 2b_u)$, where the σ_{2s}^* HOMO of

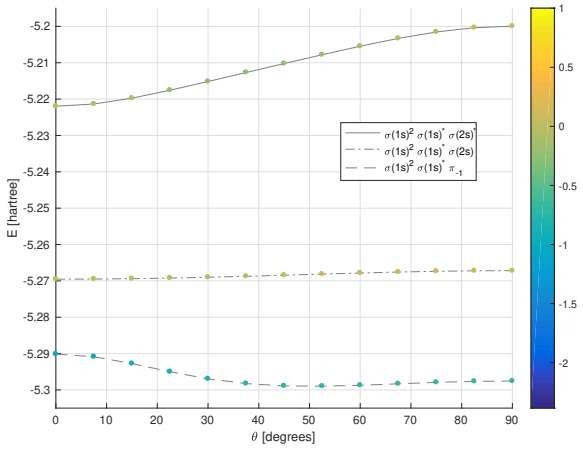

FIG. 10. Energies of the lowest triplet states at $R = 2a_0$ and $B = 0.2B_0$ plotted against the angle θ between the bond axis and magnetic axis

b_u symmetry has evolved smoothly from the π_{-1} HOMO in the parallel orientation, both being of a_u symmetry in skew orientations. In the process, the AQAM projection has decreased from -1 in the parallel orientation to -0.7 in the perpendicular orientation. This lowest triplet state has a preferred field orientation of about 50°, a compromise between the preferred perpendicular orientation of the antibonding σ orbitals and preferred parallel orientation of the π orbital, in the same way as for singlet states in Fig. 7. The energy of the lowest triplet is about 7 millihartree lower in the perpendicular orientation than in the parallel orientation, by paramagnetic stabilization of the antibonding orbitals. However, since the paramagnetic stabilization also lowers the dissociation limit, the bond is actually weaker in the perpendicular orientation.

Even though ${}^3\Pi_g(\sigma_{1s}^2\sigma_{1s}^*\pi_{-1})$ and ${}^3A_g(1a_g^2 1b_u 2b_u)$ are the lowest parallel and perpendicular triplet states at a bond distance of $2a_0$, smoothly connected to each other by field rotation, they have different radial dissociation limits, the latter having the same dissociation limit as the parallel states ${}^3\Sigma_u(\sigma_{1s}^2\sigma_{1s}^*\sigma_{2s})$ and ${}^3\Sigma_g(\sigma_{1s}^2\sigma_{1s}^*\sigma_{2s}^*)$. The ${}^3\Pi_g$ state, on the other hand, crosses the ${}^3\Sigma_u$ and ${}^3\Sigma_g$ states around $R = 4a_0$, dissociating into states of higher energy. and the minimum at $R = 2.1a_0$ is thus a manifestation of the perpendicular paramagnetic bonding mechanism.

The second triplet state in Fig. 10 changes smoothly from ${}^3\Sigma_u(\sigma_{1s}^2\sigma_{1s}^*\sigma_{2s})$ to ${}^3B_u(1a_g^2 1b_u 2a_g)$ from the parallel to the perpendicular orientation, increasing its energy slightly and its AQAM projection form zero to 0.1. The third triplet state changes more dramatically (but smoothly) from ${}^3\Sigma_g(\sigma_{1s}^2\sigma_{1s}^*\sigma_{2s}^*)$ to ${}^3B_g(1a_g^2 1b_u 1a_u)$ as the HOMO changes from σ_{2s}^* to $\pi_{\shortparallel}$ character. Its energy increases by about 20 millihartree, while its AQAM projection first decreases to -0.2 at $\theta \approx 40°$, after which it increases to 0.1 in the perpendicular orientation.

To summarize, the three lowest triplet states at $R = 2a_0$ differ in their HOMOs, which, in order of increasing energy, are $\pi_{-1} < \sigma_{2s} < \sigma^*_{2s}$ in the parallel field orientation (by paramagnetic stabilization of π_{-1}) and $\sigma^*_{2s} < \sigma_{2s} < \pi_{\shortparallel}$ in the perpendicular orientation (by paramagnetic stabilization of σ^*_{2s}). We note that, even though the π and σ^*_{2s} orbitals are of different symmetries in the parallel and perpendicular field orientations, they are of the same symmetry in skew orientations and may therefore transform smoothly into each other.

We consider next the electronic states closer to the dissociation limit, at $R = 5a_0$. In Fig. 9, there are three distinct pairs of states both in the parallel field orientation and in the perpendicular orientation—in Fig. 11, we have plotted the energies of the corresponding states against the angle θ at the fixed bond distance $R = 5a_0$. Each pair consists of two close-lying states with the same dissociation limit but of different symmetries (gerade and ungerade) arising from different occupations of bonding and antibonding orbitals. Since we are close to the dissociation limit, the electronic states are typically multiconfigurational, with large contributions from two configurations. We consider the lowest pair of electronic states first.

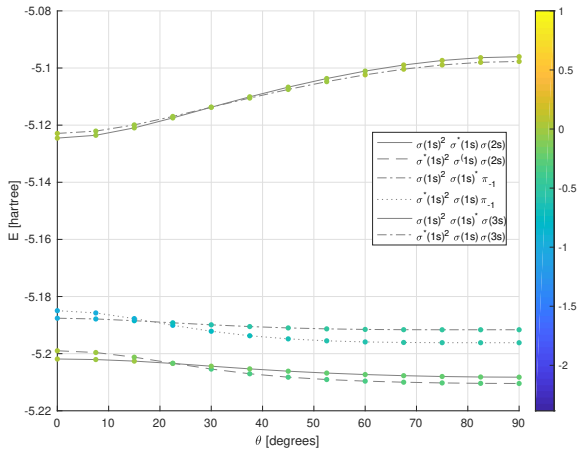

FIG. 11. Triplet states as a function of angle between the bond axis and magnetic field, with magnitudes fixed at $R = 5a_0$ and $B = 0.2B_0$, respectively.

At $R = 5a_0$, the lowest parallel state is predominantly ${}^3\Sigma_u(\sigma^2_{1s}\sigma^*_{1s}\sigma_{2s})$ with one occupied antibonding orbital, while the next state ${}^3\Sigma_g(\sigma^2_{1s}\sigma^*_{1s}\sigma^*_{2s}, \sigma^{*2}_{1s}\sigma_{1s}\sigma_{2s})$ has large contributions from two configurations, both with two occupied antibonding orbitals. Although these close-lying states have nearly reached their radial dissociation limits at this bond distance, both are lowered in energy as the angle is increased to 90°, by paramagnetic stabilization of the antibonding orbitals in the nonparallel field. With two occupied antibonding orbitals, the energy lowering is larger for the ${}^3\Sigma_g$ state, which becomes the lowest state at 22°. For this state, the AQAM projection changes from zero in the parallel field orientation to −0.3 in the perpendicular orientation; for the ${}^3\Sigma_u$ state, the AQAM projection changes less. In the perpendicular field orientation, the symmetries of the states are ${}^3A_g$ for the lower-energy state and ${}^3B_u$ for the higher state.

The next pair of states are ${}^3\Pi_g(\sigma^2_{1s}\sigma^*_{1s}\pi_{-1}, \sigma^{*2}_{1s}\sigma_{1s}\pi^*_{-1})$ and ${}^3\Pi_u(\sigma^{*2}_{1s}\sigma_{1s}\pi_{-1}, \sigma^2_{1s}\sigma^*_{1s}\pi^*_{-1})$ in the parallel orientation, both with more weight on the configuration containing the bonding orbital π_{-1}. The ${}^3\Pi_u$ state is slightly higher in energy, have a doubly occupied σ^*_{1s} orbital in the dominant configuration. As a result of paramagnetic stabilization, the gerade and ungerade states cross at about $\theta = 30°$. Furthermore, with increasing θ, the configurations containing the antibonding orbital $\pi^*_\perp$ (originating from π^*_{-1}) become more important than the configurations containing $\pi_\perp$. In the perpendicular orientation, the dominant configurations are ${}^3B_u(1a^2_g1b_u3a_g)$ and ${}^3A_g(1b^2_u1a_g3a_g)$ where $3a_g$ is the $\pi^*_\perp$ orbital. Both states have minima at roughly $R = 5a_0$, which are manifestations of perpendicular paramagnetic bonding.

Notably, there are indications of perpendicular paramagnetic bonding also in states of higher angular momentum. Tracing the third triplet state at $R = 5a_0$ in the perpendicular orientation to shorter bond distances, we find that it develops an AQAM value of −1.5 at $R \approx 2a_0$, implying that it has acquired some δ-orbital character, although the orbital Zeeman effect due to the larger magnitude of the angular momentum is not enough to offset other effects, in particular the electrostatic repulsion, at these bond lengths.

4. *Triplet potential-energy curves at $B = B_0$*

At $B = B_0$, the two lowest parallel electronic states, both with $\Lambda_{\mathbf{B}} = -1$, have the same dissociation limit and are energetically well separated from the other states. The lower state is dominated by a single electron configuration ${}^3\Pi_g(\sigma^2_{1s}\sigma^*_{1s}\pi_{-1})$, while the higher ${}^3\Pi_u$ state is more mixed, with weights 66% on $\sigma^2_{1s}\sigma^*_{1s}\pi^*_{-1}$ and 29% on $\sigma^{*2}_{1s}\sigma_{1s}\pi_{-1}$ at $R = 2a_0$.

The spectrum above these states is more complicated, with states closer together and crossings in the interval $2a_0 \le R \le 4a_0$. At $R = 2a_0$, the third electronic state is ${}^3\Delta_u(\sigma^2_{1s}\sigma^*_{1s}\delta_{-2})$ with $\Lambda_{\mathbf{B}} = -2$, while the fourth state is ${}^3\Sigma_u(\sigma^2_{1s}\sigma^*_{1s}\sigma_{2s})$ with $\Lambda_{\mathbf{B}} = 0$. The fifth state is again a mixed ${}^3\Pi_u$ state with $\Lambda_{\mathbf{B}} = -1$; it has the same dominant configurations as the second state but with weights 65% on $\sigma^{*2}_{1s}\sigma_{1s}\pi_{-1}$ and 29% on $\sigma^2_{1s}\sigma^*_{1s}\pi^*_{-1}$. The sixth state is ${}^3\Sigma_g(\sigma^2_{1s}\sigma^*_{1s}\sigma^*_{2s})$ with $\Lambda_{\mathbf{B}} = 0$.

Tracking the lowest two states from the parallel orientation through a 90° rotation is straightforward. As seen in Fig. 13, at a fixed bond distance of $R = 2a_0$, the states cross at about 40°. The bound parallel state ${}^3\Pi_g(\sigma^2_{1s}\sigma^*_{1s}\pi_{-1})$ is deformed into a nearly unbound, dissociative state ${}^3A_g(1a^2_g1b_u2b_u)$ on the perpendicular side as the bonding π_{-1} orbital transforms into the antibonding σ^*_{2s} orbital. There is, however, a minimum at the

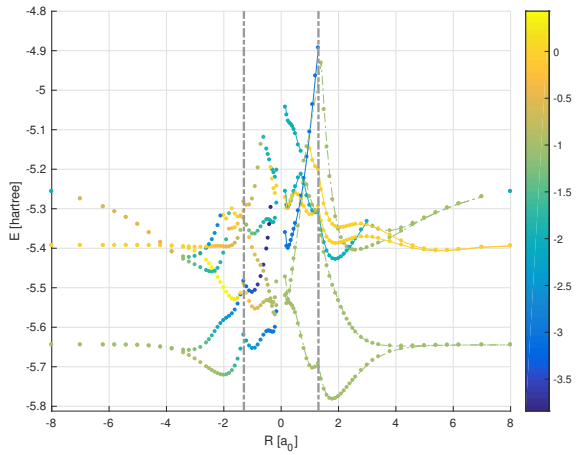

FIG. 12. Dissociation curves for triplet states in perpendicular (negative half) and parallel (positive half) magnetic field $B = B_0$.

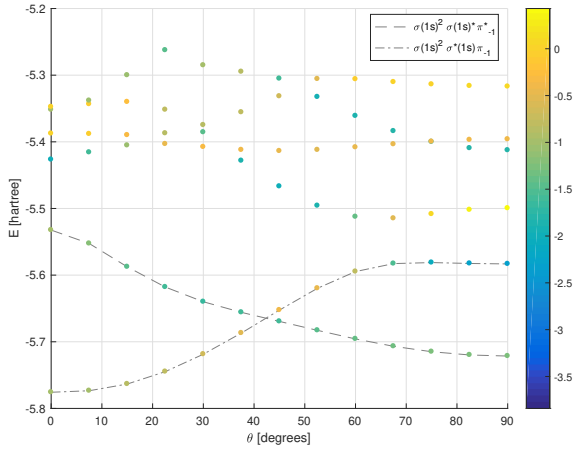

FIG. 13. Triplet states as a function of angle between the bond axis and magnetic field, with magnitudes fixed at $R = 2a_0$ and $B = B_0$, respectively.

larger bond distance of $R = 3.2a_0$, with $\Lambda_{\mathbf{B}} = -1.1$ and a depth of 14 millihartree, for this state, in part generated by paramagnetic bonding. At the same time, the unbound parallel state dominated by $^3\Pi_u(\sigma_{1s}^2\sigma_{1s}^*\pi_{-1}^*)$ transforms into the $^3B_u(1a_g^2 1b_u 2a_g)$ with $\Lambda_{\mathbf{B}} = -1.25$, which is bound by perpendicular paramagnetic bonding. Compared with the parallel orientation, the energy difference is almost 0.2 hartree—a manifestation of very strong perpendicular paramagnetic bonding. However, this state is not the global minimum over all triplet states and geometries, which instead occurs in the parallel orientation.

5. *Quintet potential-energy curves at $B = 0.2B_0$*

Dissociation curves for quintet states subject to a field $B = 0.2B_0$ are shown in Fig. 14. In the parallel orientation, the lowest-lying parallel states at $R = 4.2a_0$ alternate between $\Lambda_{\mathbf{B}} = -1$ and $\Lambda_{\mathbf{B}} = 0$. The lowest quintet state is predominantly $^5\Pi_g(\sigma_{1s}\sigma_{1s}^*\sigma_{2s}\pi_{-1})$ and covalently bound, while the second quintet is multiconfigurational $^5\Sigma_g(0.53\,\sigma_{1s}\sigma_{1s}^*\sigma_{2s}\sigma_{2s}^*, 0.21\,\sigma_{1s}\sigma_{1s}^*\sigma_{2s}^*\sigma_{2p})$ and noncovalently bound. The third and fourth parallel quintets at $R = 4.2a_0$ are predominantly $^5\Pi_u(\sigma_{1s}\sigma_{1s}^*\sigma_{2s}^*\pi_{-1})$ and $^5\Sigma_u(\sigma_{1s}\sigma_{1s}^*\sigma_{2s}\sigma_{2p})$, respectively.

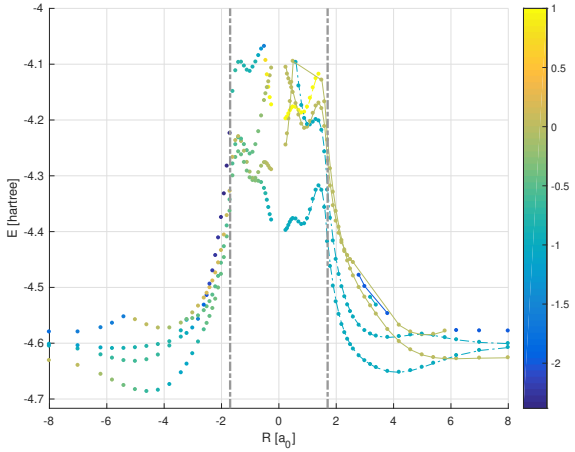

FIG. 14. Dissociation curves for quintet states in perpendicular (negative half) and parallel (positive half) magnetic field $B = 0.2B_0$.

When rotated from parallel ($\theta = 0°$) to perpendicular ($\theta = 90°$) orientation at the slightly shorter bond length of $R = 3.8a_0$, the lowest quintet state does not undergo any level crossing; see Fig. 15. From the parallel to the perpendicular orientation, the binding HOMO π_{-1} transforms into the antibonding σ_{2s}^* orbital of symmetry b_u, while the antibonding $\pi_\perp^*$ of a_g symmetry is stabilized paramagnetically. The resulting lowest perpendicular state becomes $^5A_g(0.44\,1a_g 1b_u 2b_u 3a_g, 0.27\,1a_g 1b_u 2b_u 2a_g)$ where the dominant configuration has more occupied antibonding than bonding orbitals. Nevertheless, because of paramagnetic stabilization of antibonding orbitals, the total energy decreases by more then 20 millihartree, while the dissociation energy increases from 48 to 59 millihartree as the covalent bond in the parallel orientation is replaced by a paramagnetic bond in the perpendicular orientation. Considering the relatively small magnitude of the magnetic field in this case, this provides an example of paramagnetic bonding that is orders of magnitude stronger than the initially reported bonding in the lowest H_2 triplet and He_2 singlet states [28].

As we go from the parallel to perpendicular field orientation, the AQAM projection of the lowest state de-

creases in magnitude, from −1 to −0.8, providing another example where this quantity does not directly capture the energy stabilization by the orbital Zeeman interaction. However, the radial dissociation limits are different in the parallel and perpendicular orientations, with the latter corresponding to two helium atoms in the 1s2s triplet state. Hence, from this perspective, the AQAM value changes from zero in the perpendicular radial dissociation limit to about −0.7 at the minimum, correctly indicating a stabilizing orbital Zeeman effect compared to the dissociation limit.

At $R = 3.8a_0$, the second and third quintet states in the parallel orientation are $^5\Pi_u$ and $^5\Sigma_g$, respectively. As seen from Fig. 15, these states undergo two level crossings from the parallel to perpendicular orientation, at about 20 and 70 degrees. The double crossing arises since $^5\Sigma_g$ has an energy minimum at about 45 degrees, while $^5\Pi_u$ has a maximum at about 35 degrees. We note that $^5\Sigma_g$ develops a substantial AQAM projection of −0.8 at 90 degrees and is even close to −1.1 at intermediate angles of 30–40 degrees (i.e., near the energy minimum). Both states have a lower energy at 90 degrees than at 0 degrees, with configurations $^5B_u(1a_g1b_u2a_g3a_g)$ and $^5A_g(0.39\,1a_g1b_u2b_u2a_g,\ 0.32\,1a_g1b_u2b_u3a_g)$, respectively.

The fourth perpendicular quintet state at $R = 3.8a_0$ is $^5B_g(0.49\,1a_g1b_u2a_g1a_u, 0.33\,1a_g1b_u3a_g1a_u)$. However, after a level crossing at $R = 5.8a_0$, the fourth state is $^5A_g(0.55\,1a_g1b_u3a_g3b_u, 0.30\,1a_g1b_u2a_g3b_u)$.

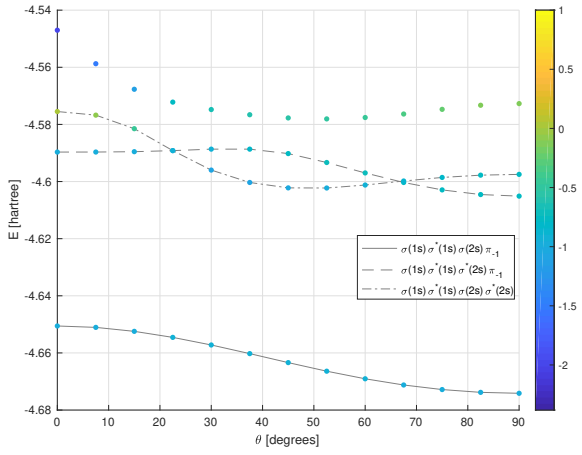

FIG. 15. Energies of the lowest quintet states as a function of angle between the bond axis and magnetic field, with magnitudes fixed at $R = 3.8a_0$ and $B = 0.2B_0$, respectively.

6. *Quintet potential-energy curves at $B = B_0$*

At a field strength of $B = B_0$, the orbital Zeeman interaction has rearranged the states so that all the states containing only σ orbitals are well above those that contain π orbitals. The lowest parallel state is dominated by the $^5\Delta_g(\sigma_{1s}\sigma^*_{1s}\pi_{-1}\pi^*_{-1})$ configuration, which is well below all other states for all bond lengths greater than $2a_0$. At a bond distance of $R = 4.2a_0$, the second quintet state is dominated by the $^5\Pi_g(\sigma_{1s}\sigma^*_{1s}\pi_{-1}\sigma_{2s})$ configuration, while the third quintet state is multiconfigurational $^5\Pi_u(0.69\,\sigma_{1s}\sigma^*_{1s}\pi^*_{-1}\sigma_{2s}, 0.22\,\sigma_{1s}\sigma^*_{1s}\pi_{-1}\sigma^*_{2s})$ The fourth quintet state is largely $^5\Phi_g(\sigma_{1s}\sigma^*_{1s}\pi_{-1}\delta_{-2})$.

In the perpendicular field orientation at field strength $B = B_0$, the lowest quintet states at bond distance $R = 3.8a_0$ are $^5A_g(1a_g1b_u2a_g2b_u)$, $^5B_g(1a_g1b_u2a_g1a_u)$, and $^5A_u(0.71\,1a_g1b_u2a_g1b_g, 0.21\,1a_g1b_u2b_u1a_u)$. The fourth quintet state is $^5B_u(1a_g1b_u2a_g3a_g)$; however, at a shorter bond distance of $R = 2.5a_0$, the fourth state has undergone a level crossing and is of the symmetry

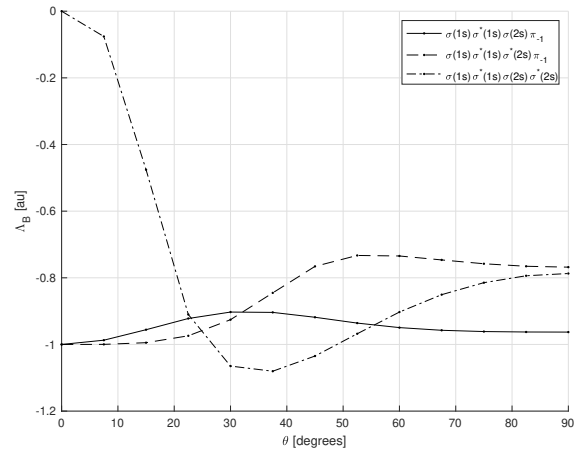

FIG. 16. AQAM value for the lowest quintet states as a function of angle between the bond axis and magnetic field, with magnitudes fixed at $R = 3.8a_0$ and $B = 0.2B_0$, respectively.

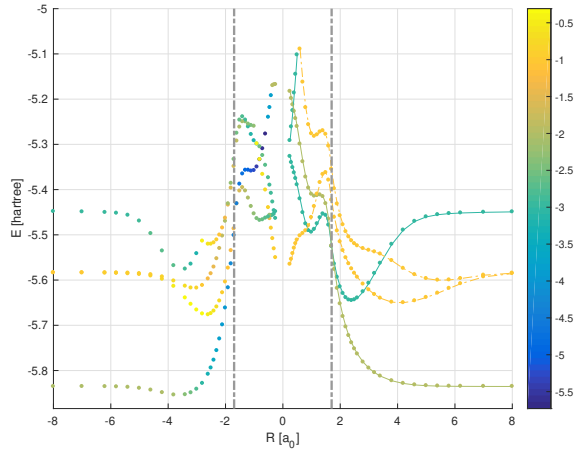

FIG. 17. Dissociation curves for quintet states in perpendicular (negative half) and parallel (positive half) magnetic field $B = B_0$.

$^5\mathrm{A_g}(1\mathrm{a_g}1\mathrm{b_u}2\mathrm{a_g}3\mathrm{b_u})$.

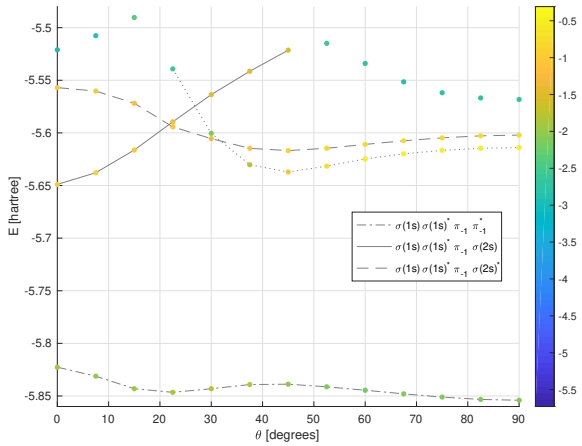

FIG. 18. Quintet states as a function of angle between the bond axis and magnetic field, with magnitudes fixed at $R = 3.8a_0$ and $B = B_0$, respectively.

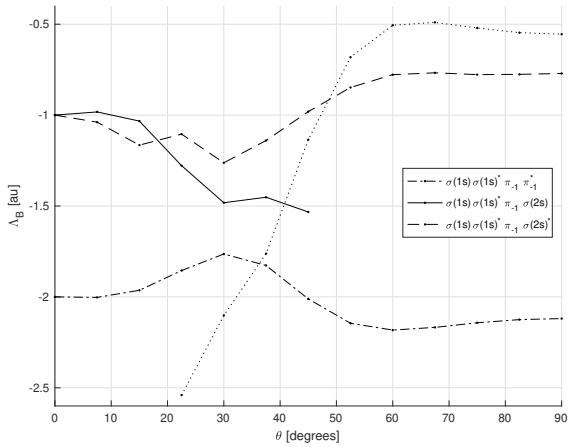

FIG. 19. AQAM value for the lowest quintet states as a function of angle between the bond axis and magnetic field, with magnitudes fixed at $R = 3.8a_0$ and $B = B_0$, respectively.

Rotation of the parallel states into perpendicular states is comparatively straightforward due to the energy separations between the dissociation curves—see Fig. 18 for rotation at the bond distance $R = 3.8a_0$. The lowest state $^5\Delta_\mathrm{g}(\sigma_{1\mathrm{s}}\sigma^*_{1\mathrm{s}}\pi_{-1}\pi^*_{-1})$ is further lowered by about 30 millihartree from 0 to 90 degrees. It is paramagnetically bound, with a dissociation energy of 20 millihartree and a global minimum located at $\theta = 90°$ and a slightly shorter bond distance $R = 3.62a_0$.

Intriguingly, the rotation curve in Fig. 18 has a second local minimum with respect to θ at about 25°. The corresponding AQAM values in Fig. 19 show that this local minimum is not associated with any increase in the magnitude $|\Lambda_\mathbf{B}|$. The stabilization at $\theta \approx 25°$ is therefore of a different origin than the stabilization at $\theta = 90°$.

IV. ENERGY SURFACES

Complete energy surfaces for the lowest singlet, triplet, and quintet states at $B = B_0$ are shown in Fig. 20, 21, and 23, respectively. These surfaces have been computed at the FCI/Lu-aug-cc-pVTZ level with a correction for basis-set superposition error (BSSE). The correction is an adapted counterpoise correction, taking into account the loss of symmetry in a magnetic field and, in particular, the inequivalence of the parallel and perpendicular orientations.

The most dramatic feature is seen in the triplet surface in Fig. 21, which is actually at each (R, θ) the minimum of two surfaces. One of these crossing states has a minimum in the perpendicular orientation and the other has a deeper minimum in the parallel orientation. The level crossing is clearly seen as a discontinuous "rift" that occurs for the shorter bond distances and angles roughly between 20° and 50°.

On the singlet surface in Fig. 20 the minimum is located at $R = 3.01a_0$ and $\theta = 90°$ and the BSSE corrected dissociation energy is 1.264 millihartree, which differs only negligibly different from the uncorrected value in Table IV. On the triplet surface in Fig. 21, the deepest minimum occurs at $R = 1.80a_0$ and $\theta = 0°$, with a BSSE corrected dissociation energy of 0.1376 hartree. The shallower minimum occurs at $R = 1.99a_0$ and has a BSSE corrected dissociation energy of 0.07676 hartree, again negligibly different from the uncorrected value. Finally, the quintet surface in Fig. 23 has two minima. The deeper minimum occurs at $R = 3.61a_0$, $\theta = 90°$, and has a BSSE corrected dissociation energy of 19.56 millihartree. The shallower minimum is located at $3.5a_0$ and $\theta = 24°$, with a dissociation energy of 11.7 millihartree.

V. CONCLUSIONS

We have studied the low-lying states of the helium dimer for different spins and magnetic-field strengths. As expected, the singlet, triplet, and quintet spectra resemble each other to a great degree, since many states have analogues with other total spin. For example, open-shell singlets have direct analogues among triplets. In general, all states are subject to a diamagnetic destabilization. However, the spin and orbital Zeeman interactions affect states differently and dramatically reorder the spectra, bringing down states of higher angular momentum. Hence, states with π and δ bonding orbitals become increasingly important in strong fields. Moreover, at large field strengths, the spin Zeeman interaction lowers the $m_\mathrm{s} = -1$ triplets below the singlets. For a field strength of $B = B_0$, the globally lowest state is even a paramagnetically bonded quintet state with $D_\mathrm{e} = 52\,\mathrm{kJ/mol}$, ori-

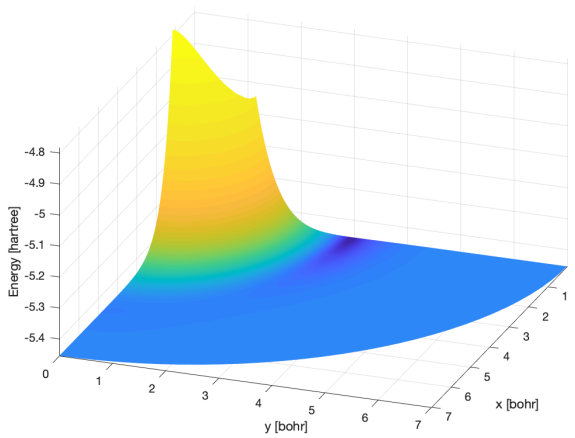

FIG. 20. The lowest singlet energy surface in a field of $B = B_0$. The axis labels are $x = R\cos(\theta)$ and $y = R\sin(\theta)$, so that the left side where $y = 0$ (and $\theta = 0°$) corresponds to the parallel orientation. The colour scale is $\ln(\eta+E(R,\theta)-E_{\min})$, with $\eta = 10^{-4}$ hartree.

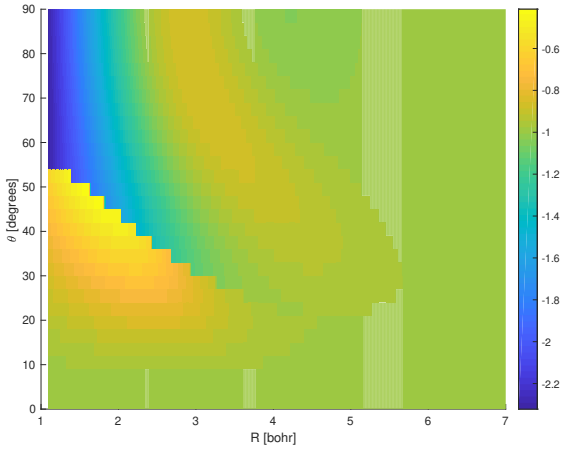

FIG. 22. The AQAM projection onto the magnetic field direction for the lowest triplet at each value of (R, θ). The level crossing between the two low-lying triplets is clearly manifested in the discontinuous "rift" that begins at $R \approx 1$ bohr and $\theta \approx 50°$.

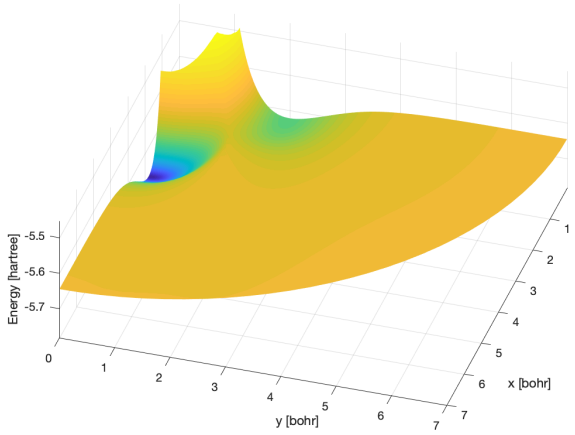

FIG. 21. The lowest triplet energy surface in a field of $B = B_0$. The axis labels are $x = R\cos(\theta)$ and $y = R\sin(\theta)$. The colour scale is $\ln(\eta + E(R,\theta) - E_{\min})$, with $\eta = 5 \times 10^{-3}$ hartree.

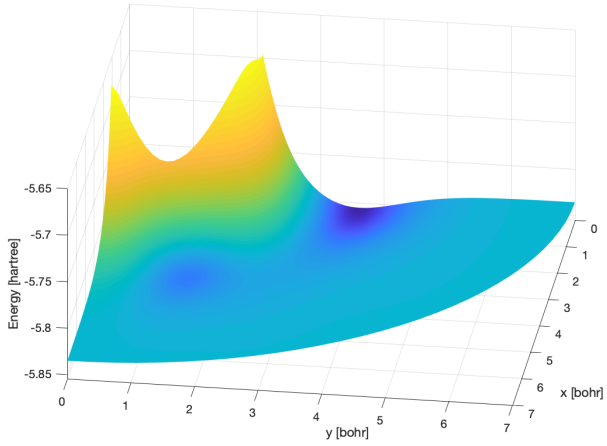

FIG. 23. The lowest quintet energy surface in a field of $B = B_0$. The axis labels are $x = R\cos(\theta)$ and $y = R\sin(\theta)$. The colour scale is $\ln(\eta + E(R,\theta) - E_{\min})$, with $\eta = 5 \times 10^{-3}$ hartree.

ented perpendicular to the magnetic field. Hence, these field strengths induce an entirely new chemistry of helium atoms.

In general, in addition to the effects of increasing field strength, the orientation with respect to the magnetic field modulates the proportion of σ, π and δ bonding, which affects the total angular momentum and the orbital Zeeman interaction. For nontrivial orientations of the bond axis with respect to the magnetic field, all spatial symmetries except inversion are lost and the canonical angular momentum ceases to be a good quantum number. To partially address this complication, we have introduced the almost quantized angular momentum (AQAM) and demonstrated that it is a very useful tool to characterize states in arbitrary orientations. Conical intersections make detailed state classification beyond the characterization provided by AQAM challenging and poorly defined. In general, energy hypersurfaces become multivalued as functions of the parameters (R, θ, B). This occurs as an effect of the symmetry breaking, which turns true crossings in the parallel orientation into avoided crossings at nontrivial angles. Two states may be continuously deformed into each along some paths in parameter space, but not others. In the radial dissociation limit, for instance, the parallel and perpendicular orientations become physically equivalent.

Nonetheless, at a fixed bond distance, continuously deforming between the parallel and perpendicular orientations can result in a state with a different radial dissociation limit.

Our results show that perpendicular paramagnetic bonding is common in excited electronic states, although the presence of conical intersections makes the identification somewhat poorly defined and dependent on the which path in parameter space is emphasized. Moreover, the effect is larger for the more diffuse σ^*_{2s} compared to the compact σ^*_{1s} orbital. As a result, the bonding mechanism is also stronger, sometimes by orders of magnitudes, in excited states than the originally described cases (lowest triplet of H_2 and lowest singlet of He_2). There are some indications of the perpendicular paramagnetic bonding mechanism involving higher angular momentum states (e.g., modulation of π into δ orbitals or δ into ϕ orbitals), although it is difficult to determine the relative contributions from σ^* and higher angular momentum orbitals.

ACKNOWLEDGMENTS

This work was supported by the Research Council of Norway through Grant No. 240674 and CoE Hylleraas Centre for Molecular Sciences Grant No. 262695. This work has also received support from the Norwegian Supercomputing Program (NOTUR) through a grant of computer time (Grant No. NN4654K).

[1] R. H. Garstang, Rep. Prog. Phys. **40**, 105 (1977).
[2] D. Lai, Rev. Mod. Phys. **73**, 629 (2001).
[3] S. Jordan, P. Schmelcher, and W. Becken, Astron. Astrophys. **376**, 614 (2001).
[4] S. Jordan, P. Schmelcher, W. Becken, and W. Schweizer, Astron. Astrophys. **336**, L33 (1998).
[5] Y. P. Kravchenko, M. A. Lieberman, and B. Johansson, Phys. Rev. A **54**, 287 (1996).
[6] O.-A. Al-Hujaj and P. Schmelcher, Phys. Rev. A **61**, 063413 (2000).
[7] M. D. Jones, G. Ortiz, and D. M. Ceperley, Phys. Rev. A **59**, 2875 (1999).
[8] W. Becken and P. Schmelcher, Phys. Rev. A **65**, 033416 (2002).
[9] A. Thirumalai and J. S. Heyl, Phys. Rev. A **79**, 012514 (2009).
[10] O.-A. Al-Hujaj and P. Schmelcher, Phys. Rev. A **70**, 023411 (2004).
[11] M. V. Ivanov and P. Schmelcher, Phys. Rev. A **61**, 022505 (2000).
[12] M. V. Ivanov and P. Schmelcher, Phys. Rev. A **60**, 3558 (1999).
[13] A. Thirumalai, S. J. Desch, and P. Young, Phys. Rev. A **90**, 052501 (2014).
[14] A. V. Turbiner and J. C. L. Vieyra, Phys. Rep. **424**, 309 (2006).
[15] J. Avron, I. Herbst, and B. Simon, Phys. Rev. Lett. **39**, 1068 (1977).
[16] A. V. Turbiner and N. L. Guevara, J. Phys. B **40**, 3249 (2007).
[17] A. V. Turbiner and N. L. Guevara, Phys. Rev. A **74**, 063419 (2006).
[18] J. Ozaki, Chem. Phys. Lett. **203**, 184 (1993).
[19] P. Schmelcher and L. S. Cederbaum, Phys. Rev. A **41**, 4936 (1990).
[20] U. Kappes, P. Schmelcher, and T. Pacher, Phys. Rev. A **50**, 3775 (1994).
[21] T. Detmer, P. Schmelcher, and L. S. Cederbaum, Phys. Rev. A **57**, 1767 (1998).
[22] T. Detmer, P. Schmelcher, and L. S. Cederbaum, J. Chem. Phys. **109**, 9694 (1998).
[23] M. Žaucer and A. Ažman, Phys. Rev. A **18**, 1320 (1978).
[24] Y. E. Lozovik and A. V. Klyuchnik, Phys. Lett. A **66**, 282 (1978).
[25] S. Basile, F. Trombetta, and G. Ferrante, Il Nuovo Cimento **9**, 457 (1987).
[26] A. V. Korolev and M. A. Lieberman, Phys. Rev. A **45**, 1762 (1992).
[27] A. Kubo, J. Phys. Chem. A **111**, 5572 (2007).
[28] K. K. Lange, E. I. Tellgren, M. R. Hoffmann, and T. Helgaker, Science **337**, 327 (2012).
[29] E. I. Tellgren, S. S. Reine, and T. Helgaker, Phys. Chem. Chem. Phys. **14**, 9492 (2012).
[30] S. Stopkowicz, J. Gauss, K. K. Lange, E. I. Tellgren, and T. Helgaker, J. Chem. Phys. **143**, 074110 (2015), https://doi.org/10.1063/1.4928056.
[31] M. Motokawa, Rep. Prog. Phys. **67**, 1995 (2004).
[32] D. Nakamura, H. Sawabe, Y. H. Matsuda, and S. Takeyama, Rev. Sci. Instrum. **84**, 044702 (2013).
[33] D. Nakamura, A. Ikeda, H. Sawabe, Y. H. Matsuda, and S. Takeyama, Rev. Sci. Instrum. **89**, 095106 (2018).
[34] A. Bykov, M. Dolotenko, N. Kolokolchikov, S. V.D., and O. Tatsenko, Physica B **274-275**, 574 (2001).
[35] B. Murdin, J. Li, M. Pang, E. Bowyer, K. Litvinenko, S. Clowes, H. Engelkamp, C. Pidgeon, I. Galbraith, N. Abrosimov, H. Riemann, S. Pavlov, H.-W. Hübers, and P. Murdin, Nature Comm. **4**, 1469 (2013).
[36] K. L. Litvinenko, M. Pang, J. Li, E. Bowyer, H. Engelkamp, V. B. Shuman, L. M. Portsel, A. N. Lodygin, Y. A. Astrov, S. G. Pavlov, H.-W. Hübers, C. R. Pidgeon, and B. N. Murdin, Phys. Rev. B **90**, 115204 (2014).
[37] Y. Kimura and K. Takazawa, Rev. Sci. Instrum. **82**, 013108 (2011).
[38] T. S. Monteneiro and K. T. Taylor, J. Phys. B **23**, 427 (1990).
[39] G. I. Pagola, M. C. Caputo, M. B. Ferraro, and P. Lazzeretti, Chem. Phys. Lett. **400**, 133 (2004).
[40] G. I. Pagola, M. C. Caputo, M. B. Ferraro, and P. Lazzeretti, J. Chem. Phys. **120**, 9556 (2004).
[41] G. I. Pagola, S. Pelloni, M. C. Caputo, M. B. Ferraro, and P. Lazzeretti, Phys. Rev. A **72**, 033401 (2005).
[42] G. I. Pagola, M. B. Ferraro, and P. Lazzeretti, J. Chem. Theor. Comp. **5**, 3049 (2009).

[43] J. Vaara, P. Manninen, and J. Lounila, Chem. Phys. Lett. **372**, 750 (2003).

[44] P. Manninen and J. Vaara, Phys. Rev. A **69**, 022503 (2004).

[45] F. London, J. Phys. Radium **8**, 397 (1937).

[46] H. F. Hameka, Mol. Phys. **1**, 203 (1958).

[47] R. Ditchfield, J. Chem. Phys. **65**, 3123 (1976).

[48] T. Helgaker and P. Jørgensen, J. Chem. Phys. **95**, 2595 (1991).

[49] E. I. Tellgren, A. Soncini, and T. Helgaker, J. Chem. Phys. **129**, 154114 (2008).

[50] "LONDON, a quantum-chemistry program for plane-wave/GTO hybrid basis sets and finite magnetic field calculations. By E. Tellgren (primary author), T. Helgaker, A. Soncini, K. K. Lange, A. M. Teale, U. Ekström, S. Stopkowicz, J. H. Austad, and S. Sen. See londonprogram.org for more information.".

[51] R. D. Reynolds and T. Shiozaki, Phys. Chem. Chem. Phys. **17**, 14280 (2015).

[52] T. J. P. Irons, J. Zemen, and A. M. Teale, J. Chem. Theory Comput. **13**, 3636 (2017), pMID: 28692291, https://doi.org/10.1021/acs.jctc.7b00540.

[53] D. B. Williams-Young, A. Petrone, S. Sun, T. F. Stetina, P. Lestrange, C. E. Hoyer, D. R. Nascimento, L. Koulias, A. Wildman, J. Kasper, J. J. Goings, F. Ding, A. E. DePrince III, E. F. Valeev, and X. Li, WIREs Computational Molecular Science , e1436https://onlinelibrary.wiley.com/doi/pdf/10.1002/wcms.1436.

[54] S. Sun, D. B. Williams-Young, T. F. Stetina, , and X. Li, J. Chem. Theor. Comp. **15**, 348 (2019).

[55] A. Ishikawa, H. Nakashima, and H. Nakatsuji, Chem. Phys. **401**, 62 (2012).

[56] H. Nakashima and H. Nakatsuji, Astrophys. J. **725**, 528 (2010).

[57] E. I. Tellgren and H. Fliegl, J. Chem. Phys. **139**, 164118 (2013).

[58] E. I. Tellgren, A. M. Teale, J. W. Furness, K. K. Lange, U. Ekström, and T. Helgaker, J. Chem. Phys. **140**, 034101 (2014).

[59] J. W. Furness, J. Verbeke, E. I. Tellgren, S. Stopkowicz, U. Ekström, T. Helgaker, and A. M. Teale, J. Chem. Theory Comput. **11**, 4169 (2015).

[60] S. Sen, K. K. Lange, and E. I. Tellgren, J. Chem. Theor. Comp. **15**, 3974 (2019).

[61] E. I. Tellgren, A. Laestadius, T. Helgaker, S. Kvaal, and A. M. Teale, J. Chem. Phys. **148**, 024101 (2018).

Paper III

Effects of strong magnetic fields on water from rigorous quantum calculations

Hemanadhan Myneni, Dariusz Kedziera, Jan W. Andselm, Jon Austad, Erik I. Tellgren, Trygve Helgaker and Krzysztof Szalewicz.
To be submitted for publication

Effects of strong magnetic fields on water from rigorous quantum calculations

Hemanadhan Myneni,[1] Dariusz Kedziera,[2] Jan W. Andzelm,[3]
Jon Austad,[4]Erik I. Tellgren,[4] Trygve Helgaker,[4] Krzysztof Szalewicz[1*]

[1]Department of Physics and Astronomy, University of Delaware,
Newark, Delaware 19716, USA
[2] Faculty of Chemistry, Nicolaus Copernicus University in Toruń,
7 Gagarin Street, 87-100 Toruń, Poland
[3] U.S. Army Research Laboratory, RDRL-WMM-G,
Aberdeen Proving Ground, MD 21005-5069, USA
[4] Centre for Theoretical and Computational Chemistry, Department of Chemistry,
University of Oslo, P.O. Box 1033 Blindern, N-0315 Oslo, Norway

*To whom correspondence should be addressed; E-mail: szalewic@udel.edu.

Whereas numerous experimental studies concerning matter in strong magnetic fields have been performed, the effects of such fields are still highly controversial. We present rigorous quantum-mechanical calculations for water and oxygen-water clusters in such fields. These calculations show that one cannot expect any measurable effects from fields of the order of 40 T, the largest available in laboratories, on structure and on most properties of water clusters and of liquid water. The only exception are properties depending on Earth gravitational field since gravitational forces can be balanced by magnetic ones.

Introduction

Magnetic water treatment devices aimed at reducing scale deposition in water pipes started to appear some time in the middle of the last century and are still available as can be quickly found by a search of the internet. This is despite the fact that several dozens of papers appeared, the earliest ones already in the 1950s, e.g., Ref. (*1*), investigating the performance of such devices and finding no effects. However, some papers, even quite recent ones, e.g., Ref. (*2*), claim to provide experimental evidence that such devices may work. A review of the subject can be found in Ref. (*3*). There have also been a large number of experimental papers finding that properties of liquid water other than the scale deposition change under the influence of strong magnetic fields. Among such properties are viscosity (*4–6*), surface-tension (*6–9*), vaporization rate (*10–13*), refraction index (*14*), and infrared and Raman spectra (*7, 15–17*). In many cases, different measurements of the same property contradict each other. On the other hand, there are also experiments on water in magnetic fields with clear-cut results such as the levitation of water droplets (*18*) or visible water surface deformation (*19*), both observed in magnetic fields of $\sim$10 T. A characteristic element of this group of experiments is that the investigated properties depend on Earth's gravitational field.

Due to low reproducibility and little consistency of the reported experimental results, one might expect that computational methods of quantum mechanics would be used for understanding the magnetic field impacts on water. In particular, one of the most common hypothetical explanations of the discussed effects is that magnetic fields significantly influence the hydrogen-bond structure of liquid water (*17, 20–22*). Indeed, water properties are closely related to this structure (*23, 24*). However, no attempt has been made to verify this hypothesis despite the fact that computational quantum methods predict water properties very well (*23–25*) (one exception are calculations on water clusters in Ref. (*6*) which, however, actually used an electric field that

the authors assumed to be equivalent to a given magnetic field). The reason for this situation was that until recently there was no software available for quantum mechanical calculation in strong magnetic fields. The situation has recently changed with the development of the LONDON code (*26–29*), capable of treating atomic or molecular systems accurately for all field orientations and strengths, i.e., not limited to linear response theory. We have performed such calculations for small water clusters in several field strengths including 40 T, the strongest fields available in laboratories.

For selected clusters and field strengths, calculations were performed at several levels of electronic structure theory and in several basis sets. The results presented here are reasonably close to the exact solutions of Schrödinger's equation in the Born-Oppenheimer (clamped nuclei) approximation despite using only the second-order of perturbation theory with the Møller-Plesset partition of the Hamiltonian (MP2) and the augmented core-valence correlation-consistent, double-zeta quality aug-cc-pCVTZ basis sets (*30*) (in the uncontracted form which results in an increased number of functions with large exponents important for describing the motions of fast core electrons that interact most strongly with magnetic fields). All calculations were performed in n-mer basis sets thereby removing the basis set superposition error. The cluster configurations are close to the global minima ones. Further technical details of our calculation as well as a tabular representation of the results are given in the Supplementary Information.

The relative effects of magnetic fields on interaction energies, defined as $\Delta E_{\rm int}(B_w)/E_{\rm int}(0)$, where $\Delta E_{\rm int}(B_w) = E_{\rm int}(B_w) - E_{\rm int}(0)$ are shown for $(H_2O)_2$, $(H_2O)_3$, and $(H_2O)_4$ in Figs. 1 as functions of the strength of the magnetic field B_w oriented along the axis $w = x, y, z$ of the coordinate system.

The most striking observation in the figures is that the changes of interaction energies for the fields up to 100 T are so small that we had to present them in ppm. In particular, for the

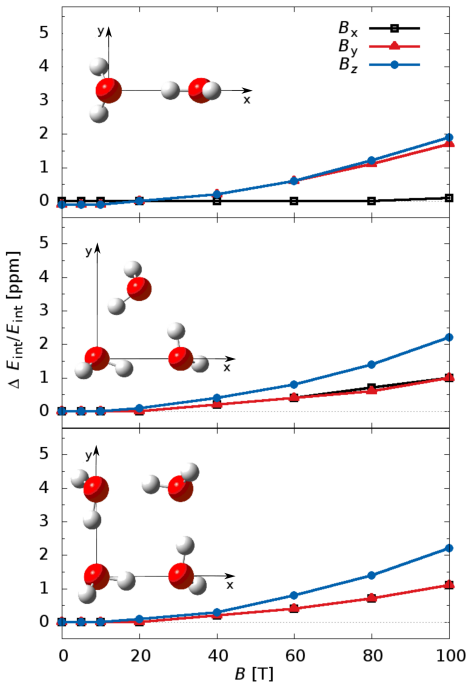

Figure 1: Dependence of the water clusters interaction energy on the strength of the magnetic field.

field of 40 T, all the changes are below 0.4 ppm. The relative changes vary very little with the size of the cluster: the values averaged over the directions of the field are 0.15, 0.23, and 0.23 ppm at 40 T for $(H_2O)_2$, $(H_2O)_3$, and $(H_2O)_4$, respectively (Fig. 1).

Clearly, sub-ppm effects of magnetic fields of up to 40 T on the interaction energies are completely negligible from the point of view of cluster properties. Even spectra of water clusters, providing the most precise data on such clusters (*23*), do not have ppm accuracy. More importantly, these conclusions extend also to liquid water. The reason is that the convergence of many-body forces in water clusters is reasonably fast. For example, for the $(H_2O)_{24}$ cluster the total interaction energy computed using two-body, three-body, and four-body interactions recovers the total interaction energy with an error of only 3% (*31*). Since the rate of convergence is approximately the same for all investigated clusters starting from the hexamer, it is

also similar for liquid water, Thus, the forces determining the structure and properties of liquid water can change only at the ppm level, which is negligible in comparison to uncertainties of any measurements on liquid water which are at the best a fraction of one percent.

Our results are in a dramatic disagreement with the calculations on water clusters by Toledo *et al.* (*6*) who found that the field of 34 T makes water dimer unbound and changes energies of water trimer and tetramer by a fraction of one percent. However, these authors performed the calculations using electric fields and making an assumption, evidently not justified, about equivalence of such fields. The only other theoretical investigations were performed using molecular dynamics or Monte Carlo simulations with empirical potential and accounting for the Lorentz force acting on the moving partial charges on atoms (*20, 22*). Since atoms move with velocities about three orders of magnitude slower than electrons, effects of this type have to be much smaller than those found by us. Thus, the effects observed in Refs. (*20, 22*) must be numerical artifacts.

The results of our calculations show that it is not possible to measure effects of magnetic field of the order of 40 T on such properties of bulk water like for example viscosity, diffusion coefficient, or infrared spectra. This conclusion, in fact, should extend to any diamagnetic matter since per atom magnetizabilites of molecules are all of the same order of magnitude. On the other hand, the behaviour of liquid water that depends on Earth gravitational field can be dramatically changed by strong magnetic fields, as in the water droplet levitation experiments (*18*). The reason is that the gravitational force is very weak compared to the Coulomb force (for two interacting electrons it is weaker by 40 orders of magnitude) and therefore it can be balanced by the magnetic force.

Another hypothesis put forward to explain the changes of water properties in strong magnetic fields observed in some experiments was that they originate from the presence of molecular oxygen in natural water (*7, 32, 33*). Whereas there are also several other molecular impurities

present, O_2 is special from the point of view of the response to magnetic fields since it is a paramagnetic molecule and paramagnetic interactions are typically three orders of magnitude stronger than diamagnetic ones. We performed calculations for the (H_2O)–O_2 and $(H_2O)_2$–O_2 clusters using the unrestricted version of MP2 (UMP2) to check if magnetic fields can significantly change intermolecular interactions in such clusters. We found that the relative differences between interaction energies of H_2O–O_2 computed in zero-field and in the field of 40 T are below 0.5 ppm (Fig. 2).

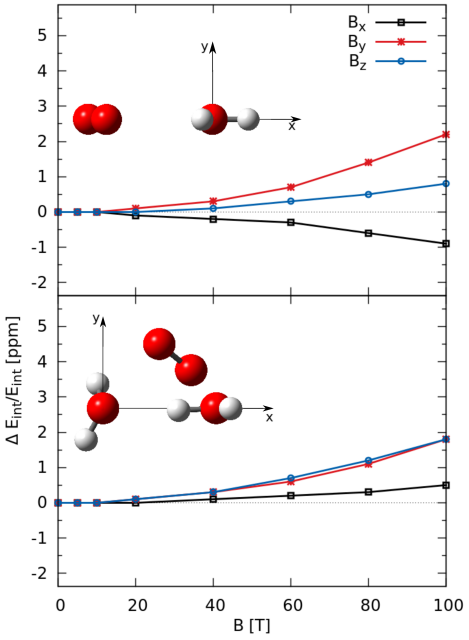

Figure 2: Dependence of the oxygen and water clusters interaction energy on the strength of the magnetic field.

However, the absolute value of the shift is not that different from the case of the water dimer, the reason for the larger ratios is that the interaction energy is only -0.45 kcal/mol in the former case, about 10 times smaller than for the water dimer. For the $(H_2O)_2$–O_2 trimer, the relative differences are smaller than 0.4 ppm, similarly as in water clusters. Thus, the presence

of oxygen will not result in any measurable changes of the structure of water (not mentioning that the concentration is 1 oxygen molecule per about 200,000 water molecules).

With the very small impacts of magnetic fields found in our calculations, one may ask if the discussed phenomena can be described well enough by linear response theory. To answer this question, we performed simple back-of-the-envelope linear response calculations. The change of a system energy due to a magnetic field B, ΔE, is given by $\Delta E = -(1/2)\xi B^2$, where ξ is the magnetizability. We used the experimental value of ξ, -218×10^{-30} J/T^2 (*34*), which close to theoretical values (*35, 36*). This calculation gives the value $\Delta E = 0.40 \times 10^{-7}$ hartree for 40 T, which agrees very well with the value of 0.45×10^{-7} hartree computed using LONDON (the total energy decreases in magnitude). Thus, linear response theory works very well for total energies. To estimate interaction energies, we assumed that the leading term in these quantities results from interactions of the induced magnetic dipoles $\mathbf{m} = \xi\mathbf{B} = 0.00047$ a.u. in 40 T. Interaction energy of two such dipoles separated by 5.5 bohr is 0.13×10^{-8} hartree for the parallel configuration and -0.27×10^{-8} hartree for the in-line head-to-tail configuration. The first case models the water dimer with the field approximately perpendicular to the hydrogen-bond axis, where the interaction energy computed by LONDON is -0.24×10^{-8} hartree, whereas the second case the field parallel to the bond, where the interaction energy computed by LONDON is -0.009×10^{-8} hartree. Thus, this simple estimate gives only the order of magnitude for the effect. Most likely the density changes induced by magnetic fields lead to changes of the exchange-repulsion term, the largest component of water-water interaction at the equilibrium.

The total energy change with magnetic field for the paramagnetic oxygen molecule can be estimated as the energy of the interaction of the 1/2 spin of the electron with the field parallel to the direction of the spin: $E_{\rm spin}(B) = B/2$ (in atomic units). Multiplying this by 2 since there are two electrons, one gets $E_{\rm spin}(B) = 0.00017$ hartree at 40 T. The change of the total energy of O_2 computed using UMP2 is 1.7×10^{-4} hartree, in a perfect agreement. This shift

is more than 3 orders of magnitude larger than the diamagnetic shift for the water molecule, as expected.

It may be surprising that despite this 3 orders of magnitude difference, the effects of magnetic fields on the *interaction* energies are about the same for the paramagnetic clusters as for the diamagnetic ones. Apparently, the unpaired spins do not affect interaction energies, i.e., the paramagnetic shifts in $(H_2O)_n$–O_2 and in O_2 perfectly cancel each other. This is confirmed by the smallness of the magnitude of the H_2O–O_2 interaction energy which is similar to interaction energies involving rare gas atoms.

In conclusion, our work shows that most measurements of properties of water (or any other diamagnetic substance) in magnetic fields up to 40 T should not be able to detect changes of the properties due to the field since the structure of water changes negligibly in such fields. The only experiments where such changes are detectable (and sometimes very pronounced) are those where magnetic forces can balance the very small gravitational forces. Another type of experiment that could possibly detect a B-dependent signal is a measurement involving directly oxygen spins. This is due to the fact that water degasifies in magnetic fields and therefore the concentration of oxygen changes.

References

1. R. Eliassen, R. T. Skrinde, W. B. Davis, *J. Am. Water Works Ass.* **50**, 1371 (1958).

2. L. Jiang, J. Zhang, D. Li, *Desalin. Water Treat.* **53**, 1275 (2015).

3. J. S. Baker, S. J. Judd, *Wat. Res.* **30**, 247 (1996).

4. K. Ishii, S. Yamamoto, M. Yamamoto, H. Nakayama, *Chem. Lett.* **34**, 874 (2005).

5. S. A. Ghauri, M. S. Ansari, *J. Appl. Phys.* **100**, 066101 (2006).

6. E. J. Toledo, T. C. Ramalho, Z. M. Magriotis, *J. Mol. Struct.* **888**, 409 (2008).

7. I. Otsuka, S. Ozeki, *J. Phys. Chem. B* **110**, 1509 (2006).

8. Y. Fujimura, M. Iino, *J. Appl. Phys.* **103**, 124903 (2008).

9. R. Cai, H. Yang, J. He, W. Zhu, *J. Mol. Struct.* **938**, 15 (2009).

10. J. Nakagawa, N. Hirota, K. Kitazawa, M. Shoda, *J. Appl. Phys.* **86**, 2923 (1999).

11. S. H. Wu, F. B. Zhang, *J. Petrochem. Univ. (China)* **232**, 954 (2006).

12. A. Szcześ, E. Chibowski, L. Hołysz, P. Rafalski, *Chem. Eng. Process* **50**, 124 (2011).

13. Y.-z. Guo, *et al.*, *Int. J. Mol. Sci.* **13**, 16916 (2012).

14. H. Hosoda, H. Mori, N. Sogoshi, A. Nagasawa, S. Nakabayashi, *J. Phys. Chem. A* **108**, 1461 (2004).

15. X. Pang, B. Deng, *Sci. China, Ser. G* **51**, 1621 (2008).

16. X.-F. Pang, B. Deng, *Physica B* **403**, 3571 (2008).

17. M. Iwasaka, S. Ueno, *J. Appl. Phys.* **83**, 6459 (1998).

18. Y. Ikezoe, N. Hirota, J. Nakagawa, K. Kitazawa, *Nature* **393**, 749 (1998).

19. K. Kitazawa, Y. Ikezoe, H. Uetake, N. Hirota, *Physica B: Cond. Mat.* **294-295**, 709 (2001).

20. K. X. Zhou, *et al.*, *J. Appl. Phys.* **88**, 1802 (2000).

21. H. Inaba, T. Saitou, K.-i. Tozaki, H. Hayashi, *J. Appl. Phys.* **96**, 6127 (2004).

22. K.-T. Chang, C.-I. Weng, *J. Appl. Phys.* **100**, 043917 (2006).

23. R. Bukowski, K. Szalewicz, G. C. Groenenboom, A. van der Avoird, *Science* **315**, 1249 (2007).

24. O. Akin-Ojo, K. Szalewicz, *J. Chem. Phys.* **138**, 024316 (2013).

25. F. Paesani, *Acc. Chem. Res.* **49**, 1844 (2016).

26. K. K. Lange, E. I. Tellgren, M. R. Hoffmann, T. Helgaker, *Science* **337**, 327 (2012).

27. E. I. Tellgren, *et al.*, *J. Chem. Phys.* **140**, 034101 (2014).

28. J. W. Furness, *et al.*, *J. Chem. Theory Comput.* **11**, 4169 (2015).

29. S. Stopkowicz, J. Gauss, K. K. Lange, T. Helgaker, *J. Chem. Phys.* **143**, 074110 (2015).

30. D. E. Woon, T. H. Dunning Jr., *J. Chem. Phys.* **103**, 4572 (1995).

31. U. Gora, R. Podeszwa, W. Cencek, K. Szalewicz, *J. Chem. Phys.* **135**, 224102 (2011).

32. S. Ueno, M. Iwasaka, T. Kitajima, *J. Appl. Phys.* **75**, 7174 (1994).

33. S. Ueno, M. Iwasaka, G. Furukawa, *IEEE Trans. Magn.* **31**, 4259 (1995).

34. D. R. Lide, *CRC Handbook of Chemistry and Physics, 84th Edition* (Taylor & Francis, Boca Raton, FL, 2004).

35. K. Ruud, T. Helgaker, K. L. Bak, P. Jørgensen, H. J. A. Jensen, *J. Chem. Phys.* **99**, 3847 (1993).

36. E. I. Tellgren, A. Soncini, T. Helgaker, *J. Chem. Phys.* **129**, 154114 (2008).

37. Neese, F. *Wiley Interdiscip Rev Comput Mol Sci.*, **2**, 73 (2012).

38. R. A. Kendall, T. H. Dunning, Jr., R. J. Harrison, *J. Chem. Phys.* **96**, 6796 (1992).

39. E. M. Mas and K. Szalewicz, *J. Chem. Phys.* **104**, 7606 (1996).

40. W. Cencek, K. Szalewicz, C. Leforestier, R. van Harrevelt, A. van der Avoird, *Phys. Chem. Chem. Phys.* , **10**, 4716, (2008).

41. A. van der Avoird, K. Szalewicz, *J. Chem. Phys.* **128**, 014302 (2008).

42. E. Miliordos, S. S. Xantheas, *J. Chem. Phys.* **142**, 234303 (2015).

Acknowledgments

This work was supported by the U. S. Army Research Laboratory and by the NSF grant CHE-1566036. D.K. acknowledges support from the NCN grant no. DEC-2012/07/B/ST4/01347.

Errata

- Multiple erroneous hyphens are removed.
- Planet Earth was sometimes written earth.
- In Acknowledgment: The word “office” was misspelled.
- Page 4: The formulation “beyond the limitations” is now “beyond the reach”.
- Vector called $\boldsymbol{q}$ is renamed to $\boldsymbol{c}$ in Section 2.2.
- Section 2.3.1 is removed from the thesis.
- The twoelectron integral notation is cleaned up in Sections 2.2 and 3.4.1.
- An explanation for using uncontracted basis sets has been provided.
- Basis sets has been coherently named throughout.
- All references to nuclear physics are removed.
- The section devoted to the discussion of size consistency is reduced to a paragraph.
- The bibliography style has been changed to ieeetr.
- Footnote 5 on page 20 is incorporated in the main text.
- Figure 2.2 in the original is removed.
- The redundant definition of the Slater determinant is removed.
- The importance of augmented functions for dispersion effects is made explicit.
- The symmetry discussion mentioning Noether’s theorem is reformulated.
- “Chemical accuracy” is replaced with a less bold choice of words.
- Explicit reference to to Section 3.5.7 is introduced in Section 4.1.
- A missing space between word and reference on page 6 is added.
- Page 26: The word “significant” was misspelled.

- Section 3.1.2: Third sentence is reformulated.
- Page 46, Equation 3.92: E_{c} on the left hand side is now E_{xc}.
- In the discussion of paper 3: Oxygen *molecules* dissolved in water, not oxygen *atoms*.
- Removed a double "so far" in Section 4.2.4.
- Page 50: Mathematical error. The CDFT Hamiltonian as written out was defined for a strictly solenoidal $\boldsymbol{A}$ (Equation 3.117 in the original version). The corrected equation and a clarification is added.
- Section 3.1.2: In the last paragraph, it was claimed that I had used core functions "when applicable". This statement is confusing and has been removed.
- Section 3.5.4: The word "adiabatic" was misspelled.
- Section 3.5: A redundant "obviously" is removed.
- The word "interaction" was consistently misspelled with an extra r.
- Section 4.1: The words "geometries", "category" and "modeling" were misspelled once.
- Section 4.2: The words "orientation", "literature", "artifact", "clear", "appears" and "feasibility" were misspelled once.
- Figure 4.2 *is* BSSE corrected. At a point in Section 4.2.3, a claim to the contrary was made. This has been rectified.
- Section 4.2.2. The word "distinctly" is replaced with "distinct".
- Section 4.2.4: Missing word, "of", is added ("regime of dimers").
- Section 4.3: The word "levitation" was misspelled.
- Section 5.1: First sentence is clarified.
- Page 117: "Submitted for publication" is now "Submitted for publication in PCCP".